Contributions to cooperative localization techniques within mobile wireless bady area networks

Jhad Hamie, Denis Benoit, Richard Cédric

UNIVERSITE DE NICE-SOPHIA ANTIPOLIS - UFR Sciences
Ecole Doctorale en Sciences Fondamentales et Appliquées

THESE

Pour obtenir le titre de :

Docteur en Sciences
de l'UNIVERSITE de Nice-Sophia Antipolis

Spécialté : PHYSIQUE

Présentée et soutenue par :

Jihad HAMIE

Contributions to Cooperative Localization Techniques within Mobile Wireless Body Area Networks

Thèse dirigée par le Professeur **Cédric RICHARD**
soutenue le 25 novembre 2013 au CEA-Leti (Minatec), Grenoble, France

Jury :

M. Laurent CLAVIER	Pr. Institut Mines Télécom / Télécom Lille 1 (Lille)	*Rapporteur*
M. Bernard UGUEN	Pr. Université Rennes 1 (Rennes)	*Rapporteur*
M. Hichem SNOUSSI	Pr. Université de Technologie de Troyes (Troyes)	*Président & Examinateur*
M. Cédric RICHARD	Pr. Université de Nice - Sophia Antipolis (Nice)	*Directeur de thèse*
M. Benoît DENIS	Dr.-Eng. CEA-Leti Minatec (Grenoble)	*CoDirecteur de thèse*
M. Jean SCHWOERER	Dr.-Eng. Orange Labs (Meylan)	*Examinateur Invité*

THESIS

to obtain the

PhD Degree

from the University of Nice - Sophia Antipolis
Specialty : Physics

by

Jihad HAMIE

Contributions to Cooperative Localization Techniques within Mobile Wireless Body Area Networks

defended at CEA-Leti Minatec, Grenoble, France
on 2013, November 25th

in front of the evaluation jury :

Reviewers :	**Pr. Laurent Clavier** Institut Mines Télécom / Télécom Lille 1 (Lille)
	Pr. Bernard Uguen Université Rennes 1 (Rennes)
President & Examinator :	**Pr. Hichem Snoussi** Université de Technologie de Troyes (Troyes)
Co-Advisors :	**Pr. Cédric Richard** Université de Nice - Sophia Antipolis (Nice)
	Dr.-Eng. Benoît Denis CEA-Leti Minatec (Grenoble)
Invited Examinator :	**Dr.-Eng. Jean Schwoerer** Orange Labs (Meylan)

Abstract

Resumé

Dans le cadre de cette thèse, on se proposait de développer de nouveaux mécanismes de radiolocalisation, permettant de positionner les noeuds de réseaux corporels sans-fil (WBAN) mobiles, en exploitant de manière opportuniste des liens radio coopératifs bas débit à l'échelle d'un même corps (i.e. coopération intra-WBAN), entre réseaux distincts (i.e. coopération inter-WBAN), et/ou vis-à-vis de l'infrastructure environnante. Ces nouvelles fonctions coopératives présentent un intérêt pour des applications telles que la navigation de groupe ou la capture de mouvement à large échelle. Ce sujet d'étude, par essence multidisciplinaire, a permis d'aborder des questions de recherche variées, ayant trait à la modélisation physique (e.g. modélisation spatio-temporelle des métriques de radiolocalisation en situation de mobilité, modélisation de la mobilité groupe...), au développement d'algorithmes adaptés aux observables disponibles (e.g. algorithmes de positionnement coopératifs et distribués, sélection et ordonnancement des liens/mesures entre les noeuds...), aux mécanismes d'accès et de mise en réseau (i.e. en support aux mesures coopératives et au positionnement itératif). Les bénéfices et les limites de certaines de ces fonctions ont été en partie éprouvés expérimentalement, au moyen de plateformes radio réelles. Les différents développements réalisés tenaient compte, autant que possible, des contraintes liées aux standards de communication WBAN émergeants (e.g. Impulse Radio - Ultra Wideband (IR-UWB) IEEE 802.15.6), par exemple en termes de bande fréquentielle ou de taux d'erreur.

Abstract

Wireless Body Area Networks (WBAN), which have been subject to growing research interests for the last past years, start covering unprecedented needs in application fields such as healthcare, security, sports or entertainment. Even more recently, such networks have been considered for new opportunistic and stand-alone radiolocation functionalities. Under mesh or quasi-mesh topologies, mobile on-body nodes can indeed be located within a cooperative fashion, considering peer-to-peer range measurements based on e.g., *Impulse Radio - Ultra Wideband* (IR-UWB) *Time of Arrival* (TOA) estimates or *Narrow-Band* (N-B) *Received Signal Strength Indicators* (RSSI) at 2.4GHz. This radiolocation add-on is viewed as an important enabling feature for coarse but opportunistic and large-scale human *Motion Capture* (MoCap) (e.g. as an alternative to costly and geographically restricted acquisition systems) and/or for robust group navigation applications in practical environments (i.e. under severe non-line of sight conditions).
In this context, the PhD investigations accounted herein aim at exploring new

WBAN cooperative localization mechanisms, which could benefit jointly from on-body links at the body scale (i.e. intra-WBAN cooperation), body-to-body links between distinct mobile users (i.e. inter-WBAN cooperation), or off-body links with respect to the infrastructure. Following a multidisciplinary approach, we have thus addressed theoretical questions related to physical modeling (e.g. space-time correlation of radiolocation metrics, human mobility...) or to algorithmic and cross-layer design (e.g. cooperative localization and tracking algorithms under realistic protocol constraints, links selection and scheduling...). A few more practical aspects have also been dealt with (e.g. post-processing of past measurement campaigns, development of adapted cross-layer simulation tools and field experiments).
More specifically, based on WBAN channel measurements, single-link ranging error models are first discussed for more realistic performance assessment. Then a *Constrained Distributed Weighted Multi-Dimensional Scaling* (CDWMDS) positioning algorithm is put forward for relative MoCap purposes at the body scale, coping with on-body nodes' asynchronism to reduce system latency and exploiting the presence of constant-length radio links for better accuracy. Scheduling and censoring rules are also proposed to limit the influence of harmful peripheral nodes. Subsequently we consider extending this algorithm for larger-scale asbolute MoCap applications within a 2-step localization approach that incorporates additional off-body links in a heterogeneous WBAN framework. Then, both individual and collective kinds of navigation are addressed, comparing a *Non Linear Least Squares* (NLLS) positioning algorithm with a centralized *Extended Kalman Filter* (EKF) tracking filter. In both MoCap and navigation scenarios, low-complexity solutions exploiting on-body deployment diversity enable to combat error propagation and strong range biases due to body shadowing, relying on on-body nodes' dispersion or graph neighbourhood to approximate the corrupted distances. Finally, experiments based on real IR-UWB radio platforms validate in part the previous proposals, while showing their practical limitations.

Keywords

Cooperative Networks, Impulse Radio (IR), IEEE 802.15.6, Localization, Low Data Rate (LDR), Decentralized Algorithms, Medium Access Control (MAC), Narrow-Band Communications, Positioning, Ranging, Ultra-Wide Band (UWB), Wireless Body Area Network (WBAN).

To my friends & my beloved family

Acknowledgment

First of all, I would like to warmly thank Prof. Hichem SNOUSSI for honoring me by accepting to be the chair-man of my thesis committee. Furthermore, I would like to address my sincere gratitude to my thesis reviewers Prof. Bernard UGUEN and Prof. Laurent CLAVIER for their careful reading and review work. My sincere thanks also goe to the thesis examiner Dr. Jean SCHWOERER for his insightful participation in my final defense committee.

A very special thanks goes out to my advisor Prof. Cedric RICHARD, who undertook be my supervisor despite his many other academic and professional commitments. His wisdom, knowledge and advice inspired and motivated me.

Foremost, I would like to express my sincere gratitude to my co-advisor Dr. Benois DENIS for the continuous support of my Ph.D study and research, for his patience, motivation, enthusiasm, and immense knowledge. His guidance helped me in all the time of research and writing of this thesis. I could not have imagined having a better co-advisor and mentor for my Ph.D study.

I thank the head and the people of the DSIS unit at CEA-Leti Minatec, for the confidence and interest they have been putting in my work and for hosting me for 3 years in excellent working conditions.

My thoughts also go to my colleagues from the LESC lab, who are good friends and are always willing to help and give their best suggestions. Many thanks to Mickael MAMAN for being always there to help me.

I'm also grateful to the members of the CORMORAN project's consortium, for their precious and insightful comments, and even more globally, to the ANR INFRA program, which has partly funded the PhD studies accounted herein.

I would also like to thank my parents, my sisters, and elder brother Ali HAMIE. They were always supporting me and encouraging me with their best wishes. Finally, I must acknowledge my best friends, Bassem and Abbas for sharing me all the good and the bad times. I greatly value their friendship and I deeply appreciate their faith in me.

Contents

List of Figures

List of Tables

Acronyms

A-B	Aggregate-and-Broadcast
AWGN	Additive White Gaussian Noise
BP	Belief propagation
BT-LE	Bluetooth - Low Energy
B2B	Body to Body
CAP	Contention Access Period
CDF	Cumulative Density Function
CDWMDS	Constrained Distributed Weighted Multi-Dimensional Scaling
CFP	Contention Free Period
CGN	Coordinated Group Navigation
CH	Cluster Head
CIR	Channel Impulse Response
CM	Channel Model
CRLB	Cramer-Rao Lower Bound
DBPSK	Differential Binary Phase Shift Keying
DOA	Directions Of Arrival
DWMDS	Distributed Weighted Multi-Dimensional Scaling
EEG	Electro-Encephalography
EKF	Extended Kalman Filter
FAP	First Arrival Path
GCS	Global Coordinates System
GDOP	Geometric Dilution Of Precision
GTS	Guaranteed Time Slots
HBC	Humand Body Communications
i.i.d.	identically independent distributed
IMU	Inertial Measurement Unit
INS	Inertial Navigation System
IoT	Internet of Things
IR-UWB	Impulse Radio - Ultra Wideband
KF	Kalman Filter
LCS	Local Coordinates System
LDR	Low Data Rate
LDR-LT	Low Data Rate-Location and Tracking
LLS	Linear Least Square
LOS	Line Of Sight
LSIMC	Large Scale Individual Motion Capture
MAC	Medium Access Control
MAP	Maximum a posteriori
MDS	Multidimensional Scaling
MEMS	Micro Electro-Mechanical Systems

MF	Matched Filtering
MMSE	Minimum Mean Squared Error
ML	Maximum Likelihood
MLL	Maximizes the Log-Likelihood
MoCap	Motion Capture
MPC	Multi Path Components
M2M	Mobile to Mobile
N-B	Narrow-Band
NBP	Non Parametric Belief Propagation
NBP-ST	Non Parametric Belief Propagation over Spanning Trees
NGBP	Non Parametric Generalized Belief Propagation
NLLS	Non Linear Least Squares
NLOS	Non Line Of Sight
PC	Personal Computer
pdf	probability density function
PER	Packet Error Rate
PL	Path Loss
PRF	Pulse Repetition Frequency
QoS	Quality of Service
RMSE	Root Mean Squared Error
RPGM	Reference Point Group Mobility Model
RSSI	Received Signal Strength Indicator
RTLS	Real Time Location Systems
RT-TOF	Round Trip - Time of Flight
SMACOF	Scaling by MAjorizing a COnvex Function
SNR	Signal to Noise Ratio
SPA	Self Positioning Algorithm
SRRC	Square-root Raised Cosine
TDMA	Time Division Multiple Access
TDOA	Time Difference of Arrival
TOA	Time Of Arrival
TOF	Time of Flight
TP-NBP	Two Phase - Non Parametric Belief Propagation
TRW-BP	Tree-Reweighted Belief Propagation
TS	Time Slot
ULP	Ultra Low Power
UWB	Ultra-Wideband
WBAN	Wireless Body Area Network
WLS	Weighted Least Squares
WSN	Wireless Sensor Network
2-WR	2-Way Ranging
3-WR	3-Way Ranging

Chapter 1

General Introduction

Contents

1.1 Location-Based Body-Centric Applications and Needs

The recent development of sensing and short-range communication integrated technologies has been disclosing interesting perspectives for mobile, personal and body-centric applications or services. More particularly, the *Wireless Body Area Networks* (WBANs), which consist of small and low-power wearable wireless devices, are on the verge of fulfilling new market needs in a variety of application fields such as emergency and rescue (e.g. remote posture detection for institutional rescuers or victims), healthcare (e.g. physiological or activity monitoring, wireless medical actuators and implants, assistance to medical diagnosis, lab-on-chip chemical analysis), entertainment (e.g. motion capture for gaming or sports analysis), personal communications and multimedia (e.g. distributed terminals, personal consumer electronics), clothing applications (e.g. garments with electronic components, smart shoes) [14], [15] (See Figure 1.1). On the one hand, WBANs rely on emerging radio technologies that claim *Ultra Low Power* (ULP) consumption, low complexity, and low cost, such as *Narrow-Band* (N-B) solutions at 2.4 GHz based on e.g., *Bluetooth - Low Energy* (BT-LE), or *Impulse Radio - Ultra Wideband* (IR-UWB) solutions, as put forward in the recent IEEE 802.15.6 standard dedicated to WBAN applications [4], [11]. On the other hand, WBAN nodes usually embed extremely low-power sensors and actuators based on e.g., *Micro Electro-Mechanical Systems* (MEMS) or even further

energy scavenging systems for power autonomy. In the near future, such wearable systems could drastically change our daily life, by participating as local (but core) building components and key contributors into the *Internet of Things* (IoT). People disseminated in the crowd with their own personal WBAN could play a significant role in cooperative and heterogeneous communication networks, by serving as distributed pieces of the overall architecture skeleton [16] (See Figures 1.2 and 1.3).

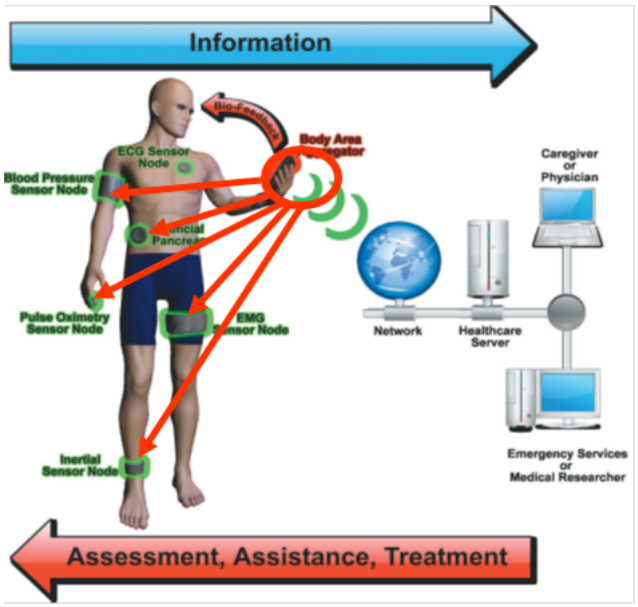

Figure 1.1: Typical WBAN deployment for medical and healthcare applications [1].

Figure 1.2: WBAN integrated in cooperative and heterogeneous networks, as a core building block of the future daily-life Internet of Things (IoT).

Figure 1.3: Cooperative WBANs interacting within their local environment (including other WBANs), enabling new site-/context-specific applications for smarter cities/homes and augmented nomadic social networking.

Besides simple WBAN considerations, numerous location-dependent services have also been appearing for the last past years, such as pedestrian navigation in indoor environments or urban canyons, location-dependent commercial offers or contextual information broadcast, assisted mobility in dangerous and/or confined environments. One common requirement is to bring high-precision location information into unaddressed applicative environments where classical satellite-based solutions can not operate properly. Many of those services are intrinsically user-centric, in the sense the location information would be required on the end-user side, possibly with decentralized resources and a limited access to the infrastructure. Among the proposed technological solutions providing such location and tracking capabilities on top of standard communication means at medium ranges, *Low Data Rate* (LDR) ULP radio technologies, very similar to that considered in the WBAN context actually, are favoured today, such as IR-UWB (e.g. IEEE 802.15.4a standard) or, more marginally, Zigbee (e.g. IEEE 802.15.4 standard).

Finally, there is also a growing interest today in acquiring the human motion and gesture at variable degrees of precision, but with non-intrusive, very low-cost, low-complexity and stand-alone technologies, as an alternative to the relatively cumbersome, geographically restricted and specific means used so far (e.g. video solutions used by professionals in the domain of motion capture). This may be particularly useful either for mass-market or more confidential applications including e.g., coarse gesture-based remote control necessitating relaxed accuracy.

In this context, the CORMORAN project, which was recently funded by the French National Research Agency (ANR 11-INFR-010) and started in 2012, aims at studying and developing solutions that could benefit from cooperation within groups of mobile WBANs, with the twofold objectives of making available new localization functions and enhancing globally the quality of the wireless communication service. Overall, fusing cooperative short-range communications *in* and *between* WBANs with radiolocation capabilities could indeed enable to cover unaddressed (or at least

still hardly addressed) applications, such as:

- augmented group navigation (e.g. fire-fighters progressing in a building on fire with physiological monitoring and relative position information, coordinated squads of soldiers on urban battle-fields);
- low-cost and infrastructure-free tracking of collective systems (e.g. real-time capture and/or sports analysis);
- nomadic social networking (e.g. sharing personal location-dependent information in a decentralized way among authorized members of a given community);
- augmented reality for collective entertainment (e.g. in mobile and interactive group gaming);
- context-dependent information diffusion (e.g. data broadcast to identified clusters of people with common interests, needs or locations);
- wireless network optimization (e.g. handover between different radio access technologies for clusters of people experiencing the same mobility patterns, optimal data routing under users mobility);
- distant health care, monitoring and rescue systems (e.g. collective launching or notification of emergency alarms, routine medical treatments at home);
- smart homes and personal multimedia (e.g. house automation, smart HiFi or eased screen browsing through coarse body capture).

As a preliminary step of the investigations carried out in the frame of COR-MORAN, the project's partners disseminated a questionnaire to professional entities, identified as possible users and/or integrators of this technology in various activity domains. The idea was to identify their actual needs and technical requirements, as well as to draw preliminary system specifications in terms of e.g., sensors/body location precision and refreshment rates, number of sensors/users and related deployment constraints, typical mobility, operating environments, calibration needs... The analysis of their feedback confirms that the most representative application scenarios could be classified into two main categories, namely the *Large Scale Individual Motion Capture* (LSIMC) and the *Coordinated Group Navigation* (CGN), as summarized in Figure 1.4.

The first feature is somehow identical to traditional *Motion Capture* (MoCap), which requires a rather high level of accuracy while locating the sensors at the body scale (most likely at high refreshment rates), but the new aim here is to provide stand-alone and larger-scale solutions (e.g. extending the service coverage in comparison with existing systems, which may be restricted into confined areas) with a limited access to fixed and costly elements of infrastructure around (i.e. fixed access points, base stations or wireless anchors). Note that depending on the underlying applications, this motion capture functionality can be intended either as relative on-body nodes localization (i.e. positioning on-body devices in a local body-strapped

	Large-Scale Individual Motion Capture		Coordinated Group Navigation
	Low Precision	High Precision	
On-Body Nodes Location Precision (Relative)	$\varepsilon_{90} < 25$ cm (worst case CDF @ 90%) $\varepsilon_{50} \approx 5$ cm (median CDF @ 50%)	$\varepsilon_{90} < 5$ cm (worst case CDF @ 90%) $\varepsilon_{50} \approx 1$ cm (median CDF @ 50%)	N/A
Average Body Location Precision (Absolute)	$\varepsilon_{90} < 1$ m (worst case CDF @ 90%) $\varepsilon_{50} \approx 0.3$ m (median CDF @ 50%)		
Nodes Location Refreshment Rate	100 ms	10 ms	1s
Maximum Speed	{5, 15} km.h^{-1}		
Anchors Density	< 0.05 anchors / m^2		< 0.01 anchors / m^2
Nb Persons per Group	N/A		{5, 10}
Maximum Inter-Body Distances	N/A		{1, 5, 10, 50}
Nb of On-Body Nodes	{5, 10, 20}		{2, 5}
Rank of Preferred On-Body Nodes Location	**An-He-Wr-To-Hi-Lg-Ba-Sh-Kn-Bd**		**Sh-To-Ba-Hi-Wr**
Environment	{Outdoor, Indoor}		Indoor
Place for Final Location Info	{Server, User}		User
Pre-Calibration (Deployment Convention to be Respected)	{None, Precise Deployment Pattern}		{None, Rough Deployment Pattern}

Figure 1.4: Technical needs and requirements for large-scale individual motion capture (in low and high precision modes) and group navigation applications, according to the CORMORAN project (where An: Ankles, He: Head, Wr: Wrist, To: Torso, Hi: Hips, Lg: Legs, Ba: Back, Sh: Shoulders, Kn: Knees, Bd: Bends stand for possible sensors' locations).

coordinates system) or absolute on-body localization (i.e. positioning on-body devices in a more global system, external to the carrying body, typically at the building or floor scale). The second set of applications, which is not necessarily coupled with the first motion capture functionalities, corresponds to classical pedestrian navigation applications (i.e. intended in a rather classical way) with relaxed positional accuracy (most likely at moderate refreshment rates) but within groups of mobile users, aiming at benefiting from their collective behaviour.

In the next sub-section, we make a brief overview of enabling on-body localization technologies and techniques (including radio solutions) that could fit into this context, trying to summarize their respective advantages and limitations.

1.2 Enabling On-Body Localization Technologies and Techniques

1.2.1 Optical Systems

Most optical systems are based on illuminated and reflective markers placed on the body [17], [10]. The localization of any on-body marker necessitates that the latter is viewed by at least two external cameras, which have known positions and orientations [18]. Figure 1.5 shows an example of typical operating scenario and deployment.
Such optical tracking systems are generally characterized by high localization accuracy (i.e. with an error of some millimeters) and they are able to support real-time MoCap and/or navigation applications (i.e. with neglected latency). However, they have limitations that may prevent from considering them in the very context, such as cost, complexity or the necessity to operate in geographically restricted and closed areas (i.e. with the test subject moving in this area). They also suffer from non-visibility problems, when the markers cannot be viewed by the surrounding cameras in cases of obstructions and/or obscurity conditions, and thus, the achieved accuracy can be affected accordingly.

1.2.2 Inertial Systems

The most common sensors used within *Inertial Measurement Units* (IMUs) for the localization of on-body devices are the accelerometers and the gyroscopes [19]. Those systems can achieve localization errors of a few centimeters [20], [21], what can be acceptable for MoCap purposes. They are usually characterized by their low cost and their relatively low complexity. Besides the interest for those sensors in the frame of MoCap applications, they have been also considered in *Inertial Navigation Systems* (INSs), for instance for pedestrian tracking and dead reckoning, delivering information related to the displacement amplitude, velocity, or heading [22], [23], [24]. Unfortunately, the used sensors are usually affected by significant drifts over time [20], which necessitate frequent periodic calibrations.

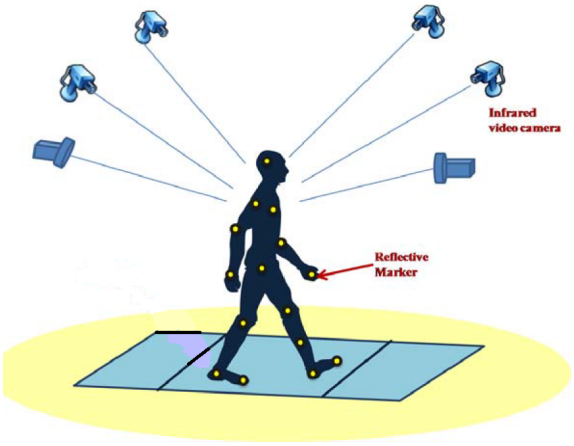

Figure 1.5: Example of typical scenario and system deployment for on-body optical tracking (e.g. based on the Infra-Red technology) [2].

1.2.3 Magnetic Systems

Magnetic systems are based on the measurements of the earth-magnetic fields measured by receivers, which can be also placed on the body [25]. Moreover, they can be based on the magnetic fields between on-body receivers and magnetic emitters placed at known positions in the localization area [26]. Those systems, which are also characterized by low cost and low complexity, could potentially enable real-time and accurate MoCap and/or navigation. However, field sensing is traditionally subject to strong disturbances due to the presence of metallic pieces in the vicinity of on-body sensors (e.g. embedded in clothes or in pieces of furniture). Finally, those disturbances can significantly degrade the localization accuracy in most of practical application environments, making this technology likely inadequate for standard non-controlled MoCap and/or navigation purposes.

1.2.4 Mechanical Systems

These systems can be based on mechanical joints placed on the body articulations in order to determine their respective rotations during the body movement. [27] provides for instance the MoCap functionality based on the combination of such mechanical and ultrasound systems. Unfortunately, those systems are not really popular in the very context due to the limited proportion of people who would accept to be equipped and potentially disturbed in their body movements. Moreover, they could hardly be used as a standalone solution for MoCap applications at the body scale (i.e. without performing data fusion with other systems).

1.2.5 Ultrasound Systems

Ultrasound on-body localization systems involve emitters placed on the body and microphones placed at known positions in the environment [27], [28], relying on the signal *Time of Flight*(TOF). However, those systems can be rather strongly affected by the interference caused by ultrasound waves transmitted from different emitters, in addition to echo effects in practical environments [29]. Those factors conduct to damage dramatically the localization performances. Note that ultrasonic TOF and inertial measurements can also be combined in the garment of wearable systems for better robustness in MoCap applications, like in [30], but at the price of much higher system and processing complexity.

1.2.6 Radio Systems

Rather similarly to ultrasound approaches, the wireless localization functionality in radiolocation systems typically relies on the analysis of radio signals transmitted with respect to multiple anchors and/or to other mobile devices (See Figure 1.6). Location-dependent radio metrics can thus be estimated over these radio links, such as the *Time Of Arrival* (TOA) of the transmitted signal or, one step ahead, the *Round Trip - Time of Flight* (RT-TOF) through handshake protocols, the *Time Difference of Arrival* (TDOA), which can be formed out of TOA estimates at synchronized receivers, or more simply the *Received Signal Strength Indicator* (RSSI), which is based on the distance-dependent average power loss. For instance, in case of RT-TOF based on TOA estimation over IR-UWB links or *Received Signal Strength Indicators* (RSSI) over N-B links, the measured metrics can directly reflect peer-to-peer ranges between radio devices. These measurements then subsequently feed positioning or tracking algorithms to deliver the coordinates of mobile nodes in a given reference system. Most of the radiolocation solutions so far have been considered for medium/large-range applications such as logistics based on asymetric *Real Time Location Systems* (RTLS) or indoor personal navigation [31], but very marginally in WBANs. However, Figure 1.6 shows an example of typical scenario and system deployment for on-body radio tracking, which could be applied in a WBAN-oriented context (e.g. with an external acquisition infrastructure).

The final positional precision is obviously related to the level of ranging precision over unitary single links. Hence, as a preliminary step of our discussions, it is worth assessing the very potential in terms of ranging capabilities (and more precisely, the expected theoretical ranging precision) of different radio technologies foreseen in our WBAN context.

For radio signals propagating at celerity c, the distance between a transmitter and a receiver is straightforwardly given by the product of the *Time Of Flight* (TOF) and c. In an ideal synchronous case, the TOF, so defined as the elapsed time for propagating the radio signal from the transmitter to the receiver, would be simply given by:

$$TOF_i = t_i - t_0 \tag{1.1}$$

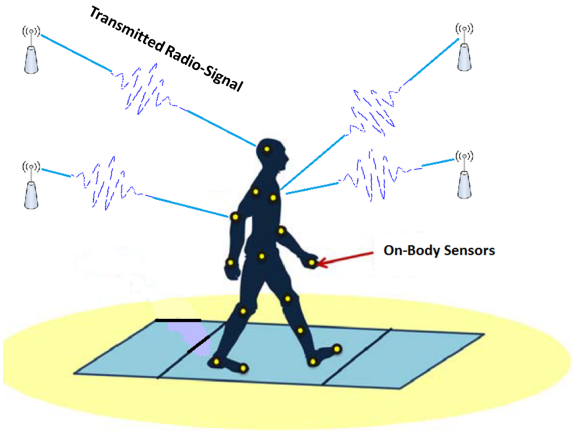

Figure 1.6: Example of typical scenario and system deployment for on-body radio tracking (e.g. with an external infrastructure).

where t_0 is the time instant at which the transmitter starts transmitting and t_i is the TOA at the receiver, estimated locally in the observation window and defined according to the local timeline (i.e. to the embedded clock).

If the transmitter and the receiver were perfectly synchronized (and thus, if t_0 was known at the receiver), then the distance could theoretically be obtained from the estimated TOA, what is however rarely the case in real systems, by nature asynchronous. For such temporal radiolocation metrics, in addition to TOA estimation accuracy, a few more challenges are indeed related to asynchronism effects among the involved devices. Some ranging protocols have thus been proposed in order to mitigate the harmful effects of synchronization errors and clock drifts, without necessitating hardware modifications and without implementing clock tracking/tuning. Those protocols consist in computing the RT-TOF, relying on e.g., *2-Way Ranging* (2-WR) or *3-Way Ranging* (3-WR) cooperative protocol transactions (i.e. exchanging packets) and unitary TOA estimates associated with the transmitted packets [32]. Only two transmissions are involved in 2-WR to remove possible clock offsets and provide peer-to-peer range measurements between two devices. One device sends a request packet first. While receiving this packet, the second node estimates its TOA and sends a response packet back to the requesting node after a known delay. The first node will receive this response after a while and will estimate its TOA as well. Finally, based on the initial transmission time, on both TOA estimates and on the known response delay, the first node can easily compute the RT-TOF. But the latter measurement can still be biased by relative clock drifts, depending on the response delay and on the respective clock precisions. Then one gradual enhancement to the 2-WR protocols leading to the 3-WR protocol consists in asking the responder device to transmit one additional packet a certain amount of time (also known in advance) after the response, so that the first requesting node estimates

and compensates for relative clock drifts out of row RT-TOF measurements. All in all, it is however also demonstrated in [33] that, as a result of such compensations, the high-level statistics (typically, the conditional bias and standard deviation) of the final error committed on corrected RT-TOF measurements is a predictable function of (and also on the same order of) the error statistics affecting unitary TOA estimates, which mostly depend on time resolution (i.e. the capability to identify and detect the first observable path in case of dense multipath, and more particularly at low SNR) and time precision (i.e. the capability to account precisely on a local timescale for a particular detection or transmission event). As an example, a simple timing error of 1 ns can lead to a distance error of 30 cm. Thus in first approximation, while illustrating the trends in terms of expected ranging precision, we will focus hereafter on TOA estimation performance only (instead of considering the full RT-TOF scheme).

In an IR-UWB context, we assume for simplicity that the transmitted waveform corresponds to a mono-pulse affected by *Additive White Gaussian Noise* (AWGN). Hence, [3] shows that the best standard deviation achieved by any unbiased TOA estimator, for instance based on *Maximum Likelihood* (ML) estimation through *Matched Filtering* (MF) and peak detection, is inversely proportional to the occupied bandwidth and bounded by

$$\sqrt{var(\hat{TOA})} = \frac{1}{2\sqrt{2}\pi\sqrt{SNR}\beta} \tag{1.2}$$

where SNR is the *Signal to Noise Ratio* and β is the effective signal bandwidth, defined as follows:

$$\beta = \sqrt{\left[\frac{\int_{-\infty}^{+\infty} f^2|S(f)|^2 df}{\int_{-\infty}^{+\infty} |S(f)|^2 df}\right]} \tag{1.3}$$

where S is the Fourier transform of the transmitted signal.
Accordingly, as shown in Figure 1.7, in the absence of further precision regarding the available processing gains (e.g. through the coherent integration of repeated pulses sequences), and considering the standard SNR levels expected for typical on-body links (i.e. at SNR<0dB), a bandwidth on the order of 1GHz (resp. 500MHz) would be for instance required for ranging precisions on the order of 5 cm (resp. 10 cm) at -5 dB. But of course, in more practical cases, one can expect that the accuracy is even more degraded due to the conjunction of multipath effects, body obstructions and receiver hardware capabilities. Note that other temporal radiolocation metrics inheriting from preliminary TOA estimation (i.e. RT-TOF or TDOA) will be influenced similarly by the occupied bandwidth. Hence, the IR-UWB technology, which relies on the transmission of short pulses whose durations are on the order of a few nanoseconds (i.e. occupying bandwidths larger than 500 MHz), is characterized by fine temporal resolution capabilities [3], [34], providing fine accuracy for TOA estimation. Thus, it is clearly encouraged for accurate range measurements between on-body devices in the general WBAN context (i.e. belonging to the same WBAN or even to neighboring WBANs), especially when considering the "WBAN scaling

factor" in comparison with more classical medium-range localization applications, in terms of both the required transmission ranges and relative levels of precision. Furthermore, it is worth recalling that the recent IEEE 802.15.6 radio standard issued for WBAN applications also promotes IR-UWB as a relevant low power physical layer for communication purposes [11]. As for RSSI-based ranging in N-B radio

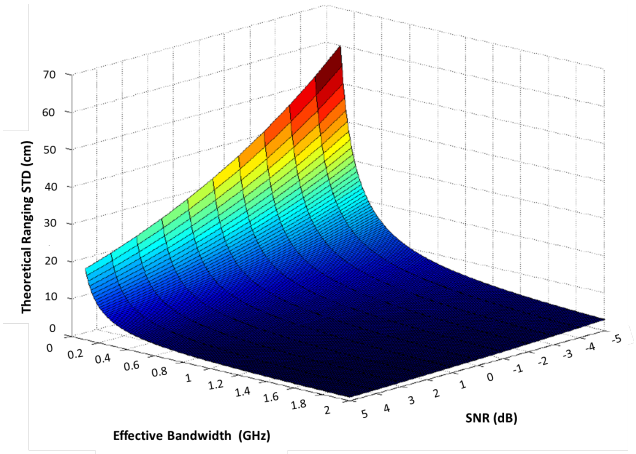

Figure 1.7: Best achievable single-link TOA-based ranging standard deviation, as a function of the effective signal bandwidth and signal to noise ratio, assuming a mono-pulse AWGN scenario [3].

systems, one simply uses the fact that the average received power decreases with the distance separating the transmitting and receiving devices, by a predictable and deterministic amount. A measure of the received power can be easily obtained without additional hardware complexity at most of existing communication radio devices. However, a *Path Loss* (PL) model is needed, along with its parameters. Assuming for simplicity that the WBAN's RSSI model is somehow similar to the most frequently cited model from [35] for indoor scenarios, one can write:

$$P_r(d) = P_0 - 10 n_p log_{10} d + \varepsilon \tag{1.4}$$

where $P_r(d)$ (in dB) is the RSSI value at a distance d, P_0 is the average RSSI value at a reference distance 1 m, n_p is the PL exponent, and ε is considered as a centered Gaussian random variable of variance σ_{sh}^2 that represents the large scale fading or shadowing.
Hence, relying on equation (1.4), and similarly to TOA, a theoretical lower bound for the standard deviation of unbiased RSSI-based range estimators can be derived as follows [3]:

$$\sqrt{var(\hat{d})} = \frac{log(10)}{10} \frac{\sigma_{sh}}{n_p} d \tag{1.5}$$

First of all, the occupied bandwidth will obviously play a role with respect to small-scale fading. However, it is common to assume within RSSI-based localization that

those effects are somehow averaged (e.g. based on consecutive RSSI measurements within the channel coherence time over one link). Furthermore, in the classical modeling presented above, the best achievable ranging performance would theoretically depend on both the channel power parameters (i.e. path loss exponent and shadowing deviation) and the distance between the two nodes. But it is adversely well known in the on-body WBAN context that: (i) the received power is less dependent on the actual distance than in any other wireless context, (ii) body shadowing is rather strong (in comparison with the nominal average received power levels), far dominating (in comparison with other effects due to e.g. small-scale fading or distance) and hardly predictable with no a priori information (e.g. highly variable as a function of the actual nodes places on the body). Overall, the achievable level of ranging precision is not only hard to predict or specify a priori over on-body links, but it is likely insufficient in comparison with the actual nominal Euclidean distances to be measured (say, on the order of one meter). Figure 1.8 shows the variations of this best achievable single-link RSSI-based ranging standard deviation, as a function of both the actual distance and the shadowing standard deviation, while assuming a path loss exponent equal to $n_p = 2$ for simplification. Hence, for a given $\sigma_{sh} = 2$, the lower standard deviation is about 23.03 cm at $d = 1$ m. This range of inaccuracy can strongly damage the on-body ranging functionality, making it hardly compliant (not to say, most likely irrelevant) with MoCap applications. However, note that RSSI shall still be useful in this on-body context, as an indirect source of information (e.g. for mitigating ambiguities), but it would be mostly meaningful over larger-range off-body and body-to-body links and in case of relatively low shadowing standard deviation (i.e. in comparison with the path loss exponent).
The previous trends have also been confirmed in [36] with joint UWB and N-B experimentations conducted in a realistic indoor environment (i.e. including typically radio obstructions and dense multipath) and in a health monitoring context based on medical WBAN. On this occasion, the ranging performances of both the IEEE 802.15.4 and the IEEE 802.15.4a standards are benchmarked, based respectively on RT-TOF measurements using integrated UWB prototypes and RSSI measurements using commercially available standard-compliant components at 2.4GHz.

One way to improve significantly the performance of wireless localization systems (especially in case of generalized radio obstructions and/or poor geometric dilution of precision) is to rely on hybrid solutions. For instance, in MoCap applications or less marginally for navigation applications, inertial measurements have already been considered on top of IR-UWB TOA in [37], [38], specific optimization-based combinations of TOA in [39], IR-UWB TDOA and AOA in [40] and [41], or even N-B RSSI fingerprints in [42]. Nevertheless, those solutions impose the use of too specific settings, system architectures, and fusion strategies. They can not either comply with a generic and opportunistic WBAN usage, since such wearable networks do not necessarily include IMUs as on-body sensors depending on the underlying application. Finally, they are expected to be more expensive and to suffer from much higher complexity and higher energy consumption.

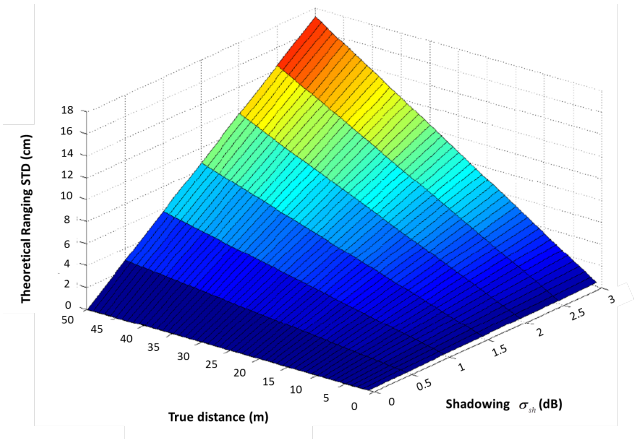

Figure 1.8: Best achievable single link RSSI-based ranging standard deviation, as a function of the actual distance and shadowing parameter (assuming a path loss exponent equal to 2).

1.3 Problem Statement, Open Issues and Personal Contributions

One major disruptive concept in modern short-range wireless communications concerns *Mobile to Mobile* (M2M) cooperation, allowing moving nodes or terminals to exchange data through peer-to-peer links. So at the origin of this PhD work one motivating intuition was that fusing cooperative short-range communications and radiolocation capabilities could be beneficial within mobile groups of interacting WBANs. First of all, at the body scale, the intrinsic cooperation possibilities offered by mesh network topologies are most often underexploited in WBANs but star or tree topologies are preferred, for being adapted to low-consumption data-oriented applications. Then, WBANs are expected to be massively present in public areas in the near future (e.g. streets, shopping malls, train stations), where direct *Body to Body* (B2B) interactions and heterogeneous network access are likely to offer the highest and most promising potential in terms of cooperation. Typically locational affinity awareness would be helpful to various WBAN-based applications. In addition, the predicted massive deployment of personal wearable networks could offer intrinsic cooperation availability in most practical environments. As already pointed out, a growing attention is also paid today to user-centric and context-aware applications, which could be explicitly covered and benefit from cooperative location-enabled WBANs. Moreover, very similar short-range LDR ULP radio technologies (i.e. IR-UWB or Zigbee) have been considered in WBANs and location-enabled WSNs so far, offering common ground for fine synergies to be exploited in the near future. Finally, from a general localization-oriented perspective, cooperation is expected to provide information redundancy and spatial diversity to enable better service coverage, as well as higher precision and robustness [43].

In the restrictive WBAN context of interest, M2M cooperative schemes can be intended and applied in various forms: either within one single wearable network (i.e. providing intra-WBAN/on-body cooperation in the case of mesh networking), between distinct wearable networks at reasonably short transmission range (i.e. providing inter-WBAN/body-to-body cooperation), or even with respect to elements of infrastructure (i.e. providing so-called off-body cooperation). Figure 1.9 shows the different kinds of cooperative links that could be involved in the very WBAN context for location-based body-centric purposes. Trivially, over each physical link, the measurement of location-dependent radio metrics for localization purposes (e.g. TOF, RSSI, TDOA, etc.) necessitates underlying communication capabilities (i.e. wireless transmissions of data packets). Nevertheless, note that some of the involved links may be exploited just for communication purposes, without performing any measurement but to transit information related to the localization functionality, such as intermediary estimated positions (or estimated accuracies) in a decentralized embodiment. Assuming heterogeneous network embodiments, the intra-WBAN communication and localization functions could be ensured either through IR-UWB (e.g. extended IEEE 802.15.6) or N-B communications at 2.4GHz (e.g. BT-LE) (respectively with RT-TOF estimation or on RSSI measurements for the latter function). As for inter-WBAN (body-to-body) and off-body links, one could rely on IR-UWB (e.g. extended from IEEE 802.15.4a) or N-B communications at 2.4GHz (e.g. Zigbee).

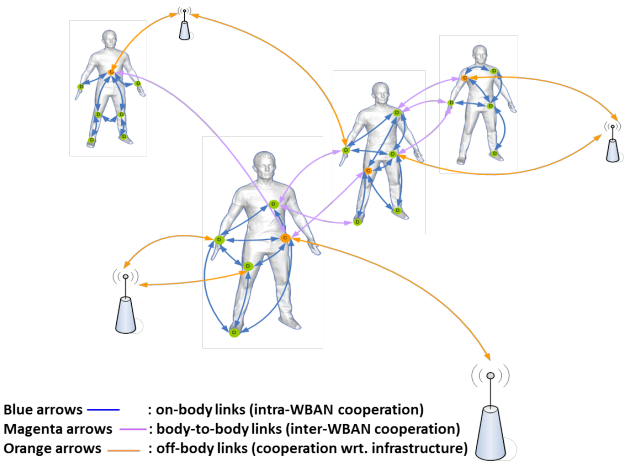

Figure 1.9: Generic cooperative WBAN deployment, with ultra short-range intra-WBAN links (blue), medium-range inter-WBAN links (magenta), and large-range off-body links (orange) for motion capture and navigation purposes.

Thus the main initial goal of these PhD investigations was to determine *if* and *to which extent* it could be relevant to exploit the three possible levels of WBAN cooperation so as to localize:

- on-body nodes at the body scale and/or at the building scale (i.e. for coarse

individual MoCap applications);

- carrying bodies belonging to a group at the building scale (i.e. for coordinated group navigation applications).

Regarding *large-scale individual motion capture* (LSIMC) needs, both relative or absolute on-body nodes positioning can be performed, depending on the targeted use cases.

For relative positioning, we consider a set of wireless devices placed on a body, which can be classified into two categories. Simple mobile (or blind) nodes with unknown positions (under arbitrary deployment) must be located relatively to reference anchor nodes, which are attached onto the body at known and reproducible positions, independently of the body attitude and/or direction (e.g. on the chest or on the back). A set of such anchors can thus define a Cartesian *Local Coordinates System* (LCS), which remains time-invariant (i.e. when expressed in the LCS) under body mobility. The estimated coordinates of the mobile nodes are then expressed into this LCS. This functionality is also occasionally depicted as *Nodes positioning at the body scale*. Possible use cases concern e.g., WBAN optimization through distance-based packet routing, WBAN self-calibration, raw gesture or posture detection for animation (e.g. gaming, augmented reality, video post-production), emergency and rescue alerts (e.g. elderly people or firefighters falling down on the floor), coarse attitude/body-based remote sensing (e.g. house automation, remote multimedia browsing and control).

As for absolute on-body nodes positioning, the considered scenario is the same as the relative one, but the coordinates system used to express the estimated on-body mobile nodes locations is no more body-strapped but external to the body. In this framework, one may thus consider as anchor nodes, some fixed elements of infrastructure (e.g. beacons/landmarks, base stations, access points or gateways) disseminated at known locations in the environment. Accordingly, the coordinates of the nodes placed on the body chest or back, which used to be time-invariant in their LCS, shall now vary in a *Global Coordinates System* (GCS) under pedestrian mobility. They directly depend on the body attitude, as well as on the motion direction and/or speed. This sub-scenario may be viewed as a combination of relative motion capture (i.e. at the body scale) and classical single-user navigation capabilities. Finally, defining the on-body nodes locations into a LCS may be still required here, as an intermediary step of the calculations. Possible use cases concern on-field sports gesture live capture and analysis, physical activity monitoring at home for non-intrusive and long-term physical rehabilitation or diet assistance.

Like in the LSIMC case, concerning *Coordinated Group Navigation* (CGN), both absolute and relative positioning are theoretically possible, although the latter is seen as less relevant.

For relative positioning, people wearing several on-body wireless sensors and forming a group of mobile users must uniquely localize themselves with respect to their mates. The inter-body range information is required, that is to say, only the relative group topology, independently of the actual locations (and orientations) in the

room or in a building. Accordingly, no external anchor nodes would be required in this embodiment. Possible use cases concern the relative deployment of soldiers or fire-fighters, people finding in nomadic social networks, proximity detection or collision avoidance in confined, blind or dangerous environments (e.g. for security, collective gaming).
Finally, the absolute positioning of moving bodies forming a group is intended in a more classical pedestrian navigation sense, where one must retrieve the absolute coordinates of several users belonging to the same mobile collective entity, with respect to an external GCS. This shall imply the use of fixed and known elements of infrastructure around. In comparison with other State-of-the-Art navigation solutions, the presence of multiple wearable on-body nodes (i.e. in the WBAN context) is expected to enhance navigation performance by providing spatial diversity and measurements redundancy (i.e. over off-body links with respect to the infrastructure and/or over inter-WBAN/body-to-body links with respect to other mobile neighbours), and possibly, further cooperative on-body information exchanges (i.e. through intra-WBAN links). Without loss of generality, this navigation-oriented scenario will aim at retrieving mostly the macroscopic positions of the bodies, but not the on-body nodes' locations in details. Hence, a reference point on the body shall be chosen to account for this average position (e.g. the geometric center of the body torso or the barycenter of all the on-body nodes). Possible use cases concern the absolute deployment of soldiers or fire-fighters in a given building, the analysis of social mobility patterns and habits in commercial centers, enhanced and/or augmented personal pedestrian navigation capabilities.

One a priori constraint imposed deliberately to our study is to rely uniquely on transmitted radio signals that would be anyway present in data-oriented WBAN contexts, that is to say, with no additional embedded sensors. One more originality of this work lies in the definition of positioning and tracking algorithms that could be operating:

- in an opportunistic, stand-alone and energy-friendly mode for daily-life and perennial usage;
- with no or limited geographic restrictions for a truly seamless and large-scale service coverage (i.e. contrarily to video systems in MoCap and/or GPS in navigation);
- with limited access to costly elements of infrastructure;
- with reasonably degraded precision in comparison with more accurate technologies (i.e. as a tolerated drawback).

The block diagram represented in Figure 1.10 shows a generic wireless localization scheme adapted to our WBAN context, where one can easily see the critical impact of both the dynamic propagation channel (i.e. under body mobility) and the protocol strategy (e.g. in terms of scheduling, response delays...) on the quality and availability of single-link measurements and in turn, on localization performance.

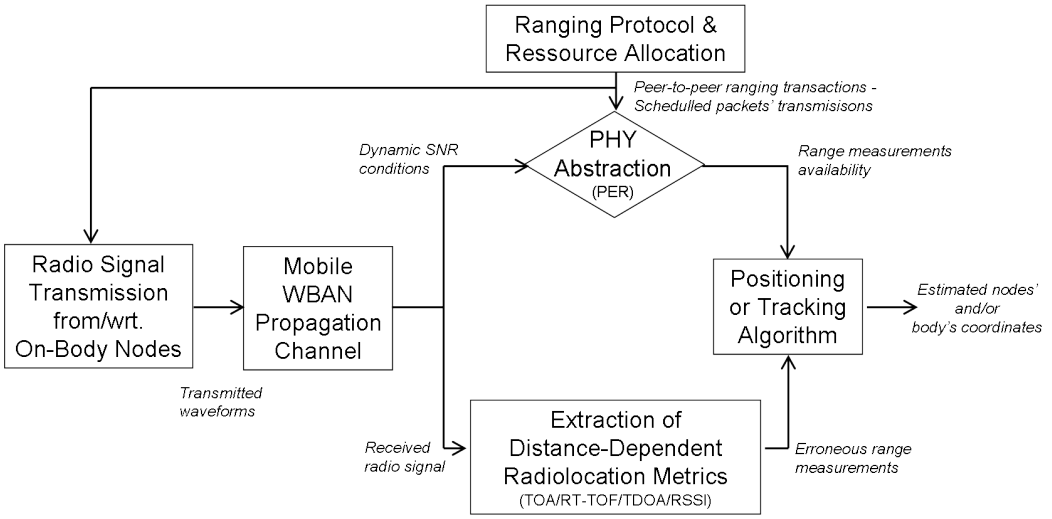

Figure 1.10: Typical localization scheme in WBAN context.

The proposed PhD topic, as stated below, is by nature multidisciplinary. It imposes to deal with various research domains, related to modeling aspects (e.g. physical layer abstraction including spatio-temporal variations of the propagation channel and radiolocation metrics under mobility, biomechanical and social human mobility, etc.), to algorithmic developments (e.g. cooperative positioning and tracking algorithms, links selection and scheduling, etc.), as well as to medium access and networking mechanisms (e.g. as a support to cooperative measurements and location updates). More precisely, several research issues, involving key building blocks of Figure 1.10, are still open or hardly explored today, such as:

- Assessing the actual impact of the physical layer on single-link ranging and final localization performances, including the evaluation of harmful propagation channel variations between on-body devices (conditioned on biomechanical and macroscopic body mobility);
- Evaluating the effects of latency introduced by communication protocols on localization performance, emphasizing the needs for cross-layer design approaches;
- Designing new positioning and tracking algorithms that can take into account the main WBAN constraints and characteristics, in terms of e.g., low complexity, reduced transmission ranges, body shadowing, and highly specific mobility pattern;

At this point, the main personal contributions issued in the frame of our PhD investigations can be summarized as follows:

- Modeling: The dynamic behaviour of IR-UWB TOA-based ranging error processes has been assessed and a realistic model has been proposed, relying on

time-variant channel measurements in representative frequency bands. This model can take into account the dynamic variations of the *Signal to Noise Ratio* (SNR) and the channel obstruction conditions, i.e. *Line Of Sight* (LOS) and *Non LOS* (NLOS), experienced over representative on-body links while walking. This contribution has led to the publication of one conference paper [44] and one journal paper [45].

- Design of localization algorithms:
  - Relative on-body positioning: We have considered adapting and enhancing a distributed localization algorithm into the new WBAN context. The nodes locations are asynchronously updated with respect to their 1-hop neighbors into a body-strapped LCS, providing better immunity against the latency effects observed within classical centralized schemes and better adaptability to local nodes velocities (e.g. in terms of refreshment rate). Among all the radio links available in a mesh topology, those that experience fixed lengths despite body mobility (e.g. between the hand's wrist and the elbow) are set as self-learnt (or a priori) geometrical constraints, limiting the number of required on-line measurements and hence, reducing the amount of over-the-air traffic and power consumption. This contribution has led to the publication of one conference paper [46]. New scheduling and censoring rules have also been proposed to prevent from error propagation among cooperative nodes, by limiting the impact of the most penalizing nodes at the body periphery. This contribution has led to the publication of one more conference paper [47]. Assuming realistic UWB TOA-based ranging error magnitudes derived from the first cited contribution, as well as realistic medium access constraints, the performance of this algorithm has been evaluated and compared with state-of-the-art solutions and theoretical bounds through simulations. This contribution has led to the publication of one journal paper [48].
  - Absolute on-body positioning: The previous algorithm has been extended within a global 2-step localization approach adapted to heterogeneous WBAN networks (i.e. considering multiple radio access technologies), incorporating also off-body links with respect to fixed infrastructure anchors. Further graph completion techniques have been applied to combat packet losses and/or body shadowing effects. One outcome is to enable absolute on-body nodes positioning at the building scale but with similar precision levels as that of relative on-body positioning at the body scale (i.e. reconciling motion capture and personal navigation). This contribution has led to the publication of one conference paper [49].
  - Absolute body positioning in groups of mobile users: New algorithms have been proposed to take benefits from body-to-body links and on-

body devices diversity under realistic collective mobility conditions. These solutions have also been evaluated through realistic simulations;

- Experiments: Field experiments based on real on-body IR-UWB devices have been carried out to partly validate the previous contributions (though focusing mostly on the LSIMC application).

The remainder of this thesis is organized as follows.

Chapter 2 provides a survey of existing works and studies in the specific WBAN context regarding the key building blocks of Figure 1.10. Firstly, aspects related to the signal waveform and to the WBAN propagation channel will be discussed. Then State-of-the-Art localization algorithms, from both general WSN and particular WBAN perspectives will be described.

Chapter 3 deals with the modeling of single-link ranging errors for the different kinds of cooperative WBAN links and radio technologies. Theoretical models based on the *Cramer-Rao Lower Bound* (CRLB), fed with realistic empirical parameters issued from WBAN channel measurement campaigns, will be considered to illustrate the best achievable bounds of ranging error over on-body, inter-body and off-body links. Furthermore, we present our novel model for dynamic intra-WBAN ranging errors based on IR-UWB TOA estimation.

In the MoCap context, Chapter 4 introduces several variants of the new *Constrained Distributed Weighted Multi-Dimensional Scaling* (CDWMDS) algorithm for relative on-body nodes positioning, relying on fixed-length links and asynchronous updates of estimated nodes locations. On this occasion, we also describe scheduling and censoring mechanisms, as well as possible extensions into heterogeneous wireless contexts, while incorporating off-body links with respect to fixed infrastructure anchors to enable large-scale absolute on-body nodes positioning.

Chapter 5 investigates navigation applications, from both personal and collective perspectives. Different algorithms will be compared, including a centralized *Extended Kalman Filter* (EKF) and a distributed *Non Linear Least Squares* (NLLS) positioning algorithm. One goal is to take benefits from the spatial diversity of deployed on-body devices to combat efficiently link losses and obstructions through intra- and inter-WBAN joint cooperation, while reducing complexity and consumption.

Chapter 6 accounts for experiments based on real IR-UWB radio platforms to validate in part some of the previous proposals, while showing their practical limitations.

Finally, Chapter 7 provides general conclusions and discloses a few research perspectives for future work.

Chapter 2

State of the Art in Wireless Body Area Networks Localization

Contents

2.1 Introduction

In this chapter, we provide a survey of State-of-the-Art contributions directly related (or at least relevant) to the radio-based localization problem in the WBAN context. We will account for these works and studies according to the block diagram already presented in the previous chapter, developing each key building block. Section 2.2 deals with transmitted waveforms and allocated frequency bandplans. In Section 2.3, aspects related to the WBAN propagation channel will be discussed from the radiolocation perspective. Then, Section 2.4 will address positioning and tracking algorithms i) in a general radiolocation context first, hence reminding the main differences between centralized/decentralized, cooperative/non-cooperative, probabilistic/non-probabilistic approaches, and then ii) focusing on existing algorithmic contributions applied into the specific frame of WBAN localization. Finally, Section 2.5 summarizes the chapter.

2.2 Transmitted Waveforms and Bandplans

In November 2007, the IEEE 802.15 Task Group 6, also known as IEEE 802.15.6, was formed to standardize WBAN, which were not covered by any existing communication standard yet. The work of this group resulted in February 2012 in

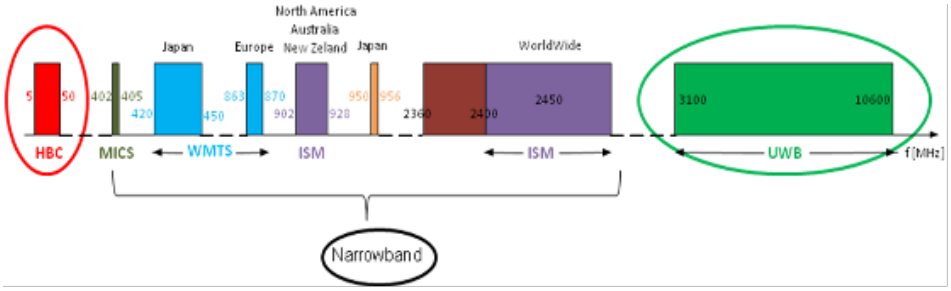

Figure 2.1: WBAN frequency bands allocation defined by the IEEE 802.15.6 standard in different countries [4].

the publication of a reference document [11], which defines *PHY*sical (PHY) and *Medium Access Control* (MAC) layers specifically optimized for short-range transmissions *in*, *on* or *around* the body, while supporting low complexity, low cost and low energy consumption.

According to the wide range of WBAN-based applications, the IEEE 802.15.6 has proposed three different PHY layers, which can be based on N-B (centered at different frequencies, including in ISM bands), IR-UWB or *Human Body Communications* (HBC). Note that the latter does not really comply with the classical definition of a radio technology in the common sense, for exploiting the propagation of waves directly on the subject's skin. As such, this physical layer will not be considered to cover our radiolocation needs in the following. Figure 2.1 shows the allocated spectrum frequencies depending on the country [4].

The standardized UWB PHY supports two groups of sub-channels with a bandwidth of 499.2 MHz [4], [11], defined as low and high bands, as shown in Table 2.1. The sub-channels are classified as optional or mandatory. As for the transmitted unitary waveforms, no strict pulse shape is really imposed but a *Square-root Raised Cosine* (SRRC) is considered as a reference shaping filter in all the bands, except in the 420 to 450 MHz bands [11], [50]. In addition to respecting the regulatory spectral mask (where applicable), a standard-compliant pulse shape $p(t)$ is constrained by the absolute value of its cross-correlation with the reference pulse respecting the SRRC spectrum. The correlation must be equal to 0.8 at least. Finally, the pulse waveform duration, the *Pulse Repetition Frequency* (PRF), and the peak PRF must be compliant with the specified timing parameters [11].

2.3 Standardized Channel Models

In the very WBAN context, many research efforts have been focusing on the characterization of the propagation channel, which plays a crucial role in the localization process and is expected to strongly impact the achievable accuracy, as already pointed out. A significant part of this work is however restricted to communication-oriented on-body scenarios so far, whereas body-to-body or off-body configurations

Band group	Channel number number	Central frequency (MHz)	Bandwidth (MHz)	Channel attribute
Low band	1	3494.4	499.2	Optional
	2	3993.6	499.2	Mandatory
	3	4492.8	499.2	Optional
High band	4	6489.6	499.2	Optional
	5	6988.8	499.2	Optional
	6	7488.0	499.2	Optional
	7	7987.2	499.2	Mandatory
	8	8486.4	499.2	Optional
	9	8985.6	499.2	Optional
	11	9984.0	499.2	Optional

Table 2.1: UWB PHY allocation defined by the IEEE 802.15.6 standard.

on the one hand, and localization-oriented scenarios on the other hand, have been more marginally treated. In this section, we will only discuss the standardized channel models, which are dedicated for WBAN communications (i.e. IEEE 802.15.6) or could be adapted to WBAN context (e.g. IEEE 802.15.4a).

2.3.1 IEEE 802.15.6 Models

WBAN channels can experience fading due to different reasons, such as energy absorption, reflection, diffraction, body posture and body shadowing. The other possible reason for fading is multipath due to scatterers disseminated in the environment around the body. Fading can be classified into two categories, namely fast fading and shadowing. Fast fading refers to the rapid changes in the amplitude of the received signal in a given short period of time. Thus, in localization context, fast fading effects can usually be removed by averaging the received signal (e.g. using a sliding window). The second type of fading is depicted as slow fading or shadowing, and is basically due to the shadowing by human body. Hence, the shadowing phenomenon reflects the slowest variations of the *Path Loss* (PL) around its mean.

IEEE 802.15.6 generally describes the WBAN channels by characterizing the total PL, including the mean PL and shadowing effects due to the human body and/or indoor obstacles [51]. Table 2.2 summarizes the different considered scenarios [4], which are grouped into classes. Each class is represented by a common *Channel Model* (CM). In the WBAN localization context, the radio devices are expected to be placed on the body but not implanted in the body. The latter configuration is indeed more indicated for medical applications (e.g. ECG, blood pressure measurements...). It is thus worth focusing on CM3 and CM4 channel models in scenarios S_4 to S_7. The most common channel model for on-body links (i.e. CM3), which has been retained by the IEEE 802.15.6 proposal, is called *Power Law Model*. This approach is used for modeling the total PL [52]. Nevertheless, the described model is generalized for both N-B links in the ISM band [2.4, 2.5] GHz and IR-UWB links in the band

Scenario	Description	Frequency Band	Channel Model
S_1	Implant to Implant	402-405 MHz	CM1
S_2	Implant to Body Surface	402-405 MHz	CM2
S_3	Implant to External	402-405 MHz	CM2
S_4	Body Surface to body Surface (LOS)	13.5, 50, 400, 600, 900 MHz 2.4, 3.1-10.6 GHz	CM3
S_5	Body Surface to body Surface (NLOS)	13.5, 50, 400, 600, 900 MHz 2.4, 3.1-10.6 GHz	CM3
S_6	Body Surface to External (LOS)	900 MHz 2.4, 3.1-10.6 GHz	CM4
S_7	Body Surface to External (NLOS)	900 MHz 2.4, 3.1-10.6 GHz	CM4

Table 2.2: List of the IEEE 802.15.6 scenarios and their description [11].

[3.1, 10.6] GHz. Thus, the power law model given in [52] is simply described by equation (2.1), where $P(d)$ is the total PL at distance d between two on-body devices. a and b are the model parameters (usually depicted as path loss exponent and reference path loss at a reference distance, respectively) and N is a normally distributed variable, zero-mean with a standard deviation σ_N.

$$P(d_{[mm]})_{[dB]} = alog_{10}(d_{[mm]}) + b + N \tag{2.1}$$

Besides the described power law models, IEEE 802.15.6 retains for CM3 scenarios a *Channel Impulse Response* (CIR) model, which was also described in [52] in the band [3.1, 10.6] GHz. This model is based on a single cluster of multipath components, as shown in the equation (2.2) below:

$$h(\tau) = \sum_{l=0}^{L-1} a_l exp(j\phi_l)\delta(\tau - \tau_l) \tag{2.2}$$

where $h(\tau)$ is the CIR, L is the total number of significant paths, a_l, τ_l and ϕ_l are respectively the amplitude, the arrival time and the phase of the $l-th$ path. The phase ϕ_l is modeled as a uniformly distributed random variable over [0, 2π]. The path amplitude a_l is modeled by an exponential decay Γ with a Ricean factor γ. The arrival time τ_l is modeled by a Poisson distribution.

Note that other on-body channel models have been retained by the IEEE 802.15.6 for CM3 scenarios at 2.4 GHz, such as the saturation model, which was described in [53] as a hybrid model merging a local propagation model (on-on) and environmental effects (i.e. due to multipath components). But the latter remains more confidential.

IEEE 802.15.6 has also considered channel models characterizing off-body radio links between on-body devices and external points, known as the CM4 model.

The normalized received power (i.e. normalized over the maximum value) is rather modeled by a gamma distribution for standing scenarios, and with a log-normal distribution for walking scenarios at 2.36 GHz [54]. The described off-body channel model also considers characterizing the CIR in the band [3.1, 10.6]GHz. The model is rather similar to the model described in equation (2.2), but additional ground effects have been considered. Further details on the related measurement set-up and data analysis can be found in [55].

So far, no model characterizing the body-to-body channels has been standardized yet. However, various proprietary models have been extracted out of real measurements in some recent works, such as [56], [57], [58] or [13]. All of them have been focusing on N-B links only.

2.3.2 IEEE 802.15.4a Models

Besides the IEEE 802.15.6 standard, other existing radio standards can fulfill in part the new needs of WBANs and localization, though non-explicitly focusing on WBAN applications and hence, requiring several adaptations at different levels (e.g. in terms of power consumption, form factor, reliability). Among those standards, the IEEE 802.15.4a standard can be viewed as an IR-UWB extension of the N-B IEEE 802.15.4 standard [59]. This standard is well known for *Wireless Sensor Network* (WSN), and supports peer-to-peer ranging capabilities up to MAC layer. In this context, some IEEE 802.15.4a channel models could be adapted for characterizing some WBAN channels, such as off-body and body-to-body channels. Moreover, the IEEE 802.15.4a provides a complete description of an on-body channel, which will be described hereafter.

In [5] an IR-UWB channel model has been characterized for on-body communications in the band [3, 5]GHz. This model has finally been extended by the IEEE 802.15.4a standard [60], and declined according to three scenarios depending on the receiver position (i.e. on the front, the side or the back of the body). Figure 2.2 recalls the three corresponding scenarios. In addition, the mean PL is modeled by a distance-dependent exponential decay, as shown in equation (2.3) below:

$$PL_{dB} = \gamma(d - d_0) + PL_{0,dB} \tag{2.3}$$

where $\gamma = 107dB/m$, d is the distance between the transmitter and the receiver around the perimeter of the body and $PL_{0,dB}$ is the measured PL at the reference distance d_0. Moreover, this model assumes the presence of two clusters of *Multi Path Components* (MPC) due to the waves' diffraction around the body and the reflection on the ground. The MPC over each cluster are correlated following a log-normal distribution.

Despite the large number and the variety of the contributions recently issued in the field of WBAN channel characterization and modeling, the available standardized models do not seem totally adapted to our problem, nor unified for a convenient usage. In our evaluation framework, while assuming single-link radiolocation metrics, we will thus either propose brand new localization-oriented models or adapt

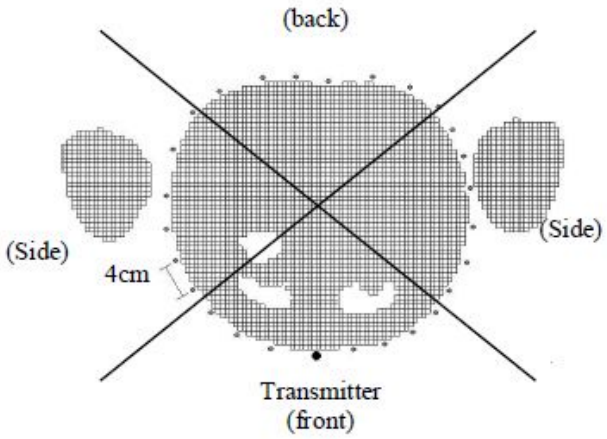

Figure 2.2: IEEE 802.15.4a on-body scenarios based on the receiver positions [5].

existing communication-oriented models derived from experimental parameters instead, which appear more adapted to our requirements (in terms of e.g., dynamic measurements, antennas placement, environment and scenarios). For instance, our intra-WBAN channel model will be mainly based on the dynamic channel measurement campaign of [6]. The off-body and body-to-body channel models will be based respectively on the experimental models of [12] and [13]. Further details about those models will be given in Chapter 3.

2.4 Localization Algorithms and Systems

As mentioned before, the localization algorithms aim at retrieving the locations of on-body devices and/or carrying bodies in our context. Those algorithms are fed directly by range measurements (i.e. through RT-TOF and/or RSSI estimation) or similarity measurements such as the connectivity information. From a pure localization perspective, we assume hereafter that a WBAN can contain two kinds of on-body wireless devices, regardless of their status in terms of networking (i.e. end-device, router, coordinator...) and/or data utility (i.e. collector, gateway, sensor node). The first category is defined by simple mobile nodes with unknown positions, which must be located relatively to reference anchor nodes, which belong to the second category. Anchor nodes have known positions in the reference coordinate system, which can be a body-strapped LCS (for relative MoCap applications) or a GCS (for LSIMC and navigation applications). In this section, we make an overview of frequently cited localization algorithms (including positioning and tracking solutions), making a distinction between centralized and decentralized, cooperative and non-cooperative, probabilistic and non-probabilistic estimation approaches, along with examples of localization systems applied into the WBAN context.

2.4.1 Taxonomy of Cooperative Localization Algorithms

2.4.1.1 Centralized vs. Distributed

Centralized localization approaches consist in collecting all the radiolocation measurements in one single computation center and to proceed with the estimation of all the blind nodes' coordinates simultaneously. From that perspective, centralized approaches are most often seen as fully centralized. Blind nodes can be both mobile or static nodes with unknown locations. Advantageously, in a body-centric approach, this computation center could be the WBAN coordinator or on-body gateway, which is usually endowed with more powerful embedded resources (i.e. in terms of energy/battery, memory and computational skills) than simple devices. But the calculi can also be externalized (e.g. hosted in a server) after relaying the measurement data to the centralized infrastructure through off-body links. There, the measurements are jointly processed and the positions for all nodes in the WBAN are simultaneously determined. Afterwards, the information can be exploited in the WBAN or sent back to any mobile node. In this approach, accuracy is expected to be optimal. However, one major drawback is the need for such on-body central nodes with computational skills and better energy autonomy, what is rather unlikely and demanding in the WBAN context. Another problem within such centralized approaches is the latency effect (i.e. the time elapsed between the collection of the required distance measurements and the final delivery of all the positions estimates, possibly while experiencing packet losses), whereas the body gesture and location can change rapidly during the collection step. Hence, to overcome the previous problems, decentralized approaches can be favored instead, although their convergence time may be also problematic.

Such distributed solutions allow each mobile node to localize itself by receiving information from its neighbors (i.e. anchors and/or mobile nodes). Hence, complexity is also distributed among the mobile nodes in comparison with the centralized approach, and the latency effect described above (i.e. mostly due to the collection of measurements) can be reduced, provided that the decentralized algorithms does not necessitate too many iterations to converge properly. In fact, distributed approaches can benefit from intrinsic asynchronism (i.e. updating the nodes positions with different refreshment rates) while localizing the mobile nodes. Accordingly the positions of the most demanding nodes (e.g. with higher velocity) can be updated at higher refreshment rates.

In the WBAN context, some centralized algorithms have been considered in [2], [8], [61], [62], [63]. For both MoCap and navigation purposes, [8] has used the *Non Linear Least Squares* (NLLS) algorithm, which consists in minimizing a global quadratic cost function using the Gradient descent method incorporating both on-body and off-body range measurements. [2] and [61] adapt a centralized classical *Multidimensional Scaling* (MDS) for on-body MoCap applications and pose estimation. In [61], the authors introduce additional constraints relying on the prior knowledge of minimal and maximal feasible distances related to the body dimensions (and thus some kinds of geographical limitations). In [62] the centralized *Maximum*

Likelihood estimator has been considered, introducing other constraints relying on the actual positions of on-body mobile nodes. However, [8] has also used a variant of the *Linear Least Square* (LLS) algorithm, which is somehow decentralized (even if the term may be debatable) in the sense that blind nodes compute their own location locally, based primarily on available external anchors or in case of limited connectivity to external points, based on already positioned on-body devices.

2.4.1.2 Cooperative vs. Non Cooperative

Localization schemes can also be classified into cooperative and non-cooperative categories. Non-cooperative approaches aim at localizing on-body nodes based on peer-to-peer range measurements with respect to anchors only [62], [63], [64]. But the number of anchors (either on-body for the relative Mocap applications, or belonging to the external infrastructure for the LSIMC and the navigation applications) in the WBAN context is likely small. One solution to compensate too frequent disconnection and/or erroneous measurements with respect to those anchors then consists in allowing peer-to-peer cooperation among mobile nodes. In our WBAN terminology herein, the term cooperative can refer to two concrete embodiments (possibly implemented simultaneously). On the one hand, intra-WBAN cooperation consists in exploiting not only radiolocation measurements between blind on-body devices to be located (either static or mobile) and anchors (either on-body or belonging to the external infrastructure), but also communication links and/or radiolocation measurements between blind devices. In this case, the latter belong necessarily to the same WBAN [8], [61]. On the other hand, inter-WBAN cooperation consists in exploiting radiolocation measurements and/or communication links between on-body devices that belong to distinct WBAN and bodies, thus exploiting body-to-body links.

Cooperative approaches can take benefits from mesh topologies. But one drawback lies in the extra over-the-air traffic and most often, in their higher complexity, e.g., in terms of synchronization requirements, coordination and/or scheduling needs, neighborhood discovery and maintenance under mobility. Hence, those two factors (i.e. complexity and traffic) represent two research topics that are worth being investigated to enhance the performance of cooperative localization in WBAN. A very preliminary comparison between cooperative and and non-cooperative localization schemes in the specific context of WBAN has been proposed in [8], showing that the achieved localization accuracy is better, but the energy consumption and the over-the-air traffic (e.g. in terms of the average number of requested superframes for localizing all the blind nodes in the WBAN) is higher in cooperative schemes than in non-cooperative schemes.

2.4.1.3 Location Estimators

Consider a WBAN of size $m + n$ nodes, where n is the number of mobile nodes to be located, and m is the number of anchors with known positions. In the following,

$\theta_t = [X_1(t), \ldots, X_n(t)]$ is the vector of unknown *d-Dimensional* (d-D) (i.e. d=2 or 3) coordinates at time t and $[X_{n+1}(t) = X_{n+1}, \ldots, X_{n+m}(t) = X_{n+m}]$ is a vector of known and time-invariant positions of anchors. In our context, note that the nodes positions can be defined either in the body-strapped LCS (e.g. for relative MoCap) or in a GCS (e.g. for LSIMC and navigation). The pair-wise radiolocation measurement performed at time t between two devices i and j is depicted by $y_{ij}(t)$, which can be either a scalar value (i.e. TOA, TDOA, TOF, RSSI) or a vector such as the CIR in rarer localization approaches. Moreover, we consider that the corresponding observed (erroneous) distance $\widetilde{d}_{ij}(t)$ can be obtained according to $\widetilde{d}_{ij}(t) = f(y_{ij}(t))$, whereas the true and estimated distances between the two devices at time t are respectively given by $d_{ij}(t) = \sqrt{((X_i(t) - X_j(t))^T(X_i(t) - X_j(t))}$ and $\widehat{d}_{ij}(t) = \sqrt{((\widehat{X}_i(t) - \widehat{X}_j(t))^T(\widehat{X}_i(t) - \widehat{X}_j(t))}$. Finally $d(t)$ is the vector containing all the available distances $d_{ij}(t)$ at time t

Weighted Least Squares Positioning The *Weighted Least Squares* (WLS) algorithm is a non-probabilistic estimator, which does not necessitate prior information about the distribution of estimated positions. In a cooperative localization context, the idea is to find the latter positions by minimizing a global cost function that incorporates quadratic errors between all the pair-wise measurements and their estimates (conditioned on the current value of the estimated coordinates, set as optimization variables). In a symetric and/or unidirectional case (i.e. assuming uniquely one available measurement per pair-wise link), the cost function is as follows:

$$\hat{\theta}_t = \underset{\theta_t}{\operatorname{argmin}}\, S(\theta_t) \tag{2.4}$$

where

$$S(\theta_t) = [\sum_{1 \le i \le n} [\sum_{i \le j \le n+m} w_{ij}(t)(\widetilde{d}_{ij}(t) - d_{ij}(t))^2 + r_i(t)||X_i(t) - \overline{X}_i(t)||^2]] \tag{2.5}$$

where $d_{ij}(t)$ denotes the Euclidean distance between nodes i and j, $w_{ij}(t)$ is a weight value, which reflects the connectivity and the accuracy of the range measurement between nodes i and j at time t, $\overline{X}_i(t)$ is a vector with prior information about the position occupied by node i at time t, while $r_i(t)$ quantifies the reliability of this prior information. If there is no prior information, then $r_i(t) = 0$, and the WLS cost function is similar to that of a blind classical NLLS cost function.

The choice of the weights should reflect the accuracy of the involved observations and unreliable measurements shall be down-weighted in the cost function. Several strategies have been adopted for the selection of $w_{ij}(t)$ such as exponential decreasing with the measured distance in [65], when the measurement noise variance is not available. Whenever a model is available, assuming for instance that measurement noise is a Gaussian distributed random process with known standard deviation $\sigma_{ij}(t)$ (e.g. increasing linearly with the true distances in a parametric description $\sigma_{ij}(t) = c_1 d_{ij}(t) + c_2$), then $w_{ij}(t)$ can be simply chosen as $\frac{1}{\sigma_{ij}(t)}$ (and thus $\frac{1}{c_1 \widetilde{d}_{ij}(t) + c_2}$ or even $\frac{1}{c_1 \widehat{d}_{ij}(t-1) + c_2}$ based on the current measurements or latest estimates) [66].

This WLS estimator is not (or at least only partly) parametric and thus it is still very popular in a wide range of localization problems, including in the WBAN context. One notorious limitation however is that the optimization problem in (2.5) is non-convex for practical cooperative configurations. Accordingly, the solution can get stuck in a local minimum depending on the starting point and hence, a relevant global solution may never be reached. A minimum of $S(\theta_t)$ can be computed using iterative numerical methods initialized at a starting position. Among these methods, one can cite the Gradient Descent, the Levenberg-Marquardt algorithm and *Scaling by MAjorizing a COnvex Function* (SMACOF) [65], [67]. Furthermore, the partial derivatives of $S(\theta_t)$ with respect to $X_i(t)$ depends only on the neighbors coordinates and thus, a local cost function can be defined at each node, where a local minimization can be performed. Hence, distributed iterative optimization solutions have been adopted such as the *Distributed Weighted Least-Squares* (DWLS) in [68] or the *Distributed Weighted Multi-Dimensional Scaling* (DWMDS) in [65], which implements a more advanced distributed version of SMACOF preventing from the increase of the cost function at each iteration. The idea still consists for each node in localizing itself, by minimizing the following cost function:

$$\hat{X}_i(t) = \underset{X_i(t)}{\operatorname{argmin}}\ S_i(t) \tag{2.6}$$

where

$$\begin{aligned} S_i(t) \quad = \quad & \sum_{j=1, j\neq i}^{n} w_{ij}(t)(\widetilde{d}_{ij}(t) - \hat{d}_{ij}(X_i(t), \hat{X}_j(t)))^2 \\ & + \sum_{j=n+1}^{n+m} 2w_{ij}(t)(\widetilde{d}_{ij}(t) - \hat{d}_{ij}(X_i(t), \hat{X}_j(t)))^2 \\ & + r_i(t)||X_i(t) - \overline{X}_i(t)||^2 \end{aligned} \tag{2.7}$$

In our work, we will adapt this DWMDS algorithm for WBAN localization purposes. More details will be given in Chapter 4.

Probabilistic Estimators In the localization context, a probabilistic estimator consists in locating the mobile nodes based on probabilistic assumptions. The latter can be based on a priori statistical models for the observed measurements conditioned on the mobile positions, like in likelihood functions. These functions can be not only conditioned on positions but also e.g., on the radio obstruction conditions over each link (i.e. LOS/NLOS), like in [69] or [70]. But other approaches can be based also on prior statistical information regarding the occupied positions by the mobile nodes them-selves. Accordingly, these algorithms are usually more accurate than simple non-probabilistic estimators like WLS. The probabilistic estimators can be classified into two categories, namely Bayesian and Non-Bayesian approaches. Non-Bayesian estimators assume that the mobile positions are treated as unknown deterministic parameters whereas mobile positions are defined as random variables with known prior distributions in Bayesian estimators.

Non-Bayesian Positioning In the Non-Bayesian context, positions are treated as unknown deterministic parameters. One common Non-Bayesian estimator is the *Maximum Likelihood* (ML) estimator, which operates by maximizing the likelihood function:

$$\hat{\theta}_t^{ML} = \underset{\theta_t}{\operatorname{argmax}}\ p(y(t)|\theta_t) \tag{2.8}$$

where the likelihood function $p(y(t)|\theta_t)$ denotes the *probability density function* (pdf) of the observation $y(t)$ conditioned upon the variable of interest θ_t.

It is known from estimation theory [71] that the ML estimator is unbiased and consistent, i.e. converges asymptotically to the *Cramer Rao Lower Bound* (CRLB) at low measurement error variances.

If we assume that the distance observations given by $\widetilde{d}_{ij}(t) = f(y_{ij}(t))$ provide sufficient statistics for the estimation of θ and that $\widetilde{d}_{ij}$ are independent, then the ML estimator is given by:

$$\hat{\theta}_t^{ML} = \underset{\theta_t}{\operatorname{argmax}}\ p(\widetilde{d}(t)|\theta_t) = \underset{\theta_t}{\operatorname{argmax}} \prod_i \prod_j p(\widetilde{d}_{ij}(t)|\theta_t) \tag{2.9}$$

The distance observations are obviously affected by ranging errors, which are most often represented as additive random variables $\widetilde{d}_{ij}(t) = d_{ij}(t) + e_{ij}(t)$. In special cases when the ranging errors are considered as Gaussian *identically independent distributed* (i.i.d.) random variables, the ML estimator simply leads to the WLS estimator, which equivalently *Maximizes the Log-Likelihood* (MLL) function, as follows:

$$\hat{\theta}_t^{MLL} = \underset{\theta_t}{\operatorname{argmax}}\ \log(p(\widetilde{d}(t)|\theta_t)) = \underset{\theta_t}{\operatorname{argmax}} \sum_i \sum_j \log(p(\widetilde{d}_{ij}(t)|\theta_t)) \tag{2.10}$$

One advantage usually put forward with M(L)L is that it can stick with arbitrarily complex measurement error behaviours, including multimodal regimes, or highly specific distributions. The counterpart is that the estimator is strongly parametric (i.e. with model parameters that necessitate prior calibration) and the underlying optimization problem is even more complex to solve out and sensitive to initial guesses than in the WLS case, thus making its application rather challenging in generic WBAN contexts (i.e. regardless of the environment) and under stringent low complexity constraints. Nevertheless, the ML algorithm has already been considered for on-body localization in a non-cooperative context in [62], but with rather simplified assumptions regarding the range measurements and with further constraints on network deployment.

Bayesian Positioning and Tracking In the Bayesian context, the positions occupied by the mobile nodes are considered as random variables. A Bayesian estimator thus considers estimating the *a posteriori* probability distribution from a

known *a priori* distribution of the occupied positions. The general Bayes' formula is given as follows:

$$p(\theta_t|y_t) = \frac{p(y_t|\theta_t)p(\theta_t)}{p(y_t)} = \frac{Likelihood \times A\ priori}{Evidence} \tag{2.11}$$

Once the *a posteriori* distribution is known, the *Maximum a posteriori* (MAP) estimator $\hat{\theta}_t$ maximizes the *a posteriori* probability distribution [71], as follows:

$$\hat{\theta}_t^{MAP} = \underset{\theta_t}{\operatorname{argmax}}\ p(\theta_t|y_t) \tag{2.12}$$

Another known estimator is the *Minimum Mean Squared Error* (MMSE) estimator $\hat{\theta}_t$, which is calculated as the mean of the *a posteriori* distribution [71], as follows:

$$\hat{\theta}_t^{MMSE} = \int \theta_t p(\theta_t|y_t) d\theta_t \tag{2.13}$$

In the dynamic localization context, the nodes positions are somehow correlated over time. Hence, one can consider tracking filters, which help to improve localization accuracy by exploiting the measurements made at multiple time instants $y_{1:t+1}$ where the time variable is indexed for simplified notations (i.e. from the past till the current time step), and thus, by benefiting also from the spatial consistency of mobile trajectories. The Bayesian formulation of the tracking filter conducts to calculate the *a posteriori* distribution $p(\theta_{t+1}|y_{1:t+1})$ as follows:

$$p(\theta_{t+1}|y_{1:t+1}) = \frac{p(y_{t+1}|\theta_{t+1}, y_{1:t})p(\theta_{t+1}|y_{1:t})}{p(y_{t+1}|y_{1:t})} \tag{2.14}$$

Furthermore, the *a priori* distribution at time $t+1$ is calculated from the *a posteriori* at time t, using the Chapman-Kolmogorov equation [71]:

$$p(\theta_{t+1}|y_{1:t}) = \int p(\theta_{t+1}|\theta_t, y_{1:t})p(\theta_t|y_{1:t}) d\theta_t \tag{2.15}$$

Thus, the dynamic extensions of the MAP and MMSE estimators are respectively given by the following equations:

$$\hat{\theta}_{t+1}^{MAP} = \underset{\theta_{t+1}}{\operatorname{argmax}}\ p(\theta_{t+1}|y_{1:t+1}) \tag{2.16}$$

$$\hat{\theta}_{t+1}^{MMSE} = \int \theta_{t+1} p(\theta_{t+1}|y_{1:t+1}) d\theta_{t+1} \tag{2.17}$$

For practicability ans tractability reasons, it is usually assumed that the state space vector θ_t to be estimated is issued from a known Markov chain of transition probability $p(\theta_t|\theta_{t-1})$, with a known initial *a priori* distribution $p(\theta_0)$. The observation model is given by:

$$y_t = h(\theta_t) + e_t \tag{2.18}$$

where h is a function relating the observation to the state space vector and e_t denotes the observation noise vector, indexing also the time variable to simplify notations. Assume that the observations are i.i.d. variables at different time instants. Then, the Chapman-Kolmogorov equation becomes as follows:

$$p(\theta_{t+1}|y_{1:t}) = \int p(\theta_{t+1}|\theta_t)p(\theta_t|y_{1:t})d\theta_t \tag{2.19}$$

If the observations are conditionally independent, then $p(y_{t+1}|\theta_{t+1}, y_{1:t}) = p(y_{t+1}|\theta_{t+1})$ and the Bayes filter equation is simplified as follows:

$$p(\theta_{t+1}|y_{1:t+1}) = \frac{p(y_{t+1}|\theta_{t+1})p(\theta_{t+1}|y_{1:t})}{p(y_{t+1}|y_{1:t})} \tag{2.20}$$

$p(y_{t+1}|y_{1:t})$ does not depend on θ_{t+1}. Hence, $p(y_{t+1}|y_{1:t})$ is obtained according to the following marginalization:

$$p(y_{t+1}|y_{1:t}) = \int p(y_{t+1}|\theta_{t+1})p(\theta_{t+1}|y_{1:t}) \tag{2.21}$$

Once the initial distribution $p(\theta_0)$ and the transition probability are known (i.e. in our case, the mobility model), the Bayes filter computes the *a posteriori* distribution of θ_t recursively at any time t. However, due to the non-linearity between the observation and θ_t in equation (2.18), equations (2.19) and (2.20) are usually analytically intractable.

Thus, the particle filter may be used, which is based on sequential Monte Carlo methods for approximating numerically the *a posteriori* densities [72]. In the WSN localization context, it has been mainly adopted for tracking applications [73], [74], for instance in vehicular or personal navigation applications. It has been also considered in the very WBAN context, but still for navigation purposes in indoor environments [63]. One advantage with the particle filter is that is can handle non-linear transitions and arbitrarily complex error densities (on both mobile state and observation processes). However, for being based on numerical approximations, it is usually too computationally demanding for low-complexity and real-time applications like in our WBAN context. It is also highly dependent on the number of used particles, as well as on specific issues like particles cloud degeneracy or impoverishment, which necessitate even more complex mechanisms such as particles resampling and regularization.

Besides, assuming Gaussian noises and linearized models (i.e. linear state-space equation and a linear observation model) conducts to the *Kalman Filter* (KF), which yields to an tractable solution of the initial Bayesian filter formulation. But in typical wireless tracking problems, due to the non-linearity of the function h, the *Extended Kalman Filter* (EKF) may be adopted instead, which consists in preserving the full KF formalism after linearizing locally the incriminated function around the predicted state. Both KF and EKF are well known and popular in the general WSN localization context [75], [76], [77], due to their simplicity and practicability for implementation.

Overall, as a summary, the particle filter is a robust Bayesian solution to the wireless tracking problem in non-linear and non-Gaussian scenarios. But the price to pay for this flexibility in terms of computational load and energy consumption tends to prevent from using it in a generic WBAN context. Besides, the complicated and disparate nature of the body limbs movement during the human motion (i.e. depending on the on-body node's placement) makes it rather difficult to maintain one single state space equation to relay θ_{t+1} and θ_t, whatever the node. Thus, the EKF are not really expected to be fully robust and convenient for MoCap applications. However, they can be more relevant for navigation purposes, where reasonable assumptions about the macroscopic body movement can be made more easily. More details about the EKF will be given in Chapter 5, where the individual and group navigation modes will be investigated.

Graph Inference and Message-Passing Recent research efforts have been focusing on iterative, cooperative and decentralized solutions relying on message-passing, such as *Belief propagation* (BP) [78], which is one of the well-known graphical models for inference in statistical physics, artificial intelligence, computer vision, etc. This kind of approaches organizes the global computation of nodes location beliefs into smaller local computations implying the exchange of packets between neighbouring mobile nodes. An implicit mapping is thus usually intended between the physical network topology and a factor-graph representation. Gradual enhancements have been proposed for the last past years in the specific WSN cooperative localization context.

For instance, the *Non Parametric Belief Propagation* approach (NBP), which is one famous particle-based approximation of the standard BP has been put forward for non-linear and non-gaussian cases [79]. But one problem with NBP is that it suffers from loopy effects and error propagation in highly connected networks. Thus some improved variants have also been proposed, considering e.g., simplifications leading to *Non Parametric Generalized Belief Propagation* (NGBP) (though usually still too complex in large-scale networks), ii) NGBP algorithms with pseudo-junction trees to reduce complexity and improve convergence (e.g. via triangulated graphs and virtual edges) and iii) *Non Parametric Belief Propagation over Spanning Trees* (NBP-ST), where the results of several independent NBP on different spanning (loop-free) trees are merged. One step ahead, the over-confidence of beliefs in loopy graphs can also be solved out by using *Tree-Reweighted Belief Propagation* (TRW-BP), for which the optimal edge appearance probability has been derived [80]. Another proposal, depicted as the *Two Phase - Non Parametric Belief Propagation* (TP-NBP) algorithm [81], [82], aims at reducing the amount of transmitted data while improving the localization error under sparser connectivity. It considers applying first the standard NBP only with respect to 1-hop neighbors for simplification and then, based on the results of this first phase, new countable sets of points are redrawn to represent each blind node, taking those points as the centers of identified modes in the beliefs plus a few more points judiciously chosen around. Finally,

the exact discrete BP is tractable over these points and packets are broadcasted up to the k-*th* neighbors.

Alternative but rather similar distributed net-factor approaches rely on net-message passing. The latter have been tested in the context of UWB cooperative positioning based on real ranging measurements [43], [83]. One more recent solution inspired by Mean Field theory is described as the *Variational Message Passing* algorithm [84]. It aims at reducing the amount of exchanged information, requiring only three scalars to account for nodes' locations and beliefs in the transmitted packets.

Despite promising recent results and a claimed simplicity, all the message-passing approaches cited above have in common to be more adapted to static and rather dense networks. Most of them also necessitate several iterations (i.e. packets' exchanges) before achieving convergence, what makes then not so relevant in our WBAN localization context.

2.4.2 WBAN Localization Systems

As regards to precise range estimation based on single-link on-body radio transmissions, preliminary IR-UWB TOA-based ranging results have been provided in [85], focusing mostly on the effect of body-induced pulse distortions with respect to various TOF-based ranging algorithms. Those results would have to be extended to cope with dynamic scenarios (e.g. introducing space-time correlations for TOA estimates under body mobility), more realistic bandwidths, waveforms and SNR in compliance with upcoming WBAN standards. Other side research activities on single-link body-to-infrastructure estimation were carried out in [36] in the context of medical body sensors (e.g. senior health monitoring application), comparing different LDR radio standards and radiolocation metrics, such as TOA-based IEEE 802.15.4a and RSSI-based IEEE 802.15.4 ranging. Finally, a first-order non-homogeneous Markov model accounting for the path arrival times in UWB WBANs has been proposed out of real measurements [86]. However, it is not exploited at all for location-dependent applications, but uniquely intended for the purpose of simulating realistic WBAN channels or assessing realistic WBAN communication performances (e.g. through multipath-combining receiver structures).

Apart from single-link characterization, positioning and tracking schemes have also been proposed in the WBAN context, enabling either navigation or motion capture functionalities. For instance, the goal in [87] is to position on-body electrodes for biomedical applications such as *Electro-Encephalography* (EEG). The proposed method relies on a radio transmission technique at low frequency bands to resist to strong body attenuation and cantilever MEMS micro-antennas, coupled with a *Self Positioning Algorithm* (SPA), feeding a LS procedure with relative RSSI-based range measurements, to infer the coordinates of each electrode in a so-called virtual coordinate system. However, cooperative measurements are exhaustively included with no links selection strategies, what is hardly compatible with real-time mobile WBAN scenarios. Then, only relative positioning is considered, i.e. retrieving only

inter-nodes distances. Finally, only one-way ranging schemes are considered, making impractical more precise ranging solutions based on signal RT-TOF estimation (e.g. with IR-UWB transmissions), as well as cooperative communications (i.e. implying bilateral data exchanges between mobile nodes). In [88], a technique to improve indoor body positioning is experimentally evaluated. Starting with the remark that antenna radiating patterns are not perfectly omni-directional, it is proposed to distribute several wireless objects on the same body to exploit spatial diversity and enhance the global precision of the body location. One RSSI-based ranging measurement is then obtained between each on-body object and each available external anchor. Two subsequent positioning methods are proposed, either averaging all the RSSI measurements into one single reading for the entire body per link with respect to an external anchor, or averaging the positions estimated for each on-body object with respect to external anchors. Even if the solution benefits from spatial diversity, strictly speaking, no inter-WBAN/intra-WBAN cooperative scheme is considered. In [63], the positioning technique concerns only one single wearable node per body. In that sense, the invoked WBAN context sounds abusive and body-to-body cooperation shall be intended from a very classical and conservative WSN perspective (i.e. excluding intra-WBAN cooperation and more complex inter-WBAN cooperation involving several links between two bodies). This technique relies on a particle filter fed with RSSI measurements collected with respect to anchors or other mobile wearable nodes. In [89], a LS positioning algorithm is put forward, based on TDOA measurements and one-way transactions between one single wearable node per body and a set of surrounding synchronized anchors. Like in the previous referenced work, the WBAN appellation is abusive here and no cooperative scheme is considered. Moreover, the transmission with respect to surrounding anchors questions the limited transmission ranges (from on-body transmitters) usually intended within standardized WBAN applications. In [90], a generic framework is put forward for medical applications. Each WBAN comprises one *Cluster Head* (CH) node and several on-body sensors. Only the CH is positioned with respect to a set of surrounding sensors deployed in the immediate environment, using a particle filter fed with *Directions Of Arrival* (DOA) that are measured at the surrounding sensors. Here, the radio links between simple nodes and the CH are unexploited for cooperative location purposes and no communication is even possible between simple nodes in this star network topology. Moreover, one single WBAN can just interact with the fixed infrastructure, whereas no body-to-body links are supported.

Even more recently, new investigations have been initiated in the field of body motion tracking through WBANs [62]. In the proposed system, mobile agent nodes equipped with transmitters and placed on the limbs (e.g. on the arms) are tracked with respect to a set of anchor nodes, which are mounted directly on a fixed part of the body (e.g. the torso), assuming both synchronous and asynchronous scenarios between agents and anchors. A geometrically constrained ML positioning algorithm (i.e. constrained topology resulting from basic bio-mechanical rules) is then considered to accommodate IR-UWB TOA measurements (potentially with a timing offset in the asynchronous case) and retrieve the locations of agent nodes. However,

in this solution, mobile-to-mobile links are not taken into account and inter-WBAN cooperation is deliberately discarded. As a complementary approach in [8], very preliminary results have been provided regarding intra-WBAN cooperative location in a specific navigation scenario, integrating realistic protocol and synchronization constraints. According to this proposal, assuming IR-UWB transmissions and temporal radiolocation metrics, TDOA measurements are performed locally at mobile wearable nodes with respect to fixed transmitters in the surrounding infrastructure and peer-to-peer TOA-based range measurements are collected between wearable mobile nodes to achieve intra-WBAN cooperation. Possible gains are claimed in terms of service coverage under low traffic (for several cooperation schemes), while pointing out obvious needs for more realistic TOA error models (e.g. space-time correlated and conditioned on body obstructions), more efficient cooperative link selection strategies (e.g. based on detected body obstructions), and finally joint inter-WBAN cooperation for enhanced group navigation.

None of the previous location algorithms can really handle joint inter/intra-WBAN cooperation. In most cases, they do not either take into account WBAN specificities, in terms of network topology, body/group mobility, space-time channel variations and correlations, or standard-compliant protocol exchanges and waveforms. Finally, refined dynamic TOA-based ranging error models are still required (e.g. conditioned on body obstructions) to assess more realistic location performances.

2.5 Conclusion

In this chapter, we have provided an overview of existing works and recent studies (explicitly or more indirectly) related to our cooperative WBAN localization problem. More precisely, we have dealt with key points of the localization system, such as the transmitted waveforms, the standardized bandplans and the channel models, the deployment topology and the localization algorithms. For the latter, while presenting possible location estimators, the discussion has been generalized (i.e. not only from a WBAN perspective, but also into a more classical WSN case).

Regarding the transmitted signal and the channel models first, the available standardized models do not seem fully adapted, nor unified. In the following, while assuming single-link radiolocation metrics within our evaluation framework, we will thus either develop a novel localization-oriented model or adapt existing communication-oriented models derived from experimental parameters instead.

Then it appears that most localization algorithms considered in the WBAN context so far favor centralized resources and synchronous calculi, which are however hardly compliant with real-time constraints under realistic human mobility (i.e. estimating all the unknown nodes' locations simultaneously, after relaying inter-nodes measurements to a central coordinator). Moreover, they often under-exploit the available potential of mesh topologies by sticking with non-cooperative links (i.e. uniquely with respect to fixed anchors). Some of these solutions also necessitate a

priori parametric models, which may be not really practical, given e.g., the unknown location-dependent mobility patterns experienced by on-body nodes (i.e. under non-calibrated and arbitrary deployments). On the contrary, considering that the DWMDS algorithm is i) distributed and asynchronous, thus adequate for real-time localization under mobility and adaptable to the local needs of on-body nodes, ii) non-probabilistic and non-parametric, in the sense no prior statistical information is absolutely required about the nodes' positions or measurements, we suggest to adapt and extend this algorithm for the relative MoCap and LSIMC applications in the following. In parallel, other classical tracking filters such as the EKF, will be also adapted for single and group navigation so as to cope with multiple on-body nodes.

The following chapter will focus on single-link ranging performances and error models in the cooperative WBAN context, considering the three possible levels of cooperation and kinds of links (i.e. on-body, body-to-body, off-body), as well as the key foreseen technologies.

Chapter 3

Single-Link Ranging and Related Error Models

Contents

3.1 Introduction

Generally speaking, the consideration of realistic ranging error statistics enables a more solid and fairer assessment of the localization performance (e.g. through realistic simulations) and in some cases, optimal algorithmic design (e.g. through outliers detection, proper measurement weighting, probabilistic location estimators...). One major problem in the WBAN context is that such localization-oriented models are still extremely rare and/or incomplete in the literature but most of them are restricted to on-body channel characterization from a pure communication-oriented perspective. Besides, in the field of cooperative WBAN localization, most of the algorithmic investigations carried out so far still consider unrealistic and synthetic TOA-based ranging errors under pedestrian mobility [2], [8], [62], [91], hence biasing somehow the performance evaluation in comparison with practical operating conditions. In particular, as far as we know, there does not exist any ranging-oriented parametric model that can really account for dynamic UWB on-body links. Apart from classical indoor representations (i.e. regardless of the WBAN context), there is no explicit ranging-oriented model either over off-body and body-to-body links.

Hence, this chapter analyzes possible models and parameters characterizing ranging errors based on the two main foreseen WBAN radio technologies, namely IR-UWB for on-body, body-to-body and off-body links on the one hand, and N-B at 2.4 GHz for body-to-body and off-body links on the other hand. In particular, Section 3.2 describes an original on-body error model, along with the retained modeling methodology, based on IR-UWB TOA estimation and exploiting real dynamic channel measurements over two representative on-body links and frequency bands [44], [45]. Then Sections 3.3 and 3.4 discuss theoretical ranging error models over off-body and body-to-body links, respectively for N-B RSSI estimation and IR-UWB TOA estimation in the presence of multipath. The latter error predictions are mainly based on CRLB calculi, fed with realistic empirical parameters issued from different WBAN channel measurement campaigns. They allow us to illustrate and discuss the best achievable ranging performance and to draw plausible bounds for further studies on localization algorithms in the following Chapters. Finally, Section 3.5 summarizes the chapter conclusions.

3.2 Empirical Modeling of On-Body Ranging Errors Based on IR-UWB TOA Estimation

In this section, we consider characterizing and modeling TOA-based ranging errors, using UWB on-body channel measurements, which were carried out under typical pedestrian walking [6].

3.2.1 Single-Link Multipath Channel Model

For the [3.1, 5.1]GHz and [3.75, 4.25]GHz bands considered hereafter, it was previously shown in [6] that on-body channels suffer from significant human shadowing, which is far dominating other distance-dependent effects. Accordingly, TOA estimation and its related error regimes are both expected to be strongly affected (and thus mostly conditioned) by dynamic body obstructions under mobility.

Over each on-body link, the received signal can be typically represented as a function of the transmitted signal as follows:

$$r(\tau) = \sum_{j=1}^{L_p} \alpha_j p(\tau - \tau_j) + n(\tau) = h(\tau) \otimes p(\tau) + n(\tau) \tag{3.1}$$

where $h(\tau) = \sum_{j=1}^{L_p} \alpha_j \delta(\tau - \tau_j)$ is the multipath CIR, $\delta(.)$ is the Dirac delta function, L_p is the number of multipath components, α_j and τ_j are respectively the amplitude and delay of the j-th multipath component, $p(\tau)$ is the transmitted pulse and $n(\tau)$ is an additive noise process.

Out of this observed signal, the TOA estimation step aims at determining the arrival time of the direct multipath component that would be ideally received in a free space propagation case. As previously pointed out and revealed by equation (3.1), the quality of TOA estimation depends on multiple factors such as the

emitted pulse energy (and hence, the received pulse energy) in comparison with the noise floor, multipath fading effects (and hence, the occupied bandwidth), or signal obstructions. It is thus possible to generate false alarms due to early noisy realizations or to miss the direct path due to poor *SNR* conditions and/or severe NLOS blockages. The latter phenomena tend to increase the apparent length of the direct path or they can even cause its absence, leading to overestimated ranges.

3.2.2 Path Detection Schemes Enabling TOA Estimation

3.2.2.1 Strongest Peak Detection

Matched Filtering (MF) usually claims low complexity and low consumption [2], which are two features particularly suitable for WBAN applications. In our ranging context, TOA estimates are first obtained through strongest peak detection, by looking for the corresponding time shifts that maximizes the cross-correlation function between the received signal that can be represented as equation (3.1), and a local template, which theoretically corresponds to the unitary transmitted waveform, as follows:

$$c(\tau') = \int_{-\infty}^{+\infty} r(\tau)p(\tau - \tau')\,\mathrm{d}\tau \tag{3.2}$$

$$\hat{\tau}_{TOA} = \underset{\tau' \in W}{\operatorname{argmax}} |c(\tau')| \tag{3.3}$$

where $c(\tau')$ is the cross correlation function, and $\hat{\tau}_{TOA}$ is the estimated TOA in the temporal observation window W. The estimated distance is $\hat{d} = \hat{\tau}_{TOA} v$, where v is the speed of light, assuming that the transmitter and the receiver are somehow synchronized, e.g. through 2-Way Ranging protocol exchanges (i.e. assuming in first approximation that the TOF is equivalent here to the TOA reading and that the errors affecting TOF measurements are restricted to that affecting TOA measurements). It will be seen in the following how to cope in part with the actual timing uncertainly when characterizing estimation errors out of real channel measurements.

3.2.2.2 First Path Detection

Getting back to the CIR expression in equation (3.1), the propagation delay τ_j obviously reveals the physical length of the j-th corresponding path. Therefore, under LOS conditions where a direct path is truly present between the transmitter and the receiver, the shortest observable propagation delay can be reasonably associated with the true Euclidean distance. This method, which is depicted hereafter as the *First Arrival Path* (FAP) detection scheme, simply consists in preliminarily estimating the CIR out of the received signal $r(\tau)$ in equation (3.1), and to associate the first estimated multipath component (i.e. among all the resolved paths) with the estimated distance between the transmitter and the receiver. Unfortunately, in NLOS conditions, this FAP may suffer from significant power attenuation that makes it subject to missed/late detections or early false alarms, thus conducting to large estimation errors and, more generally speaking, to a higher dispersion of the

measurements. Many channel estimation algorithms have already been proposed to retrieve the CIR out of the received signals, such as finger selection (e.g. for RAKE receivers) [92] or high-resolution algorithms (e.g. CLEAN), as it will be seen in the next subsection.

In the sequel, the ranging error will be simply defined as the difference between the estimated TOA-based distance described previously and the actual distance, as follows:

$$e = \hat{d} - d \tag{3.4}$$

3.2.3 Modeling Methodology

This subsection describes the methodology adopted to draw our TOA-based ranging error model out of real IR-UWB channel measurements.

3.2.3.1 Multipath Extraction from Channel Measurements

First of all, we consider the dynamic radio channels associated with the Hip-Chest and Hip-Wrist links from a past measurement campaign described in [6], where the total recording time was 4 sec and consecutive temporal channel responses were collected every 20 ms in the band [3.1, 5.1]GHz. The measurements were performed under moderate human walk mobility in a typical indoor environment, resulting in a set of 200 time-stamped channel responses. For each response, multipath components were extracted using a CLEAN-like high-resolution algorithm [93] in the bands [3.1, 5.1]GHz and [3.75, 4.25]GHz. A snapshot of the extracted CIR at the observation time-stamp t_n can hence be expressed as:

$$\hat{h}(t_n, \tau) = \sum_{j=1}^{\hat{L}_p(t_n)} \hat{\alpha}_j(t_n)\delta(\tau - \hat{\tau}_j(t_n)) \tag{3.5}$$

where $\hat{h}(t_n, \tau)$ is the CIR extracted at the observation time-stamp t_n, $\hat{L}_p(t_n)$ is the number of extracted multipath components, $\hat{\alpha}_j(t_n)$ and $\hat{\tau}_j(t_n)$ are respectively the amplitude and delay of the j-th extracted multipath component at time-stamp t_n.

Just like in [6], the dynamic power transfer function was also directly calculated out of the corresponding time-stamped frequency-domain measurements $H(t, f)$ in the band B (anyway made available for RF calibration purposes), as follows:

$$P(t_n) = \frac{1}{b}\int_B |H(t_n, f)|^2 \, \mathrm{d}f \tag{3.6}$$

where b is the bandwidth of B, and $P(t_n)$ is the time-variant power transfer function, as illustrated on Figure 3.1 for the Hip-Wrist link.

As expected, this figure shows the strong body obstruction effects on the received signal attenuation. Typically NLOS channel conditions periodically lead to severe fades due to body shadowing under mobility.

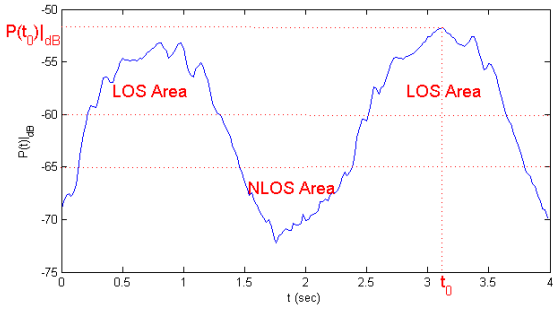

Figure 3.1: Dynamic variations of the power transfer function between the hip and the wrist under body mobility (standard walk), as a function of time t.

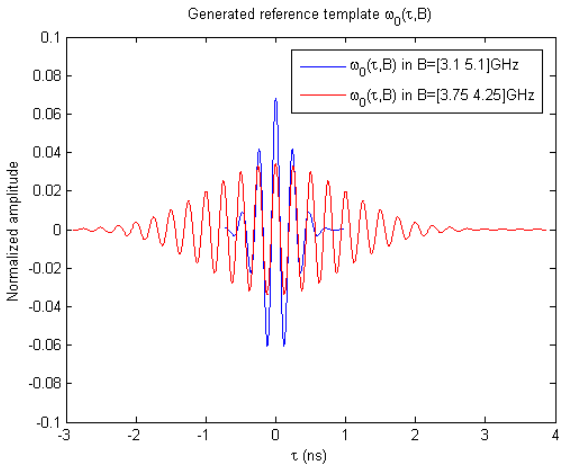

Figure 3.2: Energy-normalized templates $w_0(\tau, B)$ used for the generation of synthetic received signals and for correlation-based TOA estimation.

3.2.3.2 Generation of Synthetic Received Signals

In order to synthesize a realistic received signal out of the extracted CIRs, as a function of a given initial SNR level and occupying a given bandwidth, a reference template waveform is required. Gaussian-windowed sine waves have thus been generated in the [3.1, 5.1]GHz and [3.75, 4.25]GHz bands, the latter being in compliance with one mandatory band specified by the IEEE 802.15.6 bandplan. Figure 3.2 shows the corresponding reference templates normalized in energy. According to equation (3.1), those templates shall be convolved with the CIRs previously extracted out of real measurements, and an AWGN process with a two-sided power spectral density N_0 (i.e. $N_0 = -154\ dBm/Hz$) is filtered into the considered signal band. The resulting synthetic received signal available at the observation time-stamp t_n is thus

given by:

$$\begin{aligned} W_s(t_n,\tau) &= \hat{h}(t_n,\tau) \otimes w_0(\tau,B) + n(t_n,\tau,B) \\ &= \sum_{j=1}^{\hat{L}_p(t_n)} \hat{\alpha}_j(t_n) w_0(\tau - \hat{\tau}_j(t_n), B) + n(t_n,\tau,B) \end{aligned} \tag{3.7}$$

where $w_0(\tau, B)$ is the reference template and $n(t_n, \tau, B)$ is the band-limited noise process at the observation time-stamp t_n in the occupied band B.

For our simulation needs, in order to enable a dynamic variation of $SNR(t_n)$ and to preserve the natural relative power fluctuations due to body obstructions (as observed during the measurements campaign), we set and control the SNR values *a priori* for an arbitrary reference time stamp (preferably in LOS). In our case, the reference time t_0 is for instance chosen when the received channel exhibits a maximum of the power transfer function $P(t)$. Imposing *a priori* the reference value $SNR(t_0)$ (as an input parameter) and given the actual $P(t_n)$ (and hence $P(t_0)$) directly available from measurements at any time-stamp t_n, the instantaneous $SNR(t_n)$ is then forced and scaled artificially so as to vary realistically over the entire acquisition duration, as follows:

$$SNR(t)|_{dB} = SNR(t_0)|_{dB} + P(t)|_{dB} - P(t_0)|_{dB} \tag{3.8}$$

where $SNR(t)$ is the re-scaled instantaneous signal energy to noise ratio, $SNR(t_0)$ and $P(t_0)$ are respectively the controlled SNR value and power transfer function at time-stamp t_0, and $P(t)$ is the power transfer function at time t. In our study, $SNR(t_0)$ is viewed as an imposed input parameter, which remains constant and valuable for the whole duration of one walk cycle, and over several noise process realizations (i.e. over which TOA and ranging statistics will be drawn). Practically, before applying (3.8) to account for the overall walk duration from the reference time stamp t_0, given the fixed filtered noise power imposed by B and N_0, we re-scale the synthetic multipath impulse response $\hat{h}(t_0, \tau)$ in (3.7) into $\hat{h}_r(t_0, \tau)$ so that $W_{s,r}(t_0, \tau) = \hat{h}_r(t_0, \tau) \otimes w_0(\tau, B) + n(t_0, \tau, B)$ can respect the input parameter $SNR(t_0)$ (and thus, applying the same scaling factor to the useful signal for each random noise process realization), as follows:

$$SNR(t_0)|_{lin} = \frac{\int [W_{s,r}(t_0,\tau') - n(t_0,\tau',B)]^2 d\tau'}{N_0} \tag{3.9}$$

The rationale for parameterizing the error model with $SNR(t_0)$ are twofold: i) we have noticed that the error regime is rather stable over LOS or NLOS portions of a given walk (i.e. exhibiting approximately the same statistics under relatively small variations of the instantaneous SNR) but mostly conditioned on body shadowing and ii) $SNR(t_0)$ shall be easier to predict once for all at the beginning of the walk cycle in localization-oriented simulations (e.g. with classical free-space propagation models) for being advantageously associated with LOS conditions.

3.2.3.3 Emulated TOA Estimates and Conditional Error Regimes

At each observation time-stamp t_n, TOA estimates are thus estimated from each synthesized noisy received signal, using two kinds of estimators. The first one consists of a matched filter, as described in subsection 3.2.2.1, i.e. by looking for the time shift that maximizes the cross-correlation function between the synthetic received signal $W_{s,r}(t_n, \tau)$ and the reference template $w_0(\tau, B)$, within a given observation. In our case, the window has a time length of 5 ns like in [85], [91]. This duration is sufficient in WBAN applications to observe an arrival time corresponding to the maximum distance between two synchronized nodes placed on the same body. Thus we perform filtering here in terms of excess delay.

The second TOA estimate is based on FAP detection using a CLEAN-like approach, which can be shortly described for each time stamp t_n as follows [94]:

1) Calculate the self-correlation $r_{w_0w_0}(t_n, \tau)$ of the template and the cross-correlation $r_{w_0W_s}(t_n, \tau)$ of the template with the synthesized received signal $W_s(t_n, \tau)$.
2) Find the largest correlation peak in $r_{w_0W_s}(t_n, \tau)$, record the normalized amplitude α_k and the relative time delay τ_k of the correlation peak.
3) Substract $r_{w_0w_0}(t_n, \tau)$ scaled by α_k from $r_{w_0W_s}(t_n, \tau)$ at the time delay τ_k.
4) If a stopping criterion (e.g. a minimum threshold on the peak correlation) is not met, go to step 2. Otherwise, stop.
5) The overall CIR $\widehat{h}(t_n, \tau)$ is extracted, and the FAP is recorded as the first intime resolved multipath component $\widehat{\tau}_1(t_n)$.

The first Hip-Chest link to be considered is always assumed in LOS conditions, whereas the Hip-Wrist link varies dynamically, leading periodically and alternatively to LOS and NLOS conditions. In order to classify the obstruction conditions, the retained method is based on the power transfer function. Relying on the initial measurements, the channel is considered in LOS (resp. NLOS) conditions whenever its power transfer function is larger (resp. lower) than -60 dB (resp. -65 dB). The remaining unspecified time area is considered as a transition zone, with a steep power transition regime. Alternatively, the channel delay spread, which exhibits smaller values in LOS and higher values in NLOS conditions, could have been used to identify the channel obstruction configurations.

Finally, during the initial communication-oriented measurement campaign reported in [6], the real distance between nodes was not collected, since measurements were not carried out for localization purposes. However, in first approximation, one can try to extract this distance out of the measured TOA in time-stamp regions when the LOS conditions are clearly identified and with $SNR(t_0) = +\infty$ for the synthetic received signals in the largest bandwidth [3.1, 5.1]GHz. Practically, the first Hip-Chest link is considered as fixed and the reference distance extraction was directly realized by averaging all the TOA measurements issued from MF estimation over the walk cycle to reduce TOA estimation errors appeared during the mul-

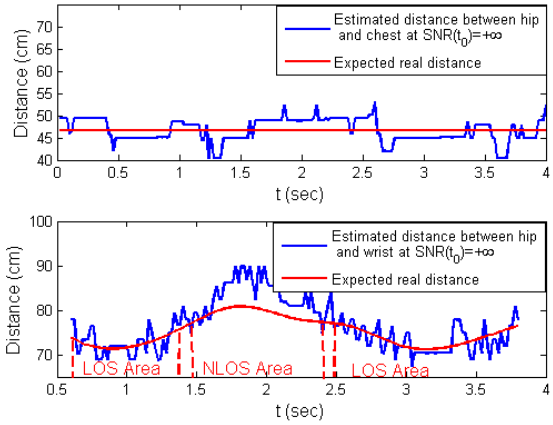

Figure 3.3: Equivalent inter-node distance retrieved out of correlation-based TOA estimation without noise (blue) and fitted reference distance after averaging with a sliding window and splines interpolation over the detected NLOS time stamp region (red), for both Hip-Chest (top) and Hip-Wrist links (bottom).

tipath extraction phase in the presence of overlapping components. Nevertheless, for the second Hip-Wrist link, a smoothing process was performed in a sliding window whose length corresponds to 20 consecutive time-stamp samples (e.g. within 20x20ms=400ms). The true distance was subsequently interpolated over NLOS areas, assuming continuity of the true distance at LOS/NLOS boundaries but discontinuity for the smoothed version of the measured distance (obtained with the sliding window). The idea consists in relying on the known extracted LOS portions, thus forming a time-stamp basis to infer the true distance in unknown NLOS time-stamp areas through spline-based data extrapolation. Figure 3.3 intends to clarify the method used to determine the reference distance, assuming the latter will correspond to the so-called "expected real" distance while computing the ranging error in the following.

3.2.4 Proposed Conditional Error Models

3.2.4.1 LOS Model

In this subsection we statistically characterize the obtained TOA-based ranging errors carried out of matched filter estimator, in the [3.1, 5.1]GHz and [3.75, 4.25]GHz frequency bands, for the two kinds of radio links. As previously mentioned, these models are conditioned on the channel obstruction status and on the reference $SNR(t_0)$. While running simulations, for each $SNR(t_0)$ value, 100 independent noise process realizations are drawn for the walk cycle duration. Over these realizations, for each frequency band, up to 20000 range measurements are then collected in LOS conditions for the Hip-Chest link, whereas 8600 and 3800 measurements are gener-

ated for the Hip-Wrist link, respectively in LOS and NLOS conditions. Moreover, we draw the model of the TOA-based ranging errors carried out of FAP detection using a CLEAN algorithm, in [3.1, 5.1]GHz frequency band, for the two kinds of radio links, but only under LOS conditions, while the FAP is almost systematically missed or falsely detected in NLOS conditions.

Strongest Path Detection Conditioned on the LOS case, a side basic *Least Square* (LS) fit has been performed between the empirical *Cumulative Density Function* (CDF) and a variety of well-known heavy tailed models (e.g. Gaussian, Generalized Extreme Value, Exponential, Weibull, lognormal...), which have been frequently cited in the literature in the field of ranging error modeling. Hence, it appears that the step-wise empirical CDF of emulated range measurements enjoys a rather satisfactory fit (in a least squares sense) to the CDF of a Gaussian random variable, whose standard deviation σ is on the order of the time base period. Figure 3.4 shows examples for both simulation-based and model-based LOS CDFs with $SNR(t_0) = 5dB$ in the band [3.1, 5.1]GHz.

Figures 3.5 and 3.6 show respectively the variations of the mean and standard deviation of the corresponding Gaussian LOS model for both links and both bands, as a function of $SNR(t_0)$. As seen in Figure 3.5, the mean varies around zero, with very low values (in comparison with the nominal expected true range value), and hence, it can be considered as null in first approximation over the explored range of $SNR(t_0)$ values. Figure 3.6 shows that the behavior of the standard deviation is asymptotically constant when $SNR(t_0)$ reaches a value of 10 dB. At high SNRs, the strongest path detected through cross-correlation indeed coincides systematically with the direct path. The asymptotic error floor at high SNR thus depends mostly on the occupied band and center frequency, as discussed in [34].

To summarize, considering the tested Hip-Chest and Hip-Wrist links, the distribution of the ranging error through correlation-based TOA estimation in LOS conditions in the [3.1, 5.1]GHz and [3.75, 4.25]GHz bands can be simply modeled as a centered Gaussian distribution, with a standard deviation depending on B and $SNR(t_0)$ (See the legend of Figure 3.6 for detailed model parameters).

First Path Detection For TOA estimation through FAP detection, the resulting pdf can be better represented by a mixture involving Gaussian and Uniform components. The Uniform distribution is weighted by the false alarm probability PF, which represents the probability to detect a wrong peak instead of the true FAP. PF is thus strongly affected by the threshold chosen within the FAP detection scheme (e.g. a smaller threshold obviously leads to higher PF), and hence, by the stopping rule in the underlying high-resolution channel estimation algorithm. Figure 3.7 shows the variation of PF as a function of $SNR(t_0)$ for both links in the [3.1, 5.1]GHz frequency band. At high $SNR(t_0)$, the behavior appears to be almost Gaussian and PF is approximately null. Figures 3.8 and 3.9 show respectively the variations of the mean and standard deviation of the corresponding Gaussian dis-

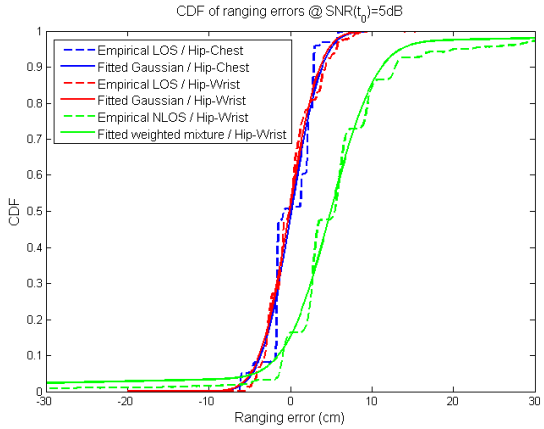

Figure 3.4: Empirical and model-based CDFs of ranging errors with a matched filter TOA estimator (i.e. strongest path detection), in both LOS and NLOS conditions, with $SNR(t_0) = 5dB$, in the band [3.1, 5.1]GHz.

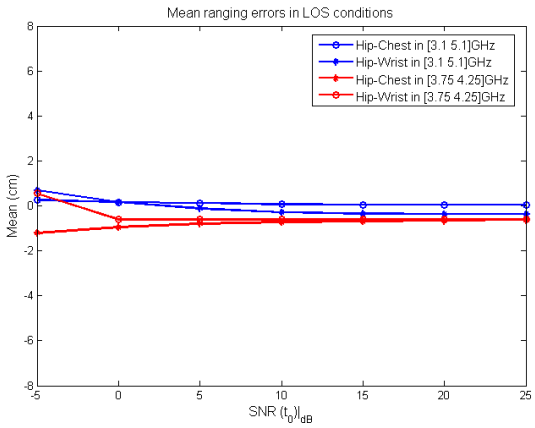

Figure 3.5: Mean of ranging errors with a matched filter TOA estimator (i.e. strongest path detection), in LOS conditions, as a function of $SNR(t_0)$.

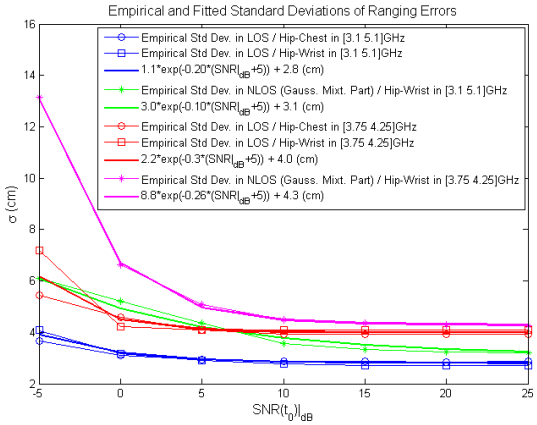

Figure 3.6: Standard deviations of ranging errors σ with a matched filter TOA estimator (i.e. strongest path detection), in LOS and NLOS conditions, as a function of $SNR(t_0)$.

tribution, for both links in the band [3.1, 5.1]GHz. These variations are compliant with the variations observed in the matched filter case in case of strongest path detection. This result shows that, in general LOS conditions, the FAP is rather in line with correlation-based TOA estimation. Thus one would tend to apply systematic strongest path detection for low complexity in such favorable conditions.

3.2.4.2 NLOS Model

As previously pointed out, in NLOS conditions (i.e. under body shadowing), the first path detection scheme being subject to much higher deviations, we mainly focus hereafter on the strongest path detection. The best fit has then been also obtained to a mixture-based model involving Gaussian and Uniform components. Figure 3.4 shows examples of both the empirical and model-based NLOS CDFs at $SNR(t_0) = 5dB$, in the [3.1, 5.1]GHz band.

The corresponding conditional pdf is then expressed as follows:

$$p(e) = \psi U(T_w) + (1 - \psi)G(\mu, \sigma^2) \tag{3.10}$$

where p is the pdf of the ranging error e in NLOS conditions, $U(T_w)$ is a uniform distribution, whose temporal support T_w depends on the receiver observation window while performing TOA estimation through cross-correlation. Again, this window is chosen to enable detection within any on-body link after synchronization (e.g considering typically a worst case distance of 1.5m), ψ is the weight of the uniform distribution, and $G(\mu, \sigma^2)$ is a Gaussian distribution with a mean μ and a variance σ^2.

The variation of those parameters in both bands of interest, as a function of $SNR(t_0)$ is represented in Figure 3.6, 3.10 and 3.11. As shown on Figure 3.11, at

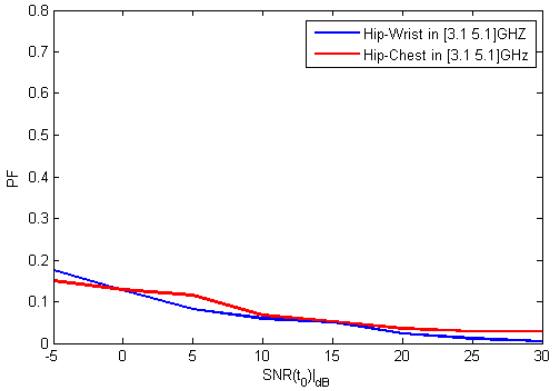

Figure 3.7: Variation of the false alarm probability for FAP TOA estimation (i.e. first path detection), using a threshold of 10 dB below the global absolute maximum of the estimated CIR, in LOS conditions, in the band [3.1, 5.1]GHz, as a function of $SNR(t_0)$.

low $SNR(t_0)$, the contribution of the uniform distribution component is high. This effect accounts for the distribution of the so-called apparent path arrival determined through cross-correlation over the entire observation window (e.g. between 0 and 5 ns), when the noise level is so high that it can cause frequent missed detections or false alarms. The uniform weight in the mixture then directly reflects the probability of having either a false alarm or a missed detection. However, at higher $SNR(t_0)$, the behavior is almost Gaussian, where the ranging error is centered around a positive mean, which can be interpreted as a positive bias caused by the obstruction of the direct path (and hence, its apparent length extension). As shown in Figure 3.6, at high $SNR(t_0)$ (i.e. larger than $10dB$), in each operating band, the behavior of the error standard deviation in LOS is similar to the standard deviation of the Gaussian part of the mixture-based NLOS model, as the uniform weight is becoming quasi-null. Similar standard deviations means that the path detection performances are thus equivalently good in terms of dispersion in LOS and NLOS conditions, given the observed strongest path. However, it is worth keeping in mind that the apparent time of flight of the first observable path in NLOS cases is shifted independently of the path power, hence leading to a non-neglected ranging bias (i.e. besides random noise terms). The fact that the NLOS bias is approximately constant over $SNR(t_0)$ for a given band is also in line with the previous remarks. This very bias value, which seems to depend mostly on the occupied band, is rather hard to predict (as a deterministic parameter) and characterize further in practice. Hence, we recommend in our final ranging error model to assume this bias as a Uniformly distributed random variable, drawn once for all within a plausible range of a few tens of cm (i.e. approximately constant over all the NLOS portions of one given walk cycle).

Finally, it is worth recalling that the standard deviation parameter depends

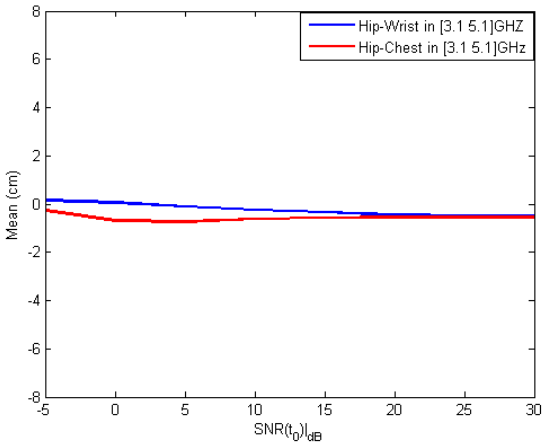

Figure 3.8: Mean of ranging errors for FAP TOA estimation (i.e. first path detection), in LOS conditions in the band [3.1, 5.1]GHz, as a function of $SNR(t_0)$.

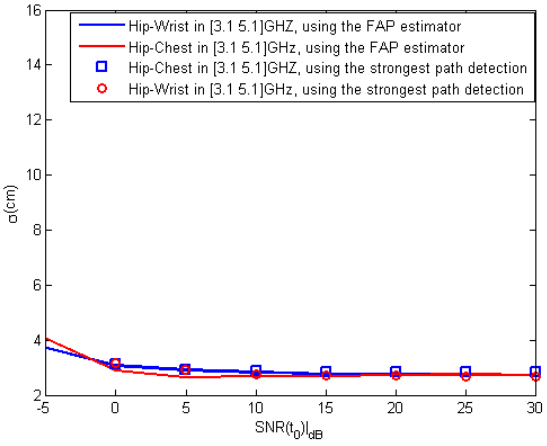

Figure 3.9: Comparison between the variations of the standard deviations of ranging errors σ using a FAP TOA estimator (i.e. first path detection using a threshold of 10 dB below the global absolute maximum of the estimated CIR) and strongest correlation peak TOA estimator, in LOS conditions, in the band [3.1, 5.1]GHz, as a function of $SNR(t_0)$.

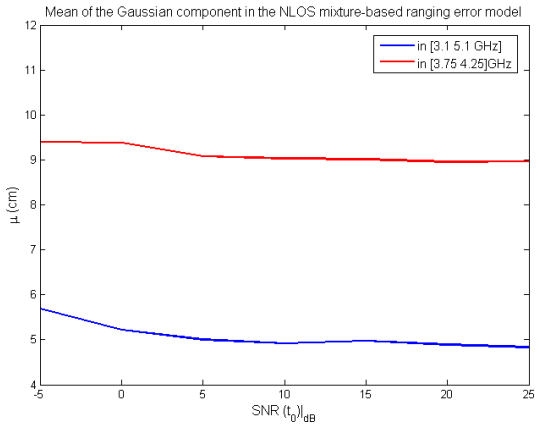

Figure 3.10: Mean value associated with the Gaussian part of the ranging error mixture-based model in NLOS conditions, as a function of $SNR(t_0)$.

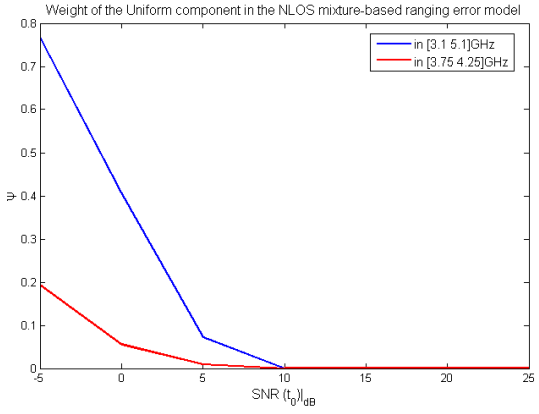

Figure 3.11: Weight of the Uniform part of the mixture-based ranging error model in NLOS conditions, as a function of $SNR(t_0)$.

mostly on B and $SNR(t_0)$. Table 3.1 shows the detailed variation of the standard deviation parameter for both Hip-Chest and Hip-Wrist links, through correlation-based TOA estimation in the [3.1, 5.1]GHz and [3.75, 4.25]GHz bands. For more practicability, Table 3.2 shows semi-analytical models that represent analytically the variation of the standard deviation parameter for both of the tested on-body links, under LOS and NLOS conditions.

$SNR(t_0)\|_{(dB)}$	-5	0	5	10	15	20	25
LOS/Hip-Chest in [3.1 5.1]GHz	3.66	3.10	2.93	2.86	2.85	2.85	2.85
LOS/Hip-Wrist in [3.1 5.1]GHz	4.07	3.18	2.91	2.76	2.72	2.70	2.69
NLOS/Hip-Wrist in [3.1 5.1]GHz	6.11	5.20	4.34	3.57	3.33	3.23	3.19
LOS/Hip-Chest in [3.75 4.25]GHz	5.43	4.59	4.09	3.91	3.91	3.91	3.91
LOS/Hip-Wrist in [3.75 4.25]GHz	7.19	4.23	4.09	4.08	4.08	4.08	4.08
NLOS/Hip-Wrist in [3.75 4.25]GHz	13.13	6.63	5.09	4.47	4.36	4.28	4.24

Table 3.1: Detailed variation of the standard deviation parameter (in cm) of the ranging error models, as a function of SNR and B, for both of the used on-body links under LOS and NLOS conditions.

Identified links	Corresponding semi-analytical model
LOS/Hip-Chest & Hip-Wrist in [3.1 5.1]GHz	$1.1 * exp(-0.2(SNR\|_{dB} + 5)) + 2.8$ (cm)
NLOS/Hip-Wrist in [3.1 5.1]GHz	$3 * exp(-0.1(SNR\|_{dB} + 5)) + 3.1$ (cm)
LOS/Hip-Chest & Hip-Wrist in [3.75 4.25]GHz	$2.2 * exp(-0.3(SNR\|_{dB} + 5)) + 4$ (cm)
NLOS/Hip-Wrist in [3.75 4.25]GHz	$8.8 * exp(-0.26(SNR\|_{dB} + 5)) + 4.3$ (cm)

Table 3.2: Semi-analytical models that corresponds to the variation of the standard deviation parameter (in cm) of the ranging error models, as a function of SNR and B, for both of the used on-body links under LOS and NLOS conditions.

3.2.4.3 Possible Generalization to Other On-Body Links

Since our described model considers the dynamic channel variations and preserves the natural relative power fluctuations due to body obstructions (i.e. for NLOS) over two representative on-body links (i.e. Hip-Wrist and Hip-Chest), it is worth illustrating the variation of the power transfer function over other on-body links. Relying on the same channel measurements campaign from [6], which has been briefly introduced in subsection 3.2.3.1, we have calculated the time-stamped power

transfer function $P(t)$ over two additional dynamic on-body links for which the true distance was unknown (i.e. Hip-Thigh and Hip-Foot), with the transmitters and the receivers placed as on Figure 3.12. Figure 3.13 then shows the dynamic variations of $P(t)|_{dB}$ over these four on-body links, for both [3.75, 4.25]GHz and [3.1, 5.1]GHz frequency bands. As it can be seen, $P(t)|_{dB}$ spans approximately in the same range for all the dynamic links (i.e. Hip-Wrist, Hip-Thigh and Hip-Foot). Moreover, the static link (i.e Hip-Chest) is characterized by a relatively stable $P(t)|_{dB}$ value as a function of the time stamp. The level is then approximately similar to that computed for dynamic links but restricted into their LOS areas. The previous observations indicate that the power transfer function relies mostly on the channel obstruction conditions and the dynamic range of investigated values is approximately the same though rather independent from the used dynamic links. Moreover, those results are also compliant with a previous remark about the relative stability of the ranging error over LOS and NLOS portions of a given walk. Finally, it is clear that $P(t)|_{dB}$ plays a critical role (through SNR normalization) with respect to the ranging error model parameters. Overall, it thus seems that the proposed error model, which has been based so far on two representative on-body links only, could be reasonably extended to other kinds of links experiencing similar power transfer conditions, being uniquely based on the LOS/NLOS and static/dynamic channel classifications.

3.3 Theoretical Modeling of Off-body and Body-to-Body Ranging Errors Based on N-B RSSI Estimation

As reminded in Chapter 1, the CRLB defines a lower bound on the variance of any unbiased estimator, given the conditional statistics (i.e. likelihood) of observations. More particularly, it has been shown that the CRLB of RSSI-based range estimates is given by equation (1.5) in the most generic case, where the RSSI has been modeled with equation (1.4), assuming that the transmit power, the reference path loss (at the reference distance) and the antenna gains are known, and that the shadowing (expressed in dB) is a Gaussian centered random variable with a known variance. Accordingly, the best ranging standard deviation is thus proportional to the ratio between the shadowing standard deviation and the path loss exponent σ_{sh}/n_p. Intuitively, a high ratio indeed implies that the dependency of the decrease of the average received power as a function of the log-distance separating the transmitter and the receiver is no longer significant nor dominating in comparison with the shadowing dispersion (i.e. around this mean power). This would make the interpretation of RSSI readings more challenging from a ranging perspective. Herein, we consider applying a similar CRLB expression for discussions, but using recent experimental channel model parameters (i.e. path loss and shadowing parameters) obtained over off-body and body-to-body links, which have been specified in the ISM band at 2.45 GHz.

Off-body links involve two kinds of wireless devices. The first one is placed on the body and the second one belongs to the surrounding infrastructure, most likely set

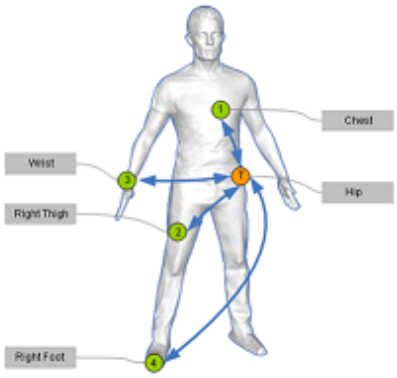

Figure 3.12: Scenario of the on-body measurements campaign carried out in [6], including four star links.

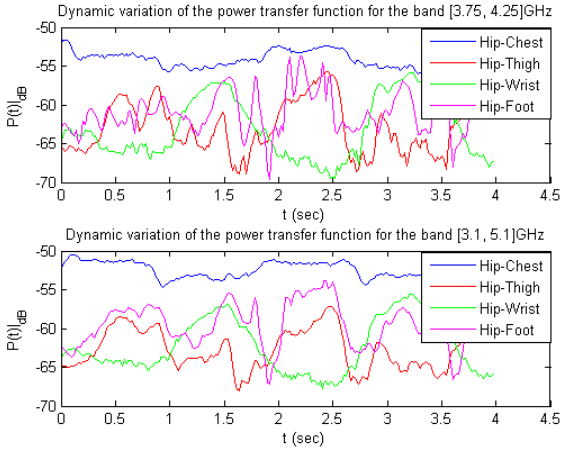

Figure 3.13: Dynamic variation of the power transfer function for 4 on-body links, in both frequency bands [3.75, 4.25]GHz (top) and [3.75, 4.25]GHz (bottom).

	LOS		NLOS	
	n_p	PL_0	n_p	PL_0
Rx heart	2	-38.92 dB	0.4	-62.62 dB
Rx left hip	2	-51.94 dB	0.1	-68.78 dB

Table 3.3: Path loss model parameters over indoor off-body N-B links at 2.45 GHz, according to [12].

as an anchor in our localization problem. These links are thus likely asymetric since on-body devices are subject to more drastic constraints in terms of transmission ranges and consumption, contrarily to elements of infrastructure.

Inspired from the off-body channel model in [12], which has been specified at 2.45 GHz according to the IEEE 802.15.4 standard, the used RSSI model can be simplified by eliminating the fast fading components (i.e. considering that one would average over a sufficient number of consecutive RSSI readings for each pair-wise link in a real system). The RSSI model is thus similar to equation (1.4), all except but the body shadowing, which mainly (and somehow deterministically) depends on the body orientation with respect to the external node. In a few scenarios however, frank LOS and NLOS configurations have been tested, with the subject body respectively facing or giving his back to the external node. Table 3.3 summarizes the corresponding parameters in an indoor environment for WBAN planar monopole antennas over two specific links, namely with on-body nodes positioned on the heart or on the left hip of the subject body.

On first remark is that the reference path loss is no longer unique but it rather strongly and adversely depends on both the on-body node's location and the antenna kind (depending on the antenna pattern). This is one more challenging point for off-body RSSI-based ranging. In other words, if this disparity can not be treated a priori as a nuisance and additional source of randomness (e.g. as part of an extended "shadowing" modeling), this practically implies that the reference path loss (again, assumed known by RSSI-based ranging algorithms) would have to be preliminarily calibrated out, not only once for all with one single reference on-body node in a given environment, but for each of the possibly occupied on-body locations, what is particularly time consuming. Another remark is that the path loss exponent $n_p < 1$ is very low in frank NLOS cases, whereas the measured power dispersion is large (on the order of 10 to 12 dB) showing that the randomness of the multipath contributions globally removes the distance dependency. But in practical cases, LOS/NLOS configurations cannot be classified so easily into binary cases over off-body (or even over body-to-body) links but there is a continuum of body shadowing configurations, as a function of the subject orientation, depending if the body partially or totally obstructs the propagation of direct radio waves. In [12] for instance, it has been shown that the power fluctuations observed over a full body rotation of 360 could be as large as 25 dB overall for a given on-body node's location (e.g. the hearth) and a given antenna (e.g. the planar monopole),

Relative Angle ()	0	45	90	135	180	225	270	315
Body Shad. (dB)	0	-2.77	-9.5	-27.34	-24.99	-17.03	-22.77	-12.4

Table 3.4: Mean body shadowing as a function of the body-to-external relative angle, over off-body N-B links at 2.45 GHz for a planar monopole antenna and an on-body device placed on the heart, according to [12].

regardless of the actual distance from the external node. In other words, from the RSSI-based ranging perspective, if the body shadowing term is still modeled as a Gaussian random variable after averaging over all the possible body orientations, with non-conditional statistics (i.e. regardless of LOS/NLOS), one could assume a standard deviation σ_{sh} on the order of 4 dB or more. For illustration purposes, Table 3.4 reports the mean body shadowing values observed as a function of the body-to-external relative angle, over off-body N-B links at 2.45 GHz for a planar monopole antenna and an on-body device placed on the heart. Considering similar results for the on-body device placed on the hip and for the same antenna, if one still wants to differentiate between LOS and NLOS cases, after partitioning respectively the results from [12] into the LOS and NLOS angular domains and considering the respective shadowing dispersions over each domain, it is thus reasonable to state that the standard deviation of the body shadowing term is around 1.5 to 2 dB in LOS and 3 dB in NLOS. Note that this representation would artificially lead to extra biases on the received power, accounting for the assumed centered regime around the mean of the body shadowing, which can be calibrated out (and likely incorporated in the original reference path loss parameter, conditioned on the LOS/NLOS obstruction configuration). As such, these extra mean terms would however not play a role in the CRLB prediction of equation (1.5).

So as to extend the discussion, still assuming that the body shadowing term ε_{sh} is a zero-mean Gaussian random variable for the evaluation of (1.5), we now carry out a parametric investigation of the conditional theoretical error model (i.e. the CRLB behaviour conditioned on LOS/NLOS and on-body device's location) as a function of the shadowing standard deviation σ_{sh}, which varies from 1 dB to 3 dB, and the real distance d separating on-body and external devices, which varies from 1 to 50 m, while relying on the n_p parameters from [12].

Figure 3.14 then shows the best achievable RSSI-based ranging error standard deviation under LOS conditions, for an on-body device placed on the heart or on the hip indifferently. This standard deviation seems to be rather penalizing, even for favorable σ_{sh} values on the order of 1.5 dB, as extracted from [12], but mostly at large transmission ranges in comparison with the actual distance (e.g. more than 5 m at 50 m). Figures 3.15 and 3.16 illustrate even more harmful effects due to NLOS conditions on off-body ranging performance at shorter ranges, especially for typical σ_{sh} values on the order of 3 dB, as extracted from [12]. Again, as shown in Table 3.3, the PL exponent n_p appears to be much smaller in NLOS than LOS conditions, meaning that the deterministic dependency of the received power on

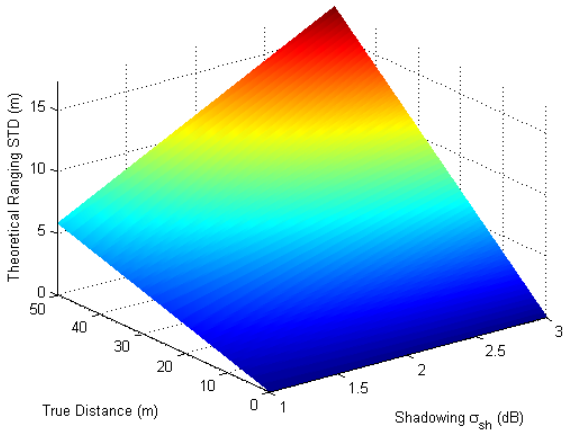

Figure 3.14: Best achievable RSSI-based ranging error standard deviation over off-body N-B links at 2.45 GHz, as a function of the actual distance and shadowing parameter, under LOS conditions, where the on-body device is either placed on heart or hip.

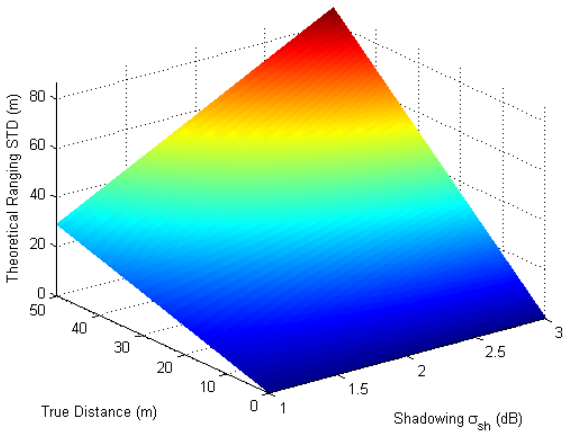

Figure 3.15: Best achievable RSSI-based ranging error standard deviation over off-body N-B links at 2.45 GHz, as a function of the actual distance and shadowing parameter, under NLOS conditions, where the on-body device is placed on heart.

	LOS		NLOS	
	n_p	PL_0	n_p	PL_0
Rx Heart	1.14	-54.02 dB	0.67	-70.77 dB
Rx Right Hip	3.33	-37.88 dB	1.15	-66.63 dB

Table 3.5: Path loss parameters over indoor body-to-body N-B links at 2.45 GHz for a Tx on the Right Hip (first carrying body) and a Rx on the Heart or the Right Hip (second carrying body), according to [13].

the true distance is no more significant but start being dominated by shadowing randomness (i.e. all the more dominated since the standard deviation is large). Accordingly, it is hard to interpret the received power for ranging purposes and the corresponding single-link errors are expected to be even larger. These results seem to confirm that RSSI cannot be reasonably considered as a meaningful location-dependent metric in NLOS cases due to hard body shadowing. Hence, RSSI shall be mainly recommended as an indirect source of ranging information over off-body links.

In [13], the authors have also proposed a new RSSI model for body-to-body links, inspired by the same underlying formalism as in equation (1.4). Table 3.5 summarizes the path loss parameters for a planar monopole antenna over two different specific body-to-body links in LOS and NLOS configurations, under the same relative angular definition as for off-body links (i.e. with one body experiencing a relative angle of 0 for LOS and 180 for NLOS, with respect to the second body). In first approximation, [13] has also considered the body shadowing as a zero-mean Gaussian variable, characterizing the corresponding standard deviation at around 6 dB over different body-to-body links and regardless of the LOS/NLOS regime. However, the behavior of the body shadowing clearly looks bi-modal instead in our own interpretation and understanding. Each of the modes actually corresponds either to the LOS case or to the NLOS case, respectively centered around +5 or -5 dB, and with a standard deviation on the order of that previously extracted for off-body links, that is to say, around 2 dB in LOS and slightly larger that 3 dB in NLOS. In other words, and in first approximation, the same kind of error regimes could be reasonably applied for both off-body and body-to-body links. Thus, similarly to the off-body discussion, we now carry out a parametric CRLB-based study of the best ranging standard deviation achievable over body-to-body links, still assuming that the body shadowing is a Gaussian variable with a standard deviation σ_{sh} that varies from 1 dB to 3 dB. Figures 3.17, 3.18, 3.19 and 3.20 show respectively the corresponding performance bounds over the two previous body-to-body links under LOS and NLOS conditions. The same observations and conclusions as in the off-body case can thus be drawn for off-body links, preventing from exploiting RSSI readings for direct ranging purposes over single links in NLOS configurations due to body shadowing.

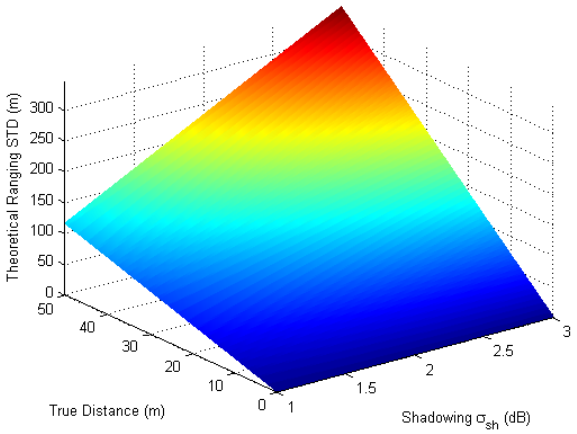

Figure 3.16: Best achievable RSSI-based ranging error standard deviation over off-body N-B links at 2.45 GHz, as a function of the actual distance and shadowing parameter, under NLOS conditions, where the on-body device is placed on hip.

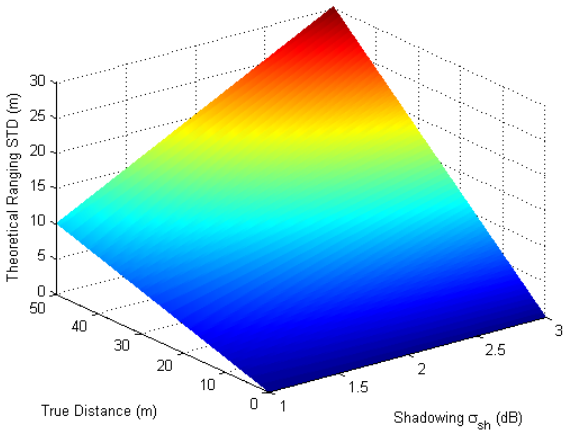

Figure 3.17: Best achievable RSSI-based ranging error standard deviation over body-to-body N-B links at 2.45 GHz, as a function of the actual distance and shadowing parameter, under LOS conditions, where the on-body devices are placed respectively on heart and hip of the two bodies.

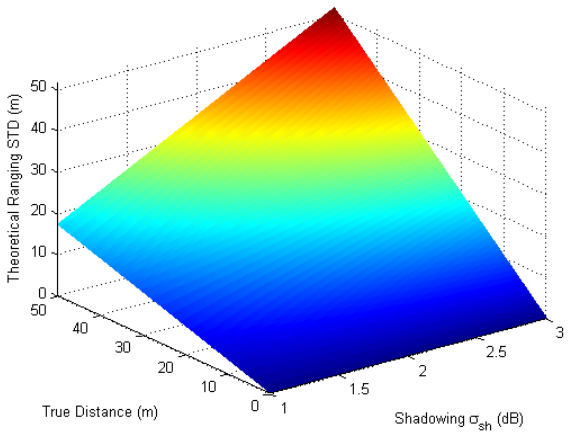

Figure 3.18: Best achievable RSSI-based ranging error standard deviation over body-to-body N-B links at 2.45 GHz, as a function of the actual distance and shadowing parameter, under NLOS conditions, where the on-body devices are placed respectively on heart and hip of the two bodies.

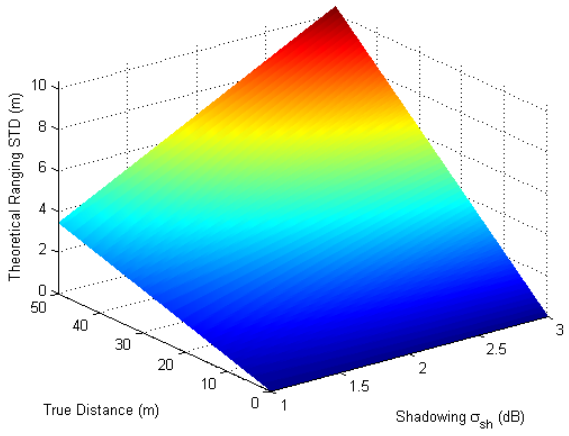

Figure 3.19: Best achievable RSSI-based ranging error standard deviation over body-to-body N-B links at 2.45 GHz, as a function of the actual distance and shadowing parameter, under LOS conditions, where the on-body devices are placed on the hips of the two bodies.

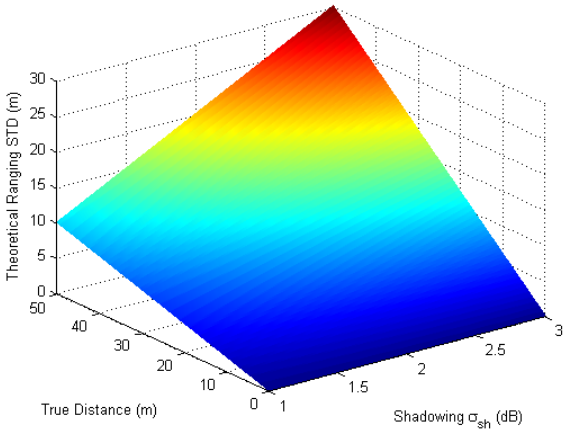

Figure 3.20: Best achievable RSSI-based ranging error standard deviation over body-to-body N-B links at 2.45 GHz, as a function of the actual distance and shadowing parameter, under NLOS conditions, where the on-body devices are placed on the hips of two bodies.

3.4 Theoretical Modeling of Off-body and Body-to-Body Ranging Errors Based on IR-UWB TOA Estimation

In Section 1.2.6, for simplification purposes and as a starting point for general discussions, we have conceptually illustrated the variation of the CRLB of unbiased TOA-based range estimators for a single pulse in a general AWGN case, as a function of the SNR and signal bandwidth. However, WBAN channels in typical indoor environments of interest are obviously considered as multipath channels, thus impacting the performance of TOA estimators. In [95], the authors have specifically characterized the CRLB of TOA estimators in UWB multipath signals. In this subsection, we thus consider computing such CRLB predictions over multipath off-body links, incorporating realistic CIR extracted after the processing of IR-UWB channel measurements. This CRLB evaluation will be performed in the [3.1, 5.1]GHz and [3.75, 4.25]GHz frequency bands. Note that the latter is compliant with one mandatory band imposed by the IEEE 802.15.6 standardization group.

We consider an experimental off-body measurement campaign described in [7], where the receiver was placed on the chest of a phantom representing the human body (with representative dielectric constants) and the transmitter was placed in the surrounding indoor environment in LOS. Figure 3.21 shows the off-body measurements scenario in [7], where the CIR is recorded in the band [3.1, 5.1]GHz at different distances separating the transmitter and receiver, spanning from 1 m to 8 m by a step of 1 m. For each response, the frequency-domain measurements was made available as an intermediary result for RF calibration purposes, and multipath components were extracted using a CLEAN-like high-resolution algorithm similar

to [93]. Each extracted CIR can hence be expressed as:

$$\hat{h}(d,\tau) = \sum_{j=1}^{\hat{L}_p(d)} \hat{\alpha}_j(d)\delta(\tau - \hat{\tau}_j(d)) \tag{3.11}$$

where $\hat{h}(d,\tau)$ is the CIR extracted at distance d as a function of the excess delay τ, $\hat{L}_p(d)$ is the number of extracted multipath components, $\hat{\alpha}_j(d)$ and $\hat{\tau}_j(d)$ are respectively the amplitude and delay of the j-th extracted multipath component at d.

Besides, rather similarly to the on-body modeling methodology presented in Section 3.2, Gaussian-windowed sine waves have been generated in the [3.1, 5.1]GHz and [3.75, 4.25]GHz bands and convolved with the extracted CIR. The latter frequency band is compliant with the channel 2 of the IEEE 802.15.4a standard [60], [96], as well as with one mandatory band imposed by the IEEE 802.15.6 standardization group. The corresponding reference templates normalized in energy have already been presented on Figure 3.2. The noise process in (3.1) is considered as an AWGN process with a two-sided power spectral density N_0 (i.e. $N_0 = -154\ dBm/Hz$) filtered in the transmitted signal band. Hence, the CRLB of any unbiased TOA estimator, as described in [95], has been computed, while assuming that the strongest path corresponds to the direct path between the transmitter and the receiver. For more mathematical details, readers are invited to look at Appendix A and [95]. Figures 3.22 and 3.23 show the best achievable TOA-based ranging error standard deviation as a function of SNR at different distances d, respectively in the [3.1, 5.1]GHz and [3.75, 4.25]GHz bands. It is noticeable that the theoretical bounds of ranging error is still inversely proportional to the bandwidth. Moreover, at a given SNR, it appears that the best ranging standard deviation is also proportional to the distance d separating the transmitter from the receiver. This phenomenon is mostly due to the fact that the number of multipath components increases at larger distances d (i.e. regardless of any imposed SNR value) and thus, for a given bandwidth, the resolution capability is altered, leading to the largest TOA-based ranging errors.

Based on the previous theoretical bounds, IR-UWB TOA estimation over off-body links in LOS conditions appears fully compliant with the requirements of both LSIMC and group navigation applications, at least from a strict resolution capability point of view and regardless of the hardware capabilities of real devices (e.g. sampling rate, antenna patterns...). For instance, with an effective bandwidth of 500 MHz, one could theoretically achieve an accuracy level of a few centimeters at $SNR = 0\ dB$ and $d = 8\ m$, as shown in Figure 3.23. Note that in the lack of NLOS channel measurements in this context however, a priori assumptions will have to be made in the following, regarding the biases introduced by body shadowing over off-body and body-to-body TOA-based range measurements.

Finally, considering the same transmitted impulse waveforms, and assuming that body-to-body links would experience similar multipath CIR conditions in comparison with off-body links, then the theoretical bounds for TOA-based ranging errors

over body-to-body links are expected to be approximately on the same order of magnitude.

Figure 3.21: UWB off-body measurement scenario in a typical indoor environment [7].

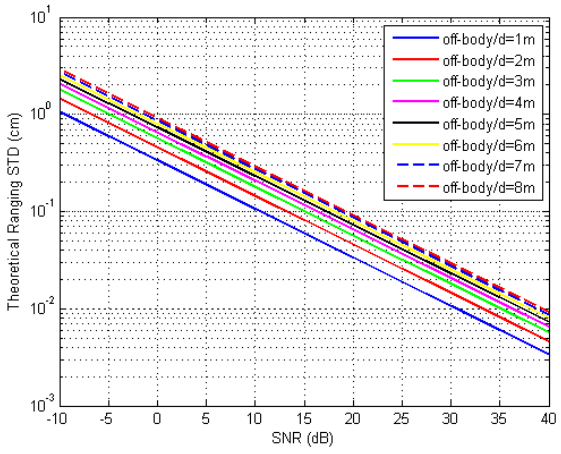

Figure 3.22: Best achievable IR-UWB TOA-based ranging error standard deviation as a function of SNR (dB), at different distances between the transmitter and the receiver in the band [3.1, 5.1]GHz.

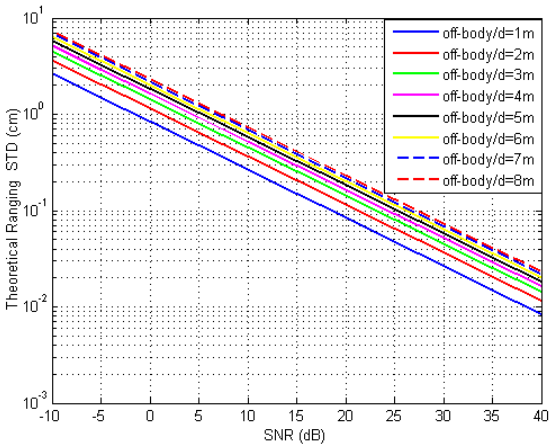

Figure 3.23: Best achievable IR-UWB TOA-based ranging error standard deviation as a function of SNR (dB), at different distances between the transmitter and the receiver in the band [3.75, 4.25]GHz.

3.5 Conclusion

In this Chapter, we have characterized and discussed possible single-link ranging error representations, exploiting recent WBAN IR-UWB and N-B channel measurements. These models rely on empirical modeling or theoretical CRLB-based predictions, fed with realistic channel parameters.

First of all, a dynamic on-body model has been proposed for IR-UWB TOA-based ranging in two key frequency bands and for two representative links. This personal contribution has led to the publication of one conference paper [44] and one journal paper [45]. The drawn model, which relies on UWB channel measurements, takes into account dynamic channel obstruction configurations (i.e. LOS/NLOS) and SNR variations under body mobility. Then the related model parameters have been studied as a function of a controlled SNR within synthetic received multipath signals. On this occasion, false and missed detection phenomena have been illustrated under low SNR and NLOS conditions, as well as asymptotically ideal detection behaviour under more favourable SNR and LOS conditions. The performances of first peak and strongest peak detection schemes have also been compared. We have shown that the ranging error distribution could be fairly well modeled as a centered Gaussian distribution in LOS conditions in case of systematic strongest path detection, and as a weighted mixture between uniform and Gaussian distributions in the case of first path detection. In NLOS conditions, ranging errors are also shown to follow a weighted mixture between uniform and Gaussian distributions in case of strongest path detection. Finally, based on the variations of the channel power transfer function observed over various on-body links and nodes' placements, a few insights have been provided for a possible extension of the previous error model to

any on-body link, depending on its instantaneous LOS/NLOS and static/dynamic status. This overall on-body model could be used for both absolute and relative nodes positioning at the body scale for individual motion capture applications. In the following however, in the lack of adequate simulation tool to generate exact time-stamped $SNR(t)$ values under mobility, the model will be simplified by using a Gaussian model, with a constant standard deviation independently of the SNR, but still in the range of the values observed over the walk cycle within the previous refined representation. Moreover, it will be assumed that the range measurements in NLOS are affected by one more positive bias that follows a uniform distribution, which is also partly compliant with the previous NLOS representation. The resulting simplified model will be used in Chapter 4 to evaluate the performance of on-body localization algorithms for relative and absolute individual MoCap purposes. Note that further comparisons will be made with the single-link statistics of on-body range measurements issued at real IR-UWB integrated platforms in Chapter 6.

Secondly, representative lower bounds have been derived for the standard deviation of N-B RSSI-based and IR-UWB TOA-based range measurements over off-body and body-to-body links. One first conclusion, as expected, is that RSSI readings in NLOS conditions due to body shadowing are hardly exploitable for ranging purposes on both kinds of links, whereas LOS conditions may provide more acceptable ranging performance, but most likely at short ranges (typically below 20 m). One second remark is that off-body and body-to-body links exhibit approximately the same behaviours in terms of ranging error statistics, in first approximation. The underlying path loss and body shadowing parameters will be reused for the simulations presented in Chapter 4 and 5, while evaluating the performance of localization algorithms for MoCap and group navigation applications.

Finally, after extracting realistic CIR out of recent UWB multipath channel measurements over off-body links in a LOS configuration, theoretical bounds for the IR-UWB TOA-based ranging standard deviation have also be calculated in two representative frequency bands at various distances, showing fine accuracy over a large range of practical SNR values. These results have been generalized to body-to-body links in first approximation. In the lack of NLOS measurement data however, in the following Chapters, additional assumptions will be made regarding the NLOS bias experienced under body shadowing in the very IR-UWB TOA-based ranging case (by nature, even more sensitive than RSSI to the specular nature of multipath components).

4

Chapter 4

Localization Algorithms for Individual Motion Capture

Contents

4.1 Introduction

Under mesh or quasi-mesh WBAN topologies (possibly coupled with off-body links with respect to the infrastructure), mobile on-body nodes can be localized in a cooperative fashion out of peer-to-peer range measurements. As seen in Chapter 1, the enabled individual MoCap applications can be classified according to the two following categories.

- "Relative On-Body Nodes Positioning" (i.e. relative MoCap): On-body mobile (or blind) nodes are located relatively to reference anchor nodes, which are attached onto the body at known and reproducible positions (i.e. independently of the body attitude and/or direction), forming a *Local Coordinate System* (LCS);
- "Absolute On-Body Nodes Positioning" (i.e. LSIMC): The *Global Coordinates System* (GCS) used to express the estimated on-body nodes' locations is no longer body-strapped but external to the body. Anchor nodes are fixed elements of infrastructure disseminated at known locations in the environment.

In this new Chapter, we describe and evaluate (through simulations) some localization algorithms adapted to the relative and/or absolute positioning of on-body nodes.

Section 4.2 deals with relative positioning first. A decentralized DWMDS localization algorithm [65], [97] is adapted into the new body sensor network context. Accordingly, on-body nodes are asynchronously updated with respect to their 1-hop neighbors in a body-strapped LCS. This approach is expected to provide better immunity against the latency observed within classical centralized and synchronous schemes, while enabling adaptability to local nodes velocity (e.g. in terms of refreshment rate). The nominal algorithm is fed with all the cooperative peer-to-peer distance measurements available in our mesh topology. According to one first enhancement, one incorporates the links that experience fixed lengths despite body mobility (e.g. between the hand's wrist and the elbow) as geometrical constraints in the positioning problem, thus leading to a *Constrained* algorithm (CDWMDS). This solution tends to limit the number of required on-line measurements and hence, to reduce over-the-air traffic and power consumption. Furthermore, while updating the locations of on-body nodes, the history of the latest estimates is used as prior information, so as to ease convergence and benefit from space-time correlation effects under continuous body movements. We also describe additional improvements of the nominal CDWMDS formulation in this section. One of them consists in applying unilateral censoring and/or scheduling of the most demanding nodes when updating estimated positions. Another point is to force the measurements symmetry for each pair of on-body nodes. The idea is to mitigate the effect of outliers or packet losses, but also to avoid error propagation and divergence issues in the retained decentralized positioning approach. Then, we apply an existing beacon-aided *Time Division Multiple Access* (TDMA) scheme that supports both peer-to-peer ranging and decentralized positioning transactions under real-time constraints. On this occasion, we make possible a more realistic performance assessment of the algorithm, while accounting for underlying latency issues and investigating the impact of network connectivity or measurements quality. Finally, we compare our solution with a more conventional *Multidimensional Scaling* (MDS) algorithm, which has been recently considered for MoCap applications in a similar WBAN context [61]. Note that the latter requires that the matrix of measured distances is completed under partial network connectivity, contrarily to our proposed asynchronous and decentralized approach.

Secondly, Section 4.3 concerns absolute positioning for LSIMC applications. We consider combining relative motion capture (i.e. at the body scale) and absolute single-user navigation (i.e. at the building scale) capabilities within an heterogeneous WBAN context. One goal is that off-body localization procedures could mutually benefit from each other, while preserving the finest precision of relative localization over large-scale trajectories, contrarily to the first cooperative localization attempt in [8], where the precision of relative localization at the body scale was degraded by the introduction of off-body links. Different options and scenarios are then compared in terms of location-dependent radio metrics (i.e. TOA, TDOA,

RSSI), synchronization constraints and transmission ranges. We also describe a specific 2-step algorithm, which first performs the relative localization of on-body nodes in the body-strapped LCS according to the previous CDWMDS algorithm, before applying transformations to express the estimated coordinates into an absolute GCS. We also take advantage of the presence of multiple on-body nodes to mitigate body obstructions and packet losses with respect to external anchors through distance approximations based on graph neighborhood information and distance completion methods.

Finally, Section 4.4 summarizes the chapter.

4.2 Relative On-Body Localization at the Body Scale

First we remind that the wireless devices placed on the body are classified into two categories. Simple mobile *nodes* with unknown positions (under arbitrary deployment) must be located relatively to reference *anchors* nodes, which are attached onto the body at known and reproducible positions, independently of the body attitude and/or mobility (e.g. on the chest or on the back). A set of such anchors defines a stable Cartesian LCS, which remains unchanged under body mobility. Mobile nodes are then located in the LCS, using peer-to-peer range measurements between pairs of devices (i.e. between mobile nodes or between nodes and fixed anchors).

Figure 4.1 shows a typical deployment scenario. In the following, $\{X_i(t)\}_{i=1...m}$ represents the $3D$ known positions of the m anchors at time t defined into the LCS, where m should be equal or larger than 3. $\{X_i(t)\}_{i=m+1...m+n}$ represents the set of the true $3D$ unknown positions of the n mobile nodes deployed on the body, at time t. Let $\widetilde{d}_{ij}(t)$ be a range measurement available at time t between nodes i and j and let l_{ij} be one constant distance (i.e. constant over time under body mobility), which will be considered hereafter as a constraint.

Given all the available range measurements, e.g. based on IR-UWB TOA estimation [34], [44], on existing constraints related to the body geometry and on the known anchors' locations, the problem that we want to solve is to estimate the positions of the mobile nodes into the LCS.

4.2.1 Relative Localization Algorithms

4.2.1.1 Conventional Multi-Dimensional Scaling (MDS)

Applied into our localization problem, the goal of MDS is to find the positions of on-body nodes so that the distances between the estimated positions fit as much as possible to a set of cooperative range measurements between the nodes. Classical MDS formulations are characterized by three basic steps, as follows. The first step consists in constructing a squared distances matrix. The second step consists in locating the nodes into a reference system, which is defined by a geometrical transformation of the LCS (i.e. rotation and translation). The third step is the restoration of the coordinates system by changing the basis of the positions estimated at the

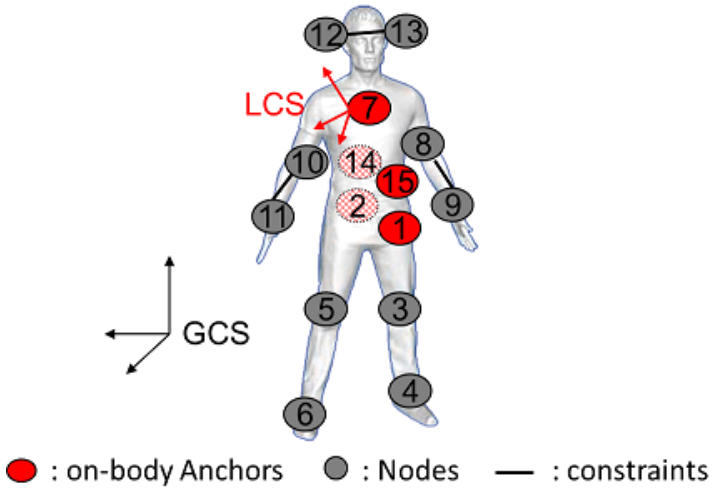

Figure 4.1: Typical deployment scenario for the relative localization of on-body wireless nodes (grey circles) with respect to a body-strapped Local Coordinate System (LCS) defined by fixed anchors (red circles).

second stage [67], [98].

First we form the overall network-level collection of on-body nodes' positions $X(t) = [X_1(t), ..., X_m(t), X_{m+1}(t)..., X_{m+n}(t)]$ at time t, including the n on-body mobile nodes and the m anchors. Assuming full network connectivity (i.e. all pairwise distance measurements are available) and that the observed distance $\delta_{ij}(t)$ between each pair of nodes i and j at time t is equal to the true corresponding distance, it comes:

$$\delta_{ij}^2(t) = d_{ij}^2(t) = (X_i(t) - Xj(t))^T(X_i(t) - Xj(t)) \tag{4.1}$$

Writing the squared distance as $d_{ij}^2(t) = X_i(t)^T X_i(t) - 2X_i(t)^T X_j(t) + X_j(t)^T X_j(t)$, and placing the centroid of the configuration at the origin, the matrix of inner products between the nodes can be expressed as follows:

$$B = X(t)X(t)^T = -\frac{1}{2}HDH \tag{4.2}$$

$$H = I - \frac{1}{n+m}\mathbf{e}^T\mathbf{e} \tag{4.3}$$

where $D = [d_{ij}^2(t)]_{i,j}$ and $\mathbf{e}$ is a $1 \times (n+m)$ vector of ones. Since B is symmetric, positive semi-definite and of rank dimensionality, it can now be written in terms of singular value decomposition as $B = UVU^T$, where V is a diagonal matrix containing the $n+m$ eigen values of B and U is the corresponding matrix of eigen vectors. Thus as $X(t)X(t)^T$, $X(t)$ is now given as:

$$X(t) = UV^{\frac{1}{2}} \tag{4.4}$$

On major problem with this classical MDS algorithm is the need for complete and noise-free distances matrices, with a full knowledge of all the pairwise distances, what is highly unlikely in realistic wireless cases (e.g. due to connectivity losses or deliberate topology restrictions). Nevertheless, such classical MDS formulation has already been considered for WBAN localization in [61], where coarse geometric constraints, relying on the prior knowledge of minimal and maximal feasible distances under radio connectivity, have been introduced to complete empty entries of the input range measurements matrix. Another problem more generally inherent within centralized approaches is the latency effect (i.e. the time elapsed between the collection of the distance measurements and the delivery of location estimates), whereas the body gesture can change rapidly during the measurements collection step, hence degrading significantly localization performances.

Motivated by the possibility to operate under partial connectivity and possibly large measurement errors, by latency reduction gains and by the natural asynchronism potential enabled for node's localization, we thus seek to estimate the nodes' positions using a distributed version of the MDS instead, as seen hereafter. A comparison between the classical MDS algorithm used in [61] and our distributed version will be presented in terms of localization accuracy in Section 4.2.3.

4.2.1.2 Proposed Constrained Distributed Weighted Multidimensional Scaling Algorithm (CDWMDS)

As seen in Chapter 2, the *Distributed Weighted Multi-Dimensional* (DWMDS) algorithm is a solution to the minimization problem of the following global stress function [67]:

$$S(t) = \sum_{1 \leq i \leq n} [\sum_{i < j \leq n+m} w_{ij}(t)(\delta_{ij}(t) - d_{ij}(X(t))^2 + r_i(t)||X_i(t) - \overline{X}_i(t)||^2] \quad (4.5)$$

where $X_i(t)$ is still a vector containing the $3D$ coordinates of node i, n and m are respectively the number of blind nodes with unknown locations and the number of anchors placed on the body, $X(t)$ is the matrix whose columns contain the positions for all the nodes at time t, $\delta_{ij}(t)$ is a so-called observed distance between node i and j at t, $d_{ij}(X(t))$ denotes the true Euclidean distance between i and j, which is equal to $\sqrt{(X_i(t) - X_j(t))^T(X_i(t) - X_j(t))}$, $w_{ij}(t)$ is a weight value, which reflects the connectivity and the accuracy of the range measurements between nodes i and j at time t, so that inaccurate measurements are down-weighted in the cost function, $\overline{X}_i(t)$ is a vector reflecting prior information about the position occupied by node i at time t, while $r_i(t)$ quantifies the reliability of such prior information. Equation (4.5) differs from a standard formulation of an MDS stress function, by the penalty term that accounts for the prior knowledge on the occupied positions.

After simple manipulations, S can be rewritten as a sum of local contributions as follows:

$$S(t) = \sum_{i=1}^{n} S_i(t) + c, \quad (4.6)$$

where $S_i(t)$ is a local cost function defined for each node i $(1 \leq i \leq n)$

$$\begin{aligned} S_i(t) &= \sum_{j=1}^{n} w_{ij}(t)(\delta_{ij}(t) - d_{ij}(X(t)))^2 + \sum_{j=n+1}^{n+m} 2w_{ij}(t)(\delta_{ij}(t) - d_{ij}(X(t)))^2 \\ &+ r_i(t)||X_i(t) - \overline{X}_i(t)||^2 \end{aligned} \tag{4.7}$$

As described in [65] and [99], the DWMDS thus allows each node i with unknown coordinates to localize itself by minimizing the defined local cost function $S_i(t)$ (i.e. $\hat{X}_i(t) = \underset{X_i(t)}{\operatorname{argmin}} S_i(t)$, where $\hat{X}_i(t)$ is a vector containing the $3D$ estimated position of node i). Unfortunately, no closed form exists for the minimum of $S_i(t)$. However, based on the neighbors information, $S_i(t)$ can be minimized iteratively using quadratic majorizing functions as in *SMACOFF* (Scaling by Majorizing a complicated function [100]). More details about the minimization process are given in [99]. As described in [65], at each time t, the dynamic equation (4.7) is iteratively resolved to estimate the nodes' positions. If $\hat{X}^{(k)}(t)$ is the matrix of the estimated positions at iteration k, node i derives its current coordinates update $\hat{X_i}^{(k)}(t)$ as follows:

$$\hat{X_i}^{(k)}(t) = a_i(t)(r_i(t)\overline{X}_i(t) + \hat{X}^{(k-1)}(t)\mathbf{b}_i^{(k-1)}(t)) \tag{4.8}$$

where

$$a_i(t) = \sum_{j=1}^{n} w_{ij}(t) + \sum_{j=n+1}^{n+m} w_{ij}(t) + r_i(t) \tag{4.9}$$

and $\mathbf{b}_i^{(k)}(t) = [b_1(t), ..., b_{n+m}(t)]$ is a vector whose entries are given by

$$\begin{aligned} b_j(t) &= w_{ij}(t)[1 - \frac{\delta_{ij}(t)}{d_{ij}(X^{(k)}(t))}] \qquad j \leq n, j \neq i \\ b_i(t) &= \sum_{j=1}^{n} \frac{w_{ij}(t)\delta_{ij}(t)}{d_{ij}(X^{(k)}(t))} + \sum_{j=n+1}^{n+m} \frac{w_{ij}(t)\delta_{ij}(t)}{d_{ij}(X^{(k)}(t))} \\ b_j(t) &= 2w_{ij}(t)[1 - \frac{\delta_{ij}(t)}{d_{ij}(X^{(k)}(t))}] \qquad j \geq n \end{aligned} \tag{4.10}$$

We point out that unlike the centralized SMACOF algorithm described in [100], the computation of (4.8) does not need to evaluate of an $n \times n$ Moore-Penrose matrix inverse.

So as to adapt this initial DWMDS formulation into the WBAN relative localization context, we propose first to take benefits from trivial geometric specificities of the human body, but without necessitating prior knowledge such as parametric models (e.g. techniques requiring articulated chains) or specific deployment patterns. Fixed-length links identified on the body are introduced as constraints while positioning (e.g. the link between the wrist and elbow on Figure 4.1), thus leading to the *Constrained* DWMDS solution (CDWMDS). More particularly, the basic idea is to substitute the distance $\delta_{ij}(t) = \widetilde{d}_{ij}(t)$ that would be measured between

	DWMDS	CDWMDS
Fixed links	$\delta_{ij}(t) = \widetilde{d}_{ij}(t)$	$\delta_{ij}(t) = l_{ij}$
Mobile links	$\delta_{ij}(t) = \widetilde{d}_{ij}(t)$	$\delta_{ij}(t) = \widetilde{d}_{ij}(t)$

Table 4.1: Comparison of the range observations used by DWMDS and CDWMDS algorithms.

nodes i and j at time t by an approximated version $\delta_{ij}(t) = l_{ij}$ over the same fixed length link, which is considered as time invariant, that is to say, independent of the body gesture, moving direction and velocity. Advantageously, during a first pre-calibration phase (already under body mobility), such fixed links can be detected and approximated distances can be learnt once for all by averaging repeated instantaneous measurements over a few time stamps, e.g. $l_{ij} = \frac{1}{N_{Cal}} \sum_{t=-N_{Cal}}^{-1} \widetilde{d}_{ij}(t)$. In this case, calibration data is collected for $t = -N_{Cal}, ..., -1$ if the localization is expected to start at $t = 0$. One claimed advantage with this proposal is that no more ranging measurements are required for these links in the steady-state localization regime. Besides localization accuracy considerations, CDWMDS hence leads to a reduction of the number of exchanged packets, and accordingly, an expected reduction of both latency and energy consumption. Note that alternatively, in case of suspected distance variability during the localization steady-state phase, the average approximation could be periodically recomputed on the wing within a sliding window, i.e. at time stamp t, $l_{ij}(t) = \frac{1}{N_{Cal}} \sum_{t'=t-N_{Cal}}^{t-1} \widetilde{d}_{ij}(t')$. As an example, in Appendix B, we propose a method to adaptively detect these on-body fixed-length links, out of the observed distance measurements. A binary decision is made (i.e. between fixed-length or mobile-length links) based on the empirical variance of the distances observed over a specified link. Table 4.1 summarizes the main differences between DWMDS and CDWMDS algorithms.

Another straightforward improvement consists in taking the latest estimated position available for node i at time $t-1$, as *a priori* information for initialization purposes in its local current cost function, i.e. assuming $\overline{X}_i(t) = \hat{X}_i(t-1)$ at t. The choice accounts for the bounded motion amplitudes of on-body nodes under human mobility. Hence, one can benefit from the space-time correlation of the true mobile location under body mobility, while speeding up convergence over k at each time stamp t.

In the following, the two previous proposals will be depicted as the nominal CDWMDS. In the next subsection we will describe a set of additional enhancements to avoid error propagation in the retained asynchronous and decentralized approach, as well as to reduce the effects of measurement outliers and packet losses.

4.2.1.3 Further Improvements

Unidirectional Censoring of Peripheral Nodes' Transmissions One first goal is to mitigate error propagation while updating nodes locations. It has been illustrated in [46] that the locations estimated for the peripheral nodes are affected

by significantly higher errors. It indeed appears that those nodes, typically located at the network edges (e.g. on the ankle) are the most rapid ones -or at least, those subject to the highest accelerations-, less connected -even if the transmission range ensures that they have more than three connected neighbours, so that their estimated locations are not ambiguous- and experiencing poor *Geometric Dilution Of Precision* (GDOP) -for being peripheral and located outside the convex hull defined by on-body anchors-.

Hence, one proposal is to allow only the update of such fast nodes with respect to their 1-hop neighbors but no updates of these neighbors with respect to the fast nodes in return, i.e. performing some kind of unidirectional censoring. The expected gains are two-fold: keep on benefiting at rapid nodes from the reliability of their slow neighbors' estimates, but also improve the average location accuracy in the entire network by avoiding error propagation from less reliable rapid nodes. In equation (4.7), the unidirectional censoring of any rapid node j would be practically applied by forcing the weight function $w_{ij}(t)$ to be null with respect to any neighboring on-body node i (i.e. $w_{ij}(t) = 0, \forall\ j \leq n$ whereas $w_{ji}(t) \neq 0$).

In the following, this proposal will be depicted as "Enhancement 1".

Scheduling of Location Updates The objective here is still to avoid error propagation, by forcing the algorithm to converge properly first after updating in priority the most reliable (and thus the slowest) nodes. Hence, rapid nodes benefit from the consolidated reliability of their slow neighbors' estimates and error propagation is minimized accordingly. Practically, considering a coordinated medium access of the multiple on-body nodes, as it will be seen hereafter, where all the protocol transactions shall be scheduled anyway (i.e. for both range measurements and position updates), one can keep track of the approximated nodes' speeds on the coordinator side, based on the latest available position estimates. Hence, at each new time stamp (and hence, at each superframe), one can draw an ordered list, setting the nodes to be updated in priority. Finally, one more degree of freedom concerns the number of updates per node per localization cycle (i.e. per superframe) or equivalently, the refreshment rate, which can be also dynamically increased for the most demanding nodes.

In the following, this proposal will be depicted as "Enhancement 2".

Forced Measurements Symmetry The objective here is to jointly mitigate measurement outliers and packet losses. Hence, we propose to force the distance measurements for each pair of nodes into being symmetric, as follows:

$$\delta_{ij}(t) = \delta_{ji}(t) = \frac{w_{ij}(t)\delta_{ij}(t) + w_{ji}(t)\delta_{ji}(t)}{w_{ij}(t) + w_{ji}(t)} \tag{4.11}$$

Practically, once the peer-to-peer range measurements between two nodes i and j are recovered independently in both directions (i.e. $\delta_{ij}(t)$ or $\delta_{ji}(t)$), our proposal consists in sharing the related information between each pair of nodes in order to mitigate possible packet losses (and thus missed measurements) that may occur

during the ranging transactions. Moreover, if we suppose that the distance observed by node i from node j is strongly affected by measurement noise and/or bias (i.e. $\delta_{ij}(t)$) but that the distance observed by node j is less noisy, outliers are mitigated or more generally speaking, the resulting apparent measurement variance is divided by a factor 2 after averaging, even in case of identically biased distance.

In the following, this proposal will be depicted as "Enhancement 3".

4.2.2 Medium Access Control For Localization-Enabled WBAN

In our WBAN localization context, one key feature of the *Medium Access Control* (MAC) is to enable ranging between the nodes, as well as further exchanges of any kind of location-dependent information. In [101] a beacon-aided TDMA superframe has been presented, which was adapted for WBAN applications running on top of the IEEE 802.15.4 radio standard. Figure 4.2 represents the MAC superframe used in [8] (and inspired from [101]) adapted for localization purposes. In our work, we also consider using this MAC superframe.

As shown in Figure 4.2, the superframe structure is delimited by a beacon, which is transmitted periodically by the coordinator (e.g. possibly one on-body anchor here) to all the nodes in order to resynchronize all the WBAN (i.e. indicating the beginning of the superframe). The beacon fully describes the MAC superframe, specifying the *Time Slot*s (TSs) allocated for each transmitting node and further information about the current network status. The *Contention Access Period* (CAP) is devoted to contention-based transmissions, while the *Contention Free Period* (CFP) is composed of guaranteed TSs allocated by the coordinator. During the inactive period, the nodes may enter in a sleep mode to reduce energy consumption. The peer-to-peer range information is derived from RT-TOF estimation, which relies on *2-Way Ranging* (2-WR) or *3-Way Ranging* (3-WR) handshake protocol transactions and unitary TOA estimates for each involved packet [32], as already seen in Chapter 1. Two guaranteed TSs are involved in the case of 2-WR protocol to investigate the peer-to-peer range measurements between two nodes i and j, where node i sends its request packet inside the assigned TS at time $\widetilde{T}_{i0}$. Once this packet is received by node j at time $\widetilde{T}_{j0}$, node j sends its response back to the requester node i inside its own dedicated TS at time $\widetilde{T}_{j1}$, after a known time of reply. Node i will receive this packet at time $\widetilde{T}_{i1}$. Hence, the estimated RT-TOF through 2-WR is simply given as follows:

$$\widetilde{TOF} = \frac{1}{2}[(\widetilde{T}_{i1} - \widetilde{T}_{i0}) - (\widetilde{T}_{j1} - \widetilde{T}_{j0})] \tag{4.12}$$

So as to estimate and compensate possible clock drift effects, the responder node j can transmit one additional packet inside a third TS at time $\widetilde{T}_{j2}$. This packet will be received by node i at time $\widetilde{T}_{i2}$, and hence a new 3-WR protocol is considered. Figure 4.3 shows a simplified representation of the ranging transactions within 3-WR. In the specific case when the first response duration is equal to the slot duration, the

final corrected RT-TOF estimate can be simply built as follows:

$$\begin{aligned} \widetilde{TOF} &= \frac{1}{2}[(\widetilde{T}_{i1} - \widetilde{T}_{i0}) - (\widetilde{T}_{j1} - \widetilde{T}_{j0})] \\ &- \frac{1}{2}[(\widetilde{T}_{i2} - \widetilde{T}_{i1}) - (\widetilde{T}_{j2} - \widetilde{T}_{j1})] \end{aligned} \tag{4.13}$$

Besides the local timer values associated with the intermediary TOA estimates, which are required to compute the RT-TOF (possibly corrected or not), the payload of the ranging packets can be advantageously exploited to carry additional information related to positioning (e.g. to collect local estimated positions to the coordinator for synchronous display, to exchange pair-wise ranges in case of forced measurements symmetry as seen before...).

Finally, note that *Aggregate-and-Broadcast* (A-B) procedures can be optionally applied to ranging packets [32], [102] so as to limit the localization-specific over-the-air traffic and especially, the number of required slots to perform all the possible pair-wise measurements in a mesh configuration. Accordingly, under full connectivity, $3n + 2m$ transmission slots would be required to guarantee ranging transactions between any pair of nodes, instead of $2n(n+m-1)$ otherwise. Such A-B procedures enable to share time resource in such a way that each node initiates specific ranging transactions with all the other nodes, and each transmitted packet can play different roles (i.e. either a request, or a response, or even a drift correction packet, depending on the receiving neighbor status and current step in the 3-Way procedure).

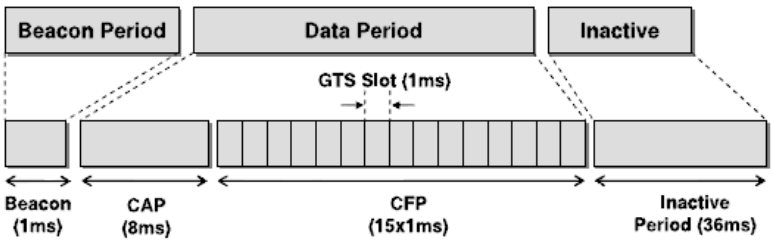

Figure 4.2: Beacon-aided TDMA MAC superframe format supporting the localization functionality [8].

4.2.3 Simulations and Results

4.2.3.1 Scenario Description

In our evaluation framework, human mobility is based on a mixed model, like in [101]. A first macroscopic mobility *Reference Point Group Mobility Model* (RPGM) accounts for the body center mobility, where the reference point as a function of time is a Random Gauss Markov process [8], [103]. The intra-WBAN mobility pattern is based on a biomechanical cylindrical model [104]. The body extremities are modeled as articulated objects, which consist of rigid cylinders connected to

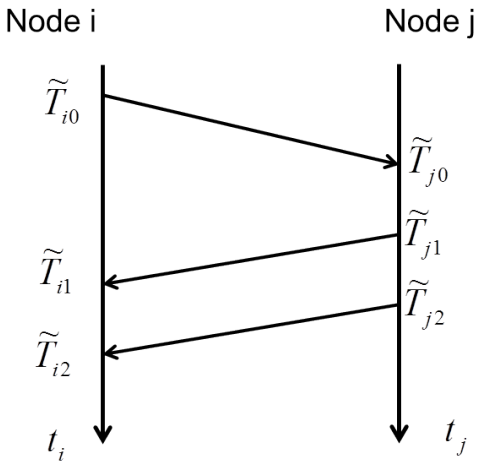

Figure 4.3: Peer-to-peer measurement procedure between nodes i and j through 2- and 3-Way ranging protocols, applying TOA estimation for each received packet.

each other by joints. A snapshot of the resulting articulated body under pedestrian mobility is represented in Figure 4.4 at an arbitrary time stamp. This biomechanical model enables the generation of true inter-node distances and obstruction conditions, whatever the time stamp.

In our scenario, for each random realization, the reference body moves in a 20m×20m×4m $3D$ environment with a constant speed of 1 m/sec for a duration of 80 sec. The network deployment is similar to that presented in Figure 4.1, where 5 anchors are positioned at fixed locations relatively to the LCS and 10 blind mobile nodes with unknown positions must be positioned.

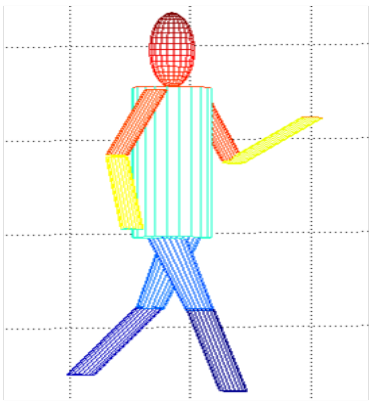

Figure 4.4: Snapshot of the biomechanical mobility model based on a piece-wise cylindrical representation and used for the generation of realistic inter-node distance measurements under body mobility.

4.2.3.2 Simulation Parameters

Regarding the physical radio parameters, we assume in first approximation that the received power is larger than the receiver sensitivity, enabling peer-to-peer communication links with a worst-case *Packet Error Rate* (PER) of 1 %, as specified by the IEEE 802.15.6 WPAN Task Group 6 [11]. This PER figure is applied onto 3-way ranging protocol transactions to emulate incomplete ranging (i.e. whenever 1 packet is lost out of 3). Inspired by the TOA-based IR-UWB ranging error model described in Chapter 3 and [44], [45], which has been specified in the IEEE 802.15.6 mandatory band centered around 4 GHz with a bandwidth of 500 MHz, ranging errors are added depending on the current LOS or NLOS channel configuration at time stamp t, as follows:

$$\begin{aligned} \widetilde{d}_{ij}(t) &= d_{ij}(t) + n_{ij}(t) \qquad && if\ LOS \\ \widetilde{d}_{ij}(t) &= d_{ij}(t) + n_{ij}(t) + b_{ij}(t) \qquad && if\ NLOS \end{aligned} \tag{4.14}$$

where $\widetilde{d}_{ij}(t)$ and $d_{ij}(t)$ are respectively the measured and the real distance between nodes i and j at time t, $n_{ij}(t)$ is a centered Gaussian random variable with a standard deviation σ, and $b_{ij}(t)$ is a bias term due to the absence of direct path when estimating TOA.

Simplifying the model from Chapter 3 and [44], [45], our first simulations are carried out using a constant σ equal to 10 cm, independently of $SNR(t)$, but still in the range of the values observed out of real measurements. $b_{ij}(t)$ is a positive bias added only into NLOS conditions, which follows a uniform distribution in [0, 10]cm, considering that the valid Rx observation would be restricted around the temporal synchronization point (i.e. applying temporal filtering of the multipath components). Moreover, $b_{ij}(t)$ is assumed constant over one walk cycle in first approximation (i.e. $b_{ij}(t) = b_{ij}, \forall t$), which is also in compliance with the first empirical observations in Chapter 3 and [44], [45] with dynamic links over NLOS portions (i.e. with reproducible bias from one walk cycle to the next).

Concerning the settings of the CDWMDS algorithm, three fixed-length link constraints are imposed, as materialized with black lines in Figure 4.1. We also assume that the weight function $w_{ij}(t)$ is equal to 1 in connectivity conditions and 0 when the nodes i and j are disconnected, regardless of the neighbor's information reliability (i.e. with no soft weighting under connectivity). The variable $r_i(t)$ associated with the prior estimated position of the current mobile node is also taken equal to 1 like in [65], for simplification. As for the benchmarked MDS algorithm, a complete matrix is required with all the distances between all the pairs of nodes. Thus, inspired from the coarse geometric constraints used in [61], which rely for each link on the prior knowledge of minimal and maximal feasible distances under radio connectivity, we substitute the missing distances $\delta_{ij}(t)$ by random variables, which follow a uniform distribution in $[\min_t(d_{ij}(t)), \max_t(d_{ij}(t))]$.

After running simulations of the walk cycle with 100 independent realizations of the ranging errors based on the TOA estimation and PER, localization performance

is assessed in terms of the *Root Mean Squared Error* (RMSE) per node or average RMSE (i.e. over all the mobile nodes), while considering different approaches. In a first evaluation, we consider updating the positions with a systematic and regular refreshment rate of 30 ms, whereas the latency introduced by the exchanged packets is not taken into account. However, in a second and more realistic approach, we consider a TDMA MAC superframe similar to that presented in Figure 4.2, where an *Aggregate-and-Broadcast* (A-B) procedure is applied to ranging packets to speed up convergence. Finally, parametric simulation-based studies have also been carried out in order to assess the performance (over all the on-body nodes) as a function of the PER and the standard deviation σ of intra-BAN ranging errors in equation (4.14).

4.2.3.3 Simulation Results

Figure 4.5 shows the RMSE performance per node for the unconstrained DWMDS and the CDWMDS algorithms. The latter is considered with self-calibrated fixed-length ranges or exact fixed-length ranges. It is thus rather clear that one can expect benefits from incorporating fixed-length constraints in comparison with the nominal DWMDS, whatever the considered node. Moreover, no significant degradations have been observed after self-learning the fixed-length distances (e.g. during a pre-calibration phase, when each constraint is calculated as the mean of the measured distances in an observation window of 9 sec) in comparison with a genius-aided introduction of the exact fixed-length distances. Overall, in this case, the average RMSE (over all the nodes) spans from 26 *cm* using DWMDS down to 23 *cm* and 22 *cm* using CDWMDS with estimated and true constraints respectively, representing a relative improvement of 15.4 %.

On Figure 4.6, we compare the RMSE per node of the standard CDWMDS algorithm (still assuming that any fixed-length constraint is learnt as the mean of the measured distances in an sliding observation window of 9 sec) with a solution applying unidirectional censoring of the fastest nodes (i.e. 4 and 6). It is thus noticeable that such censoring schemes, mitigating error propagation, are globally efficient to improve the localization performances of both penalizing and favorable nodes simultaneously. The average RMSE (i.e. over all the nodes) is for instance decreased from 23.3 cm down to 19.7 cm, representing one more improvement by 15.4 %.

The effect of introducing scheduling in the sequence of location updates is also illustrated on Figure 4.7. Blue bars represent the localization performance of CDWMDS using censoring but random scheduling for the update of nodes' locations, whereas red bars account for situations when the slowest nodes are updated in priority and the same fast peripheral nodes (i.e. 4 and 6) are updated later on. The average RMSE per node then decreases from 19.7 cm down to 17.5 cm, leading to a 11.1 % improvement. Moreover the gain is mainly spectacular for the most poorly positioned nodes. Note that with such location updates scheduling, the refreshment rate could be also adjusted depending on the local mobile speed in order to favor

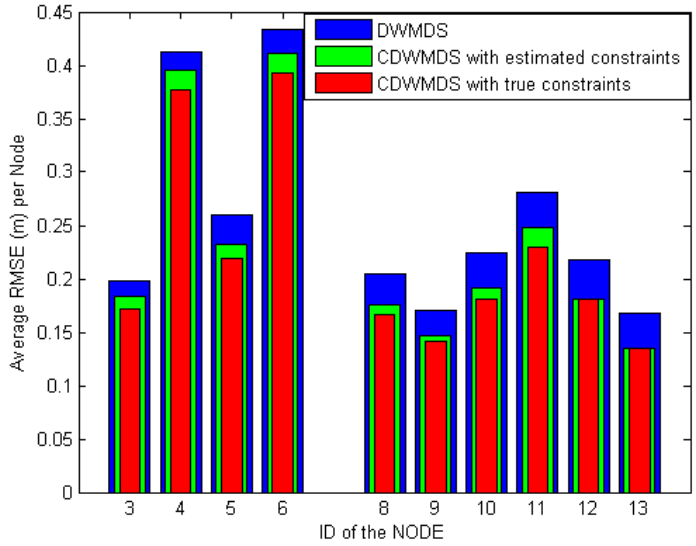

Figure 4.5: Relative localization RMSE (m) per on-body node (ID), for various asynchronous and decentralized positioning algorithms: unconstrained (DWMDS - blue), constrained (CDWMDS) with self-calibrated fixed-length ranges (green) and exact fixed-length ranges (red).

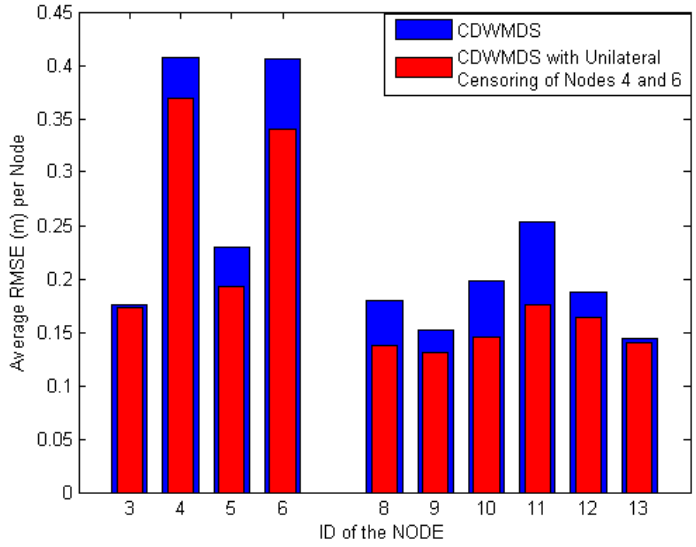

Figure 4.6: Relative localization RMSE (m) per on-body node with and without censoring of rapid nodes for $\sigma = 10\ cm$ and a refreshment rate of 30 ms.

the most demanding nodes, what was not the case in our simulations.

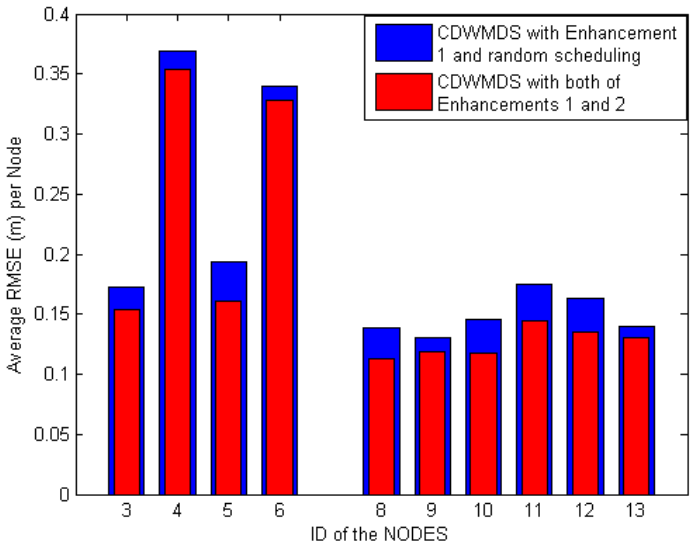

Figure 4.7: Relative localization RMSE (m) per on-body node with and without updates scheduling for $\sigma = 10\ cm$ and a refreshment rate of 30 ms.

On Figure 4.8 the blue bars represent the RMSE per node of the CDWMDS algorithm when applying the two first enhancements (i.e. censoring and scheduling), whereas red bars show the performance while forcing the symmetry of range measurements. The average RMSE (m) per node then decreases from 17.5 cm down to 15.5 cm under symmetric measurements, representing one improvement of 11.4 %.

Figure 4.9 shows a comparison of the RMSE performances per node for the standard CDWMDS and the CDWMDS under unilateral censoring of nodes 4 and 6, with the CRLB per node computed according to Appendix C under full mesh connectivity (i.e. without missing links due to deliberate censoring). For simplification purposes regarding the latter CRLB calculi, the ranging error is now considered as a centered Gaussian variable of variance $\sigma^2 = (10cm)^2$ regardless of the LOS/NLOS conditions (i.e. the bias terms applied previously under NLOS conditions are now eliminated). As shown on this figure, new enhancements would still be welcome regarding the settings of the CDWMDS algorithm (i.e. using soft weighting functions, more accurate initial positions), in order to reach the CRLB at each node. However, it also appears that the performance of CDWMDS with unilateral censoring at some nodes (i.e. nodes 4 and 6) is "better" than those theoretical bounds. This apparent contradiction simply reflects the fact that censoring sometimes outperforms the best performance that would be achieved under full mesh and cooperative connectivity, hence emphasizing the relevance of links selection and parsimonious cooperation. A new computation of the CRLB under unilateral censoring of some nodes (though not

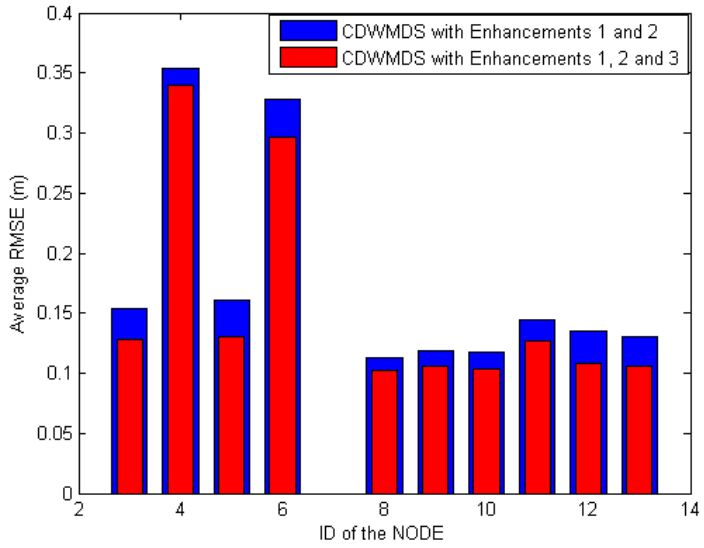

Figure 4.8: Relative localization RMSE (m) per on-body node with and without forcing measurements symmetry, with $\sigma = 10\ cm$ and a refreshment rate of 30 ms.

treated herein) would be required for a fairer comparison, but facing possibly numerical instability due to badly conditioned matrix problems, inherent to sparseness.

A comparison between MDS and CDWMDS, with and without MAC superframes, is also provided on Figures 4.10 and 4.11. First Figure 4.10 shows the variation of the average RMSE (over all the nodes) as a function of the PER. Blue, red and green curves represent respectively the localization performance of CDWMDS, CDWMDS under forced measurement symmetry and MDS algorithms, while the dashed curves represent the corresponding RMSE when considering a realistic MAC superframe. It can be seen that CDWMDS outperforms MDS, with and without MAC superframe, for each tested PER value. Moreover, the harmful effects of the latency induced by real MAC transactions (in particular between the collection of measurements and the positioning step) are also illustrated. The effect is however all the more noticeable with centralized approaches, like within MDS. As expected, it appears that forcing measurements symmetry is also an efficient way to mitigate packet losses, outliers or more simply large measurement noise occurrences (even if not outliers). Finally, the localization performance is slowly degraded as PER increases in our solution, most likely due to the jointly cooperative and decentralized nature of the proposed algorithm.

Figure 4.11 shows the variation of the average RMSE over all the nodes as a function of the standard deviation of the on-body ranging errors defined in equation (4.14). As expected, the performance is rapidly and rather strongly degraded as measurement errors increase. Indeed, the relative single-link errors become hardly

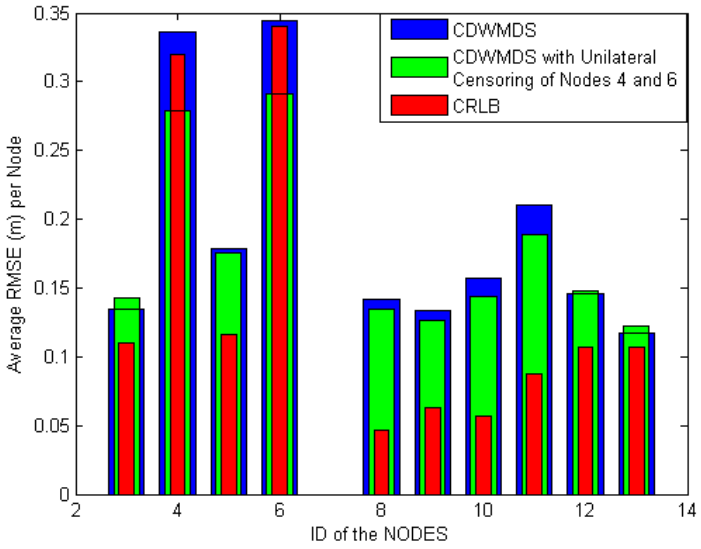

Figure 4.9: Comparison of the average RMSE (m) per on-body node with and without unilateral censoring of nodes 4 and 6, with respect to theoretical CRLB with a ranging standard deviation $\sigma = 10\ cm$, a refreshment rate of 30 ms and a PER of 1 %.

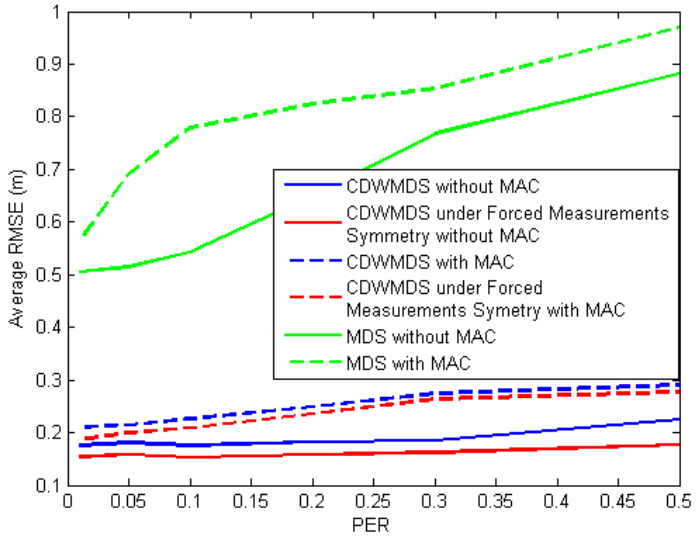

Figure 4.10: Average relative localization RMSE (m) over all the on-body nodes as a function of PER, with $\sigma = 10\ cm$.

compliant with relatively short true distances in a WBAN context. At very large noise standard deviations (e.g. larger than 20 cm), we even observe that the latency effects introduced by the use of a realistic MAC superframe are minimized, experiencing approximately similar performances (i.e. between dotted and their corresponding continuous curves in Figure 4.11). The previous observation indicates that measurement errors are far dominating in this case in comparison with latency effects (so far revealed by the presence of realistic MAC constraints), which could hence be neglected.

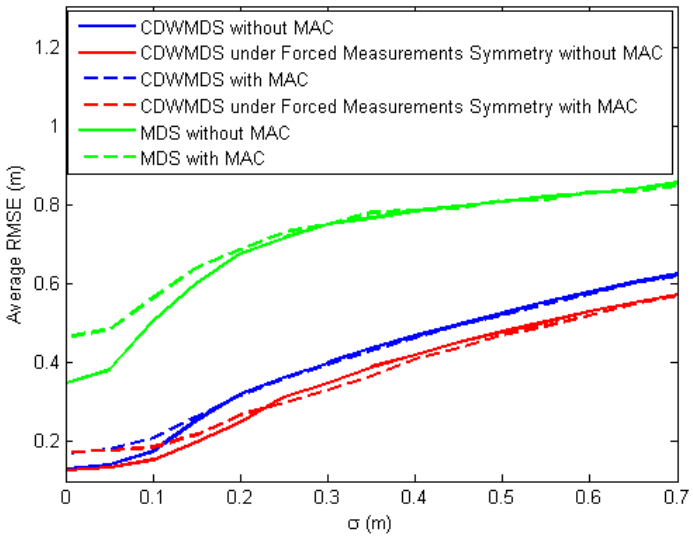

Figure 4.11: Average relative localization RMSE (m) for all the on-body nodes as a function of the standard deviation of ranging errors, with PER = 0.01.

In the next section, CDWMDS will be adapted into a 2-step algorithm for LSIMC purposes.

4.3 Large-Scale Absolute On-Body Localization

In this section, we address the absolute on-body positioning problem within a heterogeneous WBAN context. More particularly, we consider using on-body wireless links in a mesh intra-WBAN topology, as well as off-body wireless links with respect to external elements of infrastructure, set as fixed anchors. Multi-standard wireless on-body nodes are thus required, being compliant with e.g., IR-UWB IEEE 802.15.6 [4] for intra-WBAN communications and IR-UWB IEEE 802.15.4a or IEEE 802.15.4 over larger-range off-body links. Different scenarios will be compared in terms of location-dependent radio metrics (i.e. TOA, TDOA, RSSI), synchronization constraints and transmission ranges. We also describe specific algorithms to express the estimated coordinates of on-body nodes into an absolute GCS external to the

body, as well as to mitigate body obstructions and packet losses.

We first assume a set of fixed anchor nodes placed at known positions in the indoor environment and forming the building infrastructure. These nodes will be also depicted as *infrastructure anchors* in the following. A second set of wireless devices is deployed placed on the pedestrian body. These devices comprise the on-body mobile *nodes* and the reference *on-body anchors*. The latter are attached onto the body like in the relative localization case and then define a stable Cartesian LCS, which remains unchanged and time-invariant under body mobility.

Figure 4.12 shows a typical deployment scenario, where the LCS is obviously in movement and misaligned relatively to an external GCS. In the following, $\{X_i^{ac}\}_{i=1...N_a}$ represents the set of the absolute $3D$ known positions of the N_a fixed infrastructure anchors expressed in the GCS, where N_a should be equal or larger than 4. $\{X_i^a(t)\}_{i=1...n}$ and $\{X_i^r(t)\}_{i=1...n}$ represent respectively the absolute and relative $3D$ unknown positions of the n mobile nodes deployed on the body at time t, as respectively expressed in the GCS and LCS. Similarly, $\{X_i^a(t)\}_{i=n+1...n+m}$ and $\{X_i^r\}_{i=n+1...n+m}$ represent respectively the absolute $3D$ unknown positions of the m on-body anchors at time t and their corresponding relative known positions (time-invariant), where m should be equal or larger than 4. Now let $\widetilde{d}_{ij}(t)$ be one range or pseudo-range measurement available at time t between one on-body node i and a connected node j, j being one on-body node, one on-body anchor or one infrastructure anchor, and let l_{ij} be a constant distance (i.e. time-invariant over body mobility whatever the coordinates system), which will be considered as a constraint.

Given all the available measurements $\{\widetilde{d}_{ij}(t)\}_{i,j}$ at time t between cooperative on-body nodes or between on-body nodes and infrastructure anchors, on the known locations of on-body anchors and infrastructure anchors respectively in the LCS and GCS, the problem that we want to solve consists in estimating the absolute positions of the on-body nodes in the GCS.

4.3.1 Absolute Localization Algorithms

4.3.1.1 Proposed 2-Step Approach

The idea here is to start the LSIMC procedure by localizing the on-body nodes relatively to the LCS, using cooperative peer-to-peer range measurements. As seen in the previous section, the CDWMDS algorithm is relatively well suited to this relative positioning problem. It allows each on-body node to estimate its coordinates $\hat{X}_i^r(t)$ into the LCS, by minimizing the local cost function in equation (4.7), which depends uniquely on its relative neighborhood information. Once the minimization process is accomplished by all nodes, the set $\{\hat{X}_i^r(t)\}_{i=1...n}$ is available into the LCS.

The second stage consists in converting the relative locations defined into the LCS to absolute locations into the GCS. This transformation of LCS includes a rotation and a translation. Since on-body anchors are time-invariant in the LCS under mobility, it is preferable to rely on those nodes to transform the LCS. In $3D$ environments, the absolute locations of at least 4 on-body anchors are needed to find

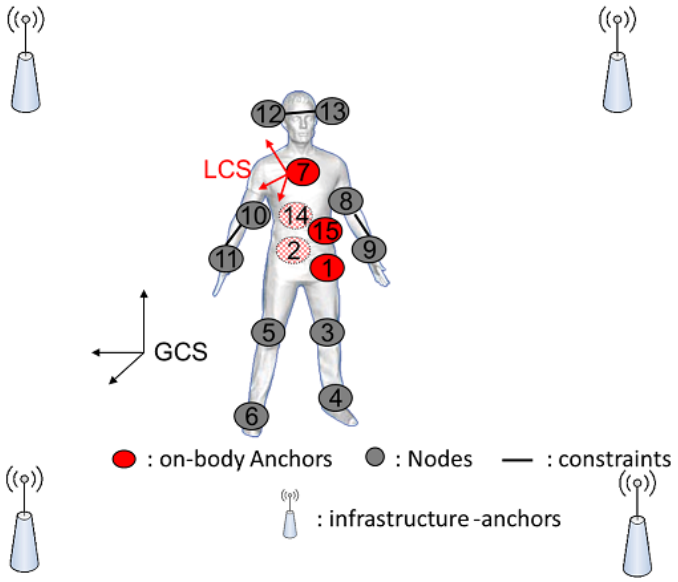

Figure 4.12: Typical deployment scenario for the absolute localization of on-body wireless nodes.

the absolute locations of the other mobile nodes. Hence, we determine the absolute localization of the on-body anchors into the GCS first.

Based on both known on-body ranges and range measurements with respect to external anchors, on-body anchors are localized through *Non-Linear Least Squares* (NLLS) optimization, by minimizing a new local cost function as follows:

$$\begin{aligned}\hat{X}_i^a(t) \;=\; \underset{X_i^a(t)}{\operatorname{argmin}}\Big[& \sum_{j=n+1, j\neq i}^{n+m} w_{ij}(t)(d_{ij}(t) - \hat{d}_{ij}(X_i^a(t), \hat{X}_j^a(t)))^2 \\ & + \sum_{k=1}^{N_a} w_{ik}(t)(\delta_{ik}(t) - \hat{d}_{ik}(X_i^a(t), X_k^{ac}))^2\Big] \end{aligned} \tag{4.15}$$

where $\hat{X}_i^a(t)$ is the vector of the estimated $3D$ coordinates of on-body anchor i into the GCS at time t, $d_{ij}(t)$ and $\hat{d}_{ij}(X_i^a(t), \hat{X}_j^a(t))$ denotes respectively the true distance between on-body anchors i and j and the corresponding distance built out of the estimated coordinates, N_a is the number of infrastructure anchors and $\delta_{ik}(t)$ is the observed distance between on-body anchor i and infrastructure anchor k.

Getting back to our initial aim of localizing on-body nodes into the GCS, the absolute coordinates can be obtained out of the relative coordinates into the LCS after a few transformations (i.e. rotation and a translation) [105], which can be represented as follows:

$$X_i^a(t) = A(t)X_i^r(t) + b(t) \tag{4.16}$$

The goal now is to estimate the rotation matrix A and the translation component b out of noisy observations, by minimizing the difference in

the least squares sense between the absolute locations of on-body anchors and the corresponding versions, which are obtained through the transformation of estimated relative positions. For a given on-body anchor l, we set $\Delta X^r(t) = [\Delta X^r_{n+1}(t), ..., \Delta X^r_{l-1}(t), \Delta X^r_{l+1}(t), ..., \Delta X^r_{n+m}]$ and $\Delta X^a(t) = [\Delta X^a_{n+1}(t), ..., \Delta X^a_{l-1}(t), \Delta X^a_{l+1}(t), ..., \Delta X^a_{n+m}]$, where $\Delta X^r_i(t) = X^r_i(t) - X^r_l(t)$ and $\Delta X^a_i(t) = X^a_i(t) - X^a_l(t)$ for $l \neq i$. The alignment problem can therefore be formulated as a standard LS optimization problem, as follows:

$$\hat{A}(t) = \underset{A(t)}{\operatorname{argmin}} \sum_{i=n+1, i\neq k}^{n+m} ||A(t)\Delta X^r_i(t) - \Delta X^a_i(t)||^2 \tag{4.17}$$

The analytical solution of this linear LS problem is given by $\hat{A}(t) = \Delta X^a(t)(\Delta X^r(t))^T(\Delta X^r(t)(\Delta X^r(t))^T)^{-1}$. Finally, the absolute locations of all the on-body mobile nodes in the GCS are simply derived from their corresponding relative versions in the LCS, as follows:

$$\hat{X}^a_i(t) = \hat{A}(t)(\hat{X}^r_i(t) - \hat{X}^r_l(t)) + \hat{X}^a_l(t) \tag{4.18}$$

The overall 2-step approach is summarized with the block diagram of Figure 4.13.

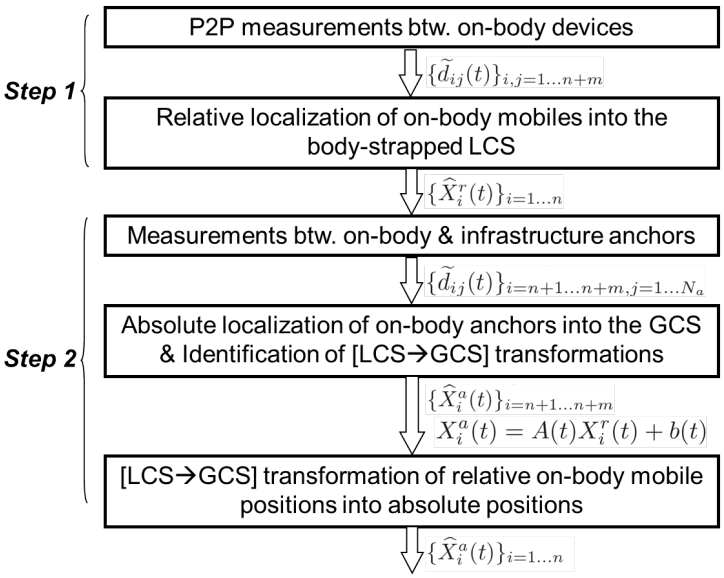

Figure 4.13: 2-step LSIMC approach.

4.3.1.2 Single Step Approach

For reference and comparison purposes, we also consider the case when the positions of all the on-body mobile nodes are directly calculated in the GCS. The idea is to

combine simultaneously all the available measurements, which can be performed between on-body devices or with respect to infrastructure anchors. Accordingly, the cost function to be minimized by each on-body device i is rather similar to that of equation (4.15) but now incorporates also cooperative distance measurements between on-body devices, as follows:

$$\begin{aligned} \hat{X}_i^a(t) &= \underset{X_i^a(t)}{\operatorname{argmin}}[\sum_{j=1,j\neq i}^{n+m} w_{ij}(t)(\delta_{ij}(t) - \hat{d}_{ij}(X_i^a(t), \hat{X}_j^a(t)))^2 \\ &\quad + \sum_{k=1}^{N_a} w_{ik}(t)(\delta_{ik}(t) - \hat{d}_{ik}(X_i^a(t), X_k^{ac}))^2] \end{aligned} \tag{4.19}$$

4.3.2 Distance Approximation and Completion Over Neighborhood Graph

A graph is usually considered as a collection of vertices (or nodes) and edges (or distances) that connect pairs of vertices [106], [107]. In the very WBAN localization context, we assume that the on-body devices and infrastructure anchors form such a graph. The edges, which can be weighted by the observation distances, then reflect connectivity between the different entities.

So as to mitigate link obstructions, as an improvement of the previous algorithms, we propose to reconstruct the graph based on connectivity and measurement information, by computing the shortest distances over neighborhood graph. The idea is to start by initializing the weight of an edge between nodes i and j by the observation distance $\widetilde{d}_{ij}(t)$ in case of connectivity, and by ∞ otherwise [105]. In a second step, we replace each weight (i.e. distance) by the shortest path separating the graph nodes in the local neighborhood, that is to say, updating $\widetilde{d}_{ij}(t^+) = min(\widetilde{d}_{ij}(t^-), \sqrt{(\widetilde{d}_{ik}(t^-)^2 + \widetilde{d}_{kj}(t^-)^2)}$. Figure 4.14 illustrate such distance approximation and/or completion with simplified examples. On the left generic case involving 4 nodes, with the initial graph exhibiting a disconnection only between node 1 and 4, the weights between nodes 1 and 2 on the one hand, and nodes 1 and 4 on the other hand, would be both reconstructed identically based on the shortest observed paths going through node 3. The right figure shows one possible application into the heterogeneous WBAN context, where a missing off-body measurement between nodes i and j (due to body shadowing) is approximated using another off-body measurement available between i and k and additional on-body information between j adn k. The selection of some kind of "triangular" approximate (i.e. $\sqrt{(\widetilde{d}_{ik}(t^-)^2 + \widetilde{d}_{kj}(t^-)^2)}$) instead of the linear one (i.e. $\widetilde{d}_{ik}(t^-) + \widetilde{d}_{kj}(t^-)$), appears more adaptable to the deployment of on-body devices with respect to the infrastructure (i.e. 2 on-body devices and an infrastructure anchor are most likely not aligned but somehow form a "triangle", even if not necessarily forming a 90° angle depending on the body orientation). Our proposal, which performs distance estimation over neighborhood graph, also generally leads to an important reduction of the ranging errors affecting the measured distances (e.g. outliers), and more noticeably

in NLOS conditions due to body shadowing. Moreover, missing distances under partial connectivity are approximated whenever one single path has been found in the graph.

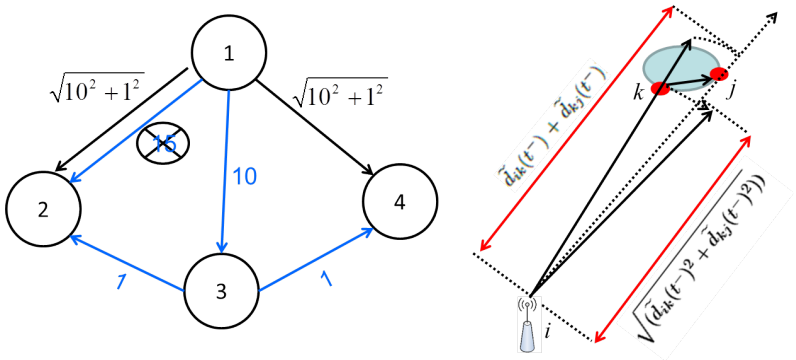

Figure 4.14: Example of distance estimation over neighborhood graph (left): the blue graph represents the initial graph based on the observation distances and connectivity information. The black graph is reconstructed based on the calculation of the shortest paths. Example of reconstructed distance through triangular and linear estimation over off-body links (right).

4.3.3 Simulations and Results

4.3.3.1 Scenario Description

In our evaluation framework, the simulation of human mobility is based on the same mixed model as in subsection 4.2.3.1, with a snapshot illustrated on figure 4.4. Furthermore, the scene is surrounded by 8 infrastructure anchors set at the corners. The network deployment is similar to that presented on Figure 4.12, with 5 on-body anchors and 10 blind on-body nodes.

4.3.3.2 Simulation Parameters

Concerning the physical radio parameters, we differentiate intra-WBAN and off-body links. We first assume IR-UWB over on-body radio links. We still consider that the received power is larger than the receiver sensitivity, which allows peer-to-peer communications with a worst-case PER of 1%, as specified by the IEEE 802.15.6 standard [11]. This PER figure is applied to each single packet involved in 3-way ranging protocol transactions within the same TDMA scheme as previously [101], thus emulating similarly incomplete ranging transactions (i.e. whenever at least one packet is lost out of 3). Based on the TOA-based IR-UWB model from Chapter 3, we consider exactly the same error model and parameters as in Section 4.2.3.2 for relative on-body localization, with ranging errors according to equation

LOS	NLOS
σ_n=0.3 m	σ_n=0.5 m
$b_{ij}(t) = 0$	$b_{ij}(t) \in [1, 2]$ m

Table 4.2: TOA-based ranging error parameters over indoor off-body IR-UWB links, according to [8].

(4.14), a constant standard deviation $\sigma_n = 10\,cm$ and NLOS random positive biases uniformly distribution in $[0\,10]cm$.

As for off-body links between on-body devices and infrastructure anchors, radiolocation measurements can be delivered either through IR-UWB TOA or N-B RSSI estimation. In case of IR-UWB (e.g. according to the IEEE 802.15.4a standard), the conditional TOA-based ranging error model is similar to that of equation (4.14), but noise parameters have been adjusted according to [8] and [108], as reported in Table 4.2. NLOS conditions are assumed to be caused uniquely by body shadowing here. Regarding N-B RSSI-based ranging (e.g. according to the IEEE 802.15.4 standard in a band centered around 2.4GHz), inspired by the off-body channel model from Chapter 3 and [12], the path-loss model used in our simulations is simplified after eliminating fast fading components (i.e. considering that one would average over a sufficient number of consecutive RSSI readings per link in a real system), as follows:

$$PL(d) = PL_0 + 10nlog_{10}(d/d_0) + S \tag{4.20}$$

where $PL(d)$ is the path-loss in dB between two devices separated by a distance d, PL_0 represents the path-loss in dB at a reference distance $d_0 = 1\ m$, n is the path-loss exponent and S represents the body shadowing.

As previously, we also suppose that the latter shadowing term is normally distributed with a zero mean and standard deviation $\sigma_S = 2$ dB, which represent a plausible median value for both conditional LOS and NLOS regimes, as seen in Chapter 3 in Table 3.4. Note that the RSSI radiolocation metrics will be integrated only in the 2-step localization scenario, where the infrastructure anchors are just connected to on-body anchors. We have classified those links into two different sets depending on the locations of their involved on-body nodes. In first approximation, generalizing the model in [12] and reported in Table 3.3 for a WBAN planar monopole antenna and two different specific links, the two sets of links are thus associated with the same channel parameters as that observed for an antenna placed either on the heart or on the left hip. The estimated RSSI-based distance is finally extracted from RSSI readings using the ML estimator proposed in [109], as follows:

$$\widetilde{d}_{ij}(t) = exp(M_{ij} - L_{ij}^2) \tag{4.21}$$

where $M_{ij} = \frac{\sigma_S ln(10)}{10n_{ij}}$ and $L_{ij} = \frac{(PL_{ij} - PL_0)ln(10)}{10n_{ij}} + ln(d_0)$.

Concerning the localization algorithm settings, three fixed-length link constraints are imposed to the CDWMDS algorithm, as materialized with black lines in Figure 4.12. We also set $w_{ij}(t) = 1$ in connectivity conditions and 0 otherwise, regardless to neighbor's information reliability (i.e. with no soft weighting under connectivity). $r_i(t)$ is also equal to 1 for simplifications. Finally, localization updates are realized in average with a refreshment rate of 30 ms.

Based on the previous models and settings, simulations have been carried out to illustrate and compare the LSIMC performances of both single- and 2-step localization approaches. We have also considered several options for off-body links (in the latter 2-step embodiment), integrating different radiolocation metrics, namely TOA, TDOA -formed from TOA- and RSSI. Additional simulations aim at illustrating the benefits from estimating the distances over neighborhood graph in order to mitigate obstructions and too large measurement errors. Running trials of the walk cycle with 100 independent realizations of measurement error processes, the performance is assessed in terms of the estimation *Root Mean Squared Error* (RMSE) for each on-body mobile node, like in the relative localization case.

4.3.3.3 Simulation Results

As shown on Figure 4.15, mostly due to severe obstructions and partial connectivity conditions, the performances of the standard 2-step RSSI-based and 1-step TOA-based approaches look rather poor and definitely not compliant with the requested LSIMC level of precision, even if the TOA-based option seems slightly better. However, based on IR-UWB TOA estimation over off-body links (i.e. TOA or TDOA) in the 2-step approach, rather clear gains can already be observed in comparison with the single-step approach, even though the resulting average precision would be mostly interesting to navigation application and still meaningless for LSIMC, with an average RMSE over all the on-body nodes respectively equal to 1.1 m and 1.2 m using the TOA and TDOA metrics over off-body links, hence justifying further enhancements.

On Fig 4.16, we show similar results, but with the additional distance approximation and completion technique, which consists in identifying the shortest distance over neighborhood graph. The average RMSE per node is then decreased from 1.1 m down to 0.31 m, leading to a significant improvement by 72 %. On the one hand, rather comparable levels of precision can now be achieved for absolute on-body localization at the building scale in comparison with the best performance of relative on-body localization at the body-scale in Section 4.2. On the other hand, penalized nodes located at the body extremities, which classically suffer from lower connectivity, poor geometric dilution of precision and higher accelerations (e.g. nodes 4, 6, 9 and 11 in our example), now seem to enjoy better robustness in comparison with other nodes. Considering relaxed deployment constraints and the claimed WBAN low consumption, these results could make this coarse LSIMC solution a reasonable alternative to costly, power greedy and geographically restricted technologies.

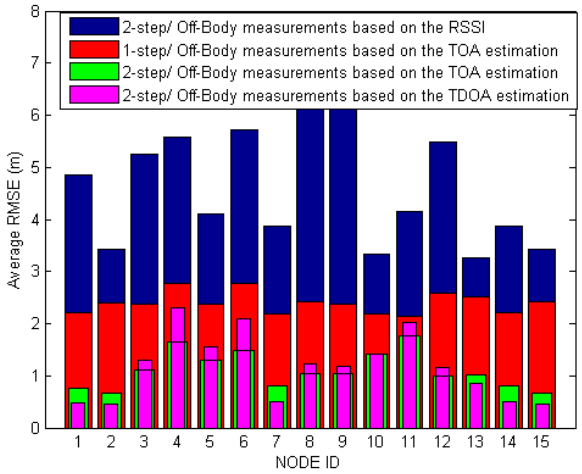

Figure 4.15: Absolute localization RMSE of estimated locations per on-body node (ID) with both single- and two-step LSIMC based on TOA, TDOA and RSSI metrics over off-body links.

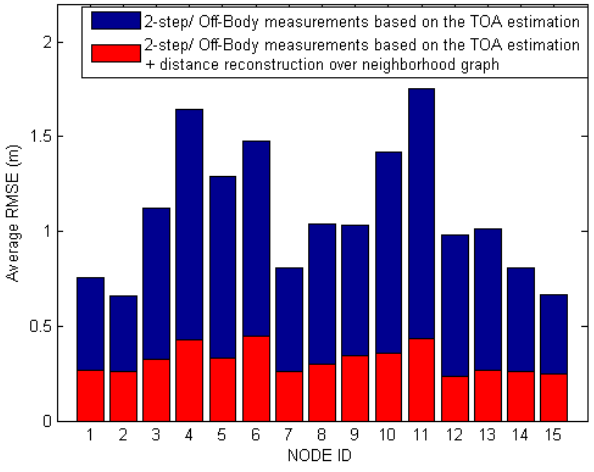

Figure 4.16: Absolute localization RMSE per on-body node (ID) with two-step LSIMC based on TOA metrics over off-body links and distances estimation over neighborhood graph.

4.4 Conclusion

In this Chapter, we have addressed the problem of relative and absolute on-body localization for individual MoCap purposes.

In Section 4.2, we have dealt with relative body motion capture only. The corresponding personal contributions have led to the publication of two conference papers [46], [47] and one journal [48]. A decentralized and cooperative DWMDS algorithm, which can asynchronously estimate unknown on-body nodes locations, has been adapted in the very context. We have introduced learnt fixed-length geometric constraints that correspond to time-invariant Euclidean inter-node distances under body mobility. Furthermore, the initial CDWMDS has been enhanced through scheduling and censoring to mitigate error propagation and harmful effects due to location-dependent node speed disparities. It has been also shown that forcing measurements symmetry could help to mitigate outliers and packet losses. Moreover, CDWMDS has been proved to outperform with a classical MDS algorithm in terms of localization accuracy for various PER values and ranging standard deviations with and without realistic MAC superframe, hence illustrating rather fine robustness against latency effects. However, given the remaining limitations still observed in terms of achievable precision, which is hardly compliant with high precision MoCap needs (especially when compared with theoretical bounds at some pathological nodes), axes of improvement can be identified, such as a judicious coupling with tracking/smoothing algorithms, better initialization or a soft weighting of the available measurements.

In Section 4.3, we have addressed the problem of absolute motion capture over large-scale indoor trajectories in location-enabled heterogeneous wireless body area networks. The related personal contribution has led to the publication of one conference paper [49]. Two approaches have been presented to estimate the absolute locations of on-body nodes in a global coordinates system, considering different radiolocation metrics over off-body links with respect to infrastructure anchors. One 2-step solution relies on preliminary relative localization at the body scale and applies further transformations through the absolute localization of on-body anchors. At first sight, body shadowing seems very challenging, not to say redhibitory to achieve precision levels compatible with high-precision MoCap needs. However we have proposed another algorithm that estimates the shortest path between on-body and infrastructure anchors over neighborhood graph to compensate for possible radio obstructions and most penalizing large measurement errors. Thanks to the latter improvement, approximately the same levels of precision as that obtained for relative on-body localization could be theoretically achieved over large-scale trajectories. This makes our radio-based solution still attractive for coarse absolute MoCap applications, even if new improvements are still foreseen, such as the use of body-to-body cooperation.

The next Chapter will precisely concern cooperative navigation functionalities in groups of WBANs, relying on such body-to-body links and on-body deployment diversity. On this occasion, different localization and tracking algorithms will be

also evaluated and compared.

Chapter 5

Localization Algorithms for Individual and Collective Navigation

Contents

5.1 Introduction

As seen in Chapter 1, in our WBAN context, one can make a distinction between classical individual navigation on the one hand, where the on-body nodes belong to one single body, whose "macroscopic" position must be estimated with respect to a GCS, and collective navigation (CGN) on the other hand, which consists in retrieving the absolute positions of several mobile users belonging to the same group, each user wearing his own WBAN. In the first case, cooperative on-body and off-body links are considered (i.e. just like for LSIMC in the previous Chapter), whereas additional body-to-body links may be involved in the latter case. In both scenarios, we assume that fixed and known elements of infrastructure are disseminated in the environment for absolute localization purposes. In terms of radiolocation metrics and radio standards, we consider peer-to-peer range measurements through TOA estimation over IR-UWB links or RSSI estimation over N-B links, like previously. We also admit various combinations of such cooperative links and measurements, hence assuming a heterogeneous WBAN context.

This Chapter addresses both individual and collective kinds of navigation. For this sake, a NLLS positioning algorithm and a centralized EKF tracking algorithm are considered. Furthermore, a new individual navigation scheme is proposed, in which the propagation of the positioning errors is avoided and the overall system complexity could be reduced. Besides, different cooperation scenarios are also compared in terms of localization accuracy.

The structure is as follows. After providing the generic problem formulation, Section 5.2 deals with positioning and tracking solutions for individual navigation, considering the new proposed cooperation scheme, whereas Section 5.3 investigates the CGN problem, introducing body-to-body cooperation. Finally, Section 5.5 concludes the Chapter.

5.2 Individual Navigation

We first assume that $\{X_i\}_{i=n+1\ldots n+m}$ is a set of vectors containing the absolute $3D$ known positions $X_i = [x_i, y_i, z_i]$ of the m fixed infrastructure anchors expressed in the GCS, where m should be equal to or larger than 4. $\{X_i(t)\}_{i=1\ldots n}$ is a set of vectors representing the unknown absolute $3D$ positions $X_i(t) = [x_i(t), y_i(t), z_i(t)]$ of the n on-body nodes at time t, also expressed in the GCS.

Now let $\widetilde{d}_{ij}(t)$ be one range (or pseudo-range) measurement available at time t between one on-body node i and a connected node j, j being another on-body node (belonging to the same WBAN or to a distinct WBAN) or one infrastructure anchor. Given all the available measurements $\{\widetilde{d}_{ij}(t)\}_{i,j}$ at time t, e.g. based on IR-UWB TOA or RSSI estimation, and given the known locations of the infrastructure anchors, the problem that we want to solve consists in estimating in the GCS the absolute positions of the carrying bodies, relying on their on-body nodes.

As said before, in the individual navigation context, the presence of a few nodes on a single body (most likely, a smaller set than in the LSIMC case) is expected to improve the performance in terms of both precision and robustness, by providing spatial diversity and measurements redundancy on the one hand (i.e. especially in case of NLOS obstructions with respect to the infrastructure), as well as practical "averaging" possibilities (i.e. each on-body node contributing to the refinement of the global body position). More precisely, a reference point on each body shall be chosen to account for the "macroscopic" position in the room or in the building, such as the geometric center of the body torso or the centroid of all the on-body nodes. In our work, for performance assessment, the latter true centroid position is retained as the reference macroscopic position of the body. Figure 5.1 shows a typical deployment scenario, including 4 on-body nodes and 4 anchors.

5.2.1 Classical Approach

In a first intuitive scheme, all the on-body nodes can be preliminarily positioned in the GCS, and then a macroscopic body position is obtained as the centroid of

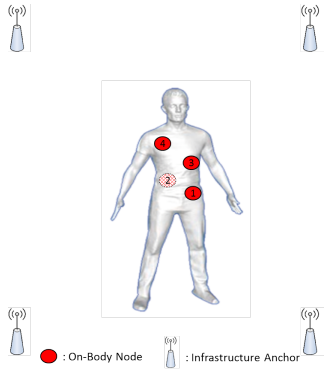

Figure 5.1: Typical WBAN deployment scenario for individual navigation.

the previous estimates. Figure 5.2 shows an example of flowchart diagram corresponding to this simple approach, assuming n on-body nodes. Note that each node is actually localized using all the available peer-to-peer range measurements (i.e. with respect to external anchors and/or even to other on-body nodes) and their neighbors' information.

In this case, if we suppose that the estimated position of one node is strongly biased, then the computation of the centroid position may be affected accordingly. Furthermore, in cooperative (and decentralized) scenarios, where the localization of one particular node is based on the estimated positions of its neighbors, the error can propagate rapidly over the entire network, causing possibly divergence. Hence, as an alternative, the following subsection defines a new proposal for computing the centroid more efficiently and avoid such error propagation.

5.2.2 New Proposal

The proposed scheme consists in localizing directly the reference centroid, instead of performing the preliminary localization of on-body nodes before averaging the resulting estimated positions. Thus intermediary distances are estimated instead, corresponding to the distances separating this on-body centroid from the deployed external anchors, based on the coarse prior knowledge of the relative dispersion ("statistical" or deterministic) of on-body nodes and based on the available range measurements between these on-body nodes and external anchors. Figure 5.3 shows a flowchart diagram for this new navigation scheme.

If $d_{iA}(t)$ denotes the true distance between on-body node i and external anchor

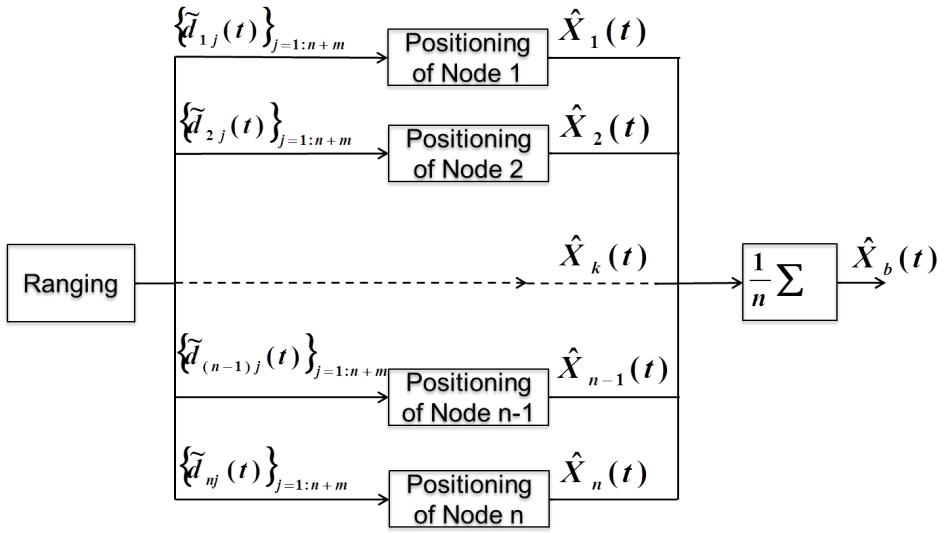

Figure 5.2: Example of classical scheme for individual navigation, based on the posterior computation of the on-body nodes' centroid.

A at time t, then

$$\begin{aligned}\frac{1}{n}\sum_{i=1}^{n} d_{iA}^2(t) &= \frac{1}{n}\sum_{i=1}^{n} x_i^2(t) - \frac{2x_A}{n}\sum_{i=1}^{i=n} x_i(t) + x_A^2 \\ &+ \frac{1}{n}\sum_{i=1}^{n} y_i^2(t) - \frac{2y_A}{n}\sum_{i=1}^{n} y_i(t) + y_A^2 \\ &+ \frac{1}{n}\sum_{i=1}^{n} z_i^2(t) - \frac{2z_A}{n}\sum_{i=1}^{n} z_i(t) + z_A^2 \end{aligned} \quad (5.1)$$

Similarly if $d_{bA}(t)$ denotes the true distance between the on-body centroid of coordinates $X_b(t) = [x_b(t) = \frac{1}{n}\sum_{i=1}^{n} x_i(t),\ y_b(t) = \frac{1}{n}\sum_{i=1}^{n} y_i(t),\ z_b(t) = \frac{1}{n}\sum_{i=1}^{n} z_i(t)]$ and anchor A, then

$$\begin{aligned} d_{bA}^2(t) &= (\frac{1}{n}\sum_{i=1}^{n} x_i(t))^2 - \frac{2x_A}{n}\sum_{i=1}^{n} x_i(t) + x_A^2 \\ &+ (\frac{1}{n}\sum_{i=1}^{n} y_i(t))^2 - \frac{2y_A}{n}\sum_{i=1}^{n} y_i(t) + y_A^2 \\ &+ (\frac{1}{n}\sum_{i=1}^{n} z_i(t))^2 - \frac{2z_A}{n}\sum_{i=1}^{n} z_i(t) + z_A^2 \end{aligned} \quad (5.2)$$

By subtracting equation (5.2) from equation (5.1), one can straightforwardly get:

$$\begin{aligned}\frac{1}{n}\sum_{i=1}^{n} d_{iA}^2(t) - d_{bA}^2(t) &= \frac{1}{n}(\sum_{i=1}^{n} x_i^2(t)) - (\frac{1}{n}\sum_{i=1}^{n} x_i(t))^2 \\ &+ \frac{1}{n}(\sum_{i=1}^{n} y_i^2(t)) - (\frac{1}{n}\sum_{i=1}^{n} y_i(t))^2 \\ &+ \frac{1}{n}(\sum_{i=1}^{n} y_i^2(t)) - (\frac{1}{n}\sum_{i=1}^{n} y_i(t))^2 \end{aligned} \tag{5.3}$$

Now let the sets of all the on-body coordinates at time t, namely $\{x_i(t)\}_{i=1...n}$, $\{y_i(t)\}_{i=1...n}$ and $\{z_i(t)\}_{i=1...n}$, be viewed as sample realizations of three unknown independent random variables $x(t)$, $y(t)$ and $z(t)$ (i.e. somehow accounting for the uncertainty of on-body deployment). Then, equation (5.3) could be rewritten into:

$$\begin{aligned}\frac{1}{n}\sum_{i=1}^{n} d_{iA}^2(t) - d_{bA}^2(t) &\approx E(x^2(t)) - (E(x))^2 + E(y^2(t)) \\ &- (E(y))^2 + E(z^2(t)) - (E(z))^2 \end{aligned} \tag{5.4}$$

where $E(.)$ denotes the statistical expectation operator and the left term, according to equation (5.3) involves the sample-based empirical versions of the exact statistical moments of x, y and z.

In other words, once $E(x^2(t)) - (E(x))^2 + E(y^2(t)) - (E(y))^2 + E(z^2(t)) - (E(z))^2$ is known a priori and $\{\widetilde{d_{iA}}(t)\}_{i=1...n}$, $\forall A$ have been collected to substitute $\{d_{iA}(t)\}_{i=1...n}$ into equation (5.4), then $d_{bA}(t)$, $\forall A$ can be also estimated and classical algorithms can be applied to localize the centroid.

From a practical point of view, the prior knowledge of the on-body nodes' dispersion can be obtained by letting the user deploy the nodes within a reasonably constrained area (e.g. considering that on-body nodes' coordinates are uniformly or normally distributed within a square of known edge length and drawn on a specific piece of clothes, typically on the torso). In a more extreme case, one could also impose fixed on-body locations to the user. In this situation, the prior knowledge of the on-body nodes' relative dispersion is no more statistical but purely deterministic and geometric (e.g. setting the on-body nodes at the corner of the square area) so that the right wing of equation (5.3) can be explicitly computed regardless of the chosen GCS. As a realistic compromise, the knowledge of this dispersion could be "statistical" in some dimensions under arbitrary deployment (e.g. in the coronal plane) but likely deterministic in others (e.g. along the sagittal axis).

The expected gains from this new proposal are three-fold: i) keep on benefiting from measurements diversity and redundancy with respect to anchors thanks to on-body nodes, ii) avoiding the error propagation that would be caused by biased intermediary on-body location estimates in the classical approach, iii) enabling the computation of one single position, thus contributing to reduce system complexity, computational load and consumption.

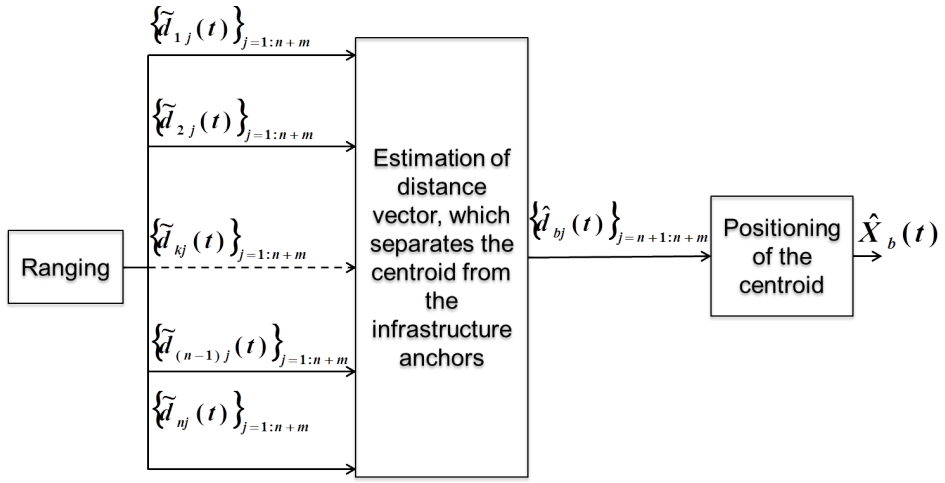

Figure 5.3: New proposed scheme for individual navigation, where one single body position is computed, based on intermediary estimated distances between the on-body centroid and external anchors.

5.3 Collective Navigation

In this application, a few mobile users wearing on-body nodes and forming a group, must be localized with respect to an external GCS. The localization can then rely on peer-to-peer range measurements between on-body nodes and infrastructure anchors over off-body links, and/or with respect to other on-body nodes on the same or different bodies (i.e. over on- and body-to-body links). Figure 5.4 shows a typical deployment with 3 users. Similarly to individual navigation, each user belonging to the group is tracked by estimating his macroscopic position, for instance defined as the centroid of his deployed on-body nodes.

5.4 Simulations and Results

5.4.1 Scenario Description

In our evaluation framework, a group of 3 persons is defined, where each body is assumed to move randomly and independently from each other (at least in terms of directions), for simplicity. The human mobility of each user is based on a mixed model similar to that already presented in Subsection 4.2.3.1. A snapshot of the resulting animated group is represented on Figure 5.5.

Furthermore, for each random trial, the different bodies move in a $20\,m \times 20\,m \times 4\,m$ 3D environment at the constant speed of $1\,m/sec$ for an overall duration of $112 sec$. The scene is surrounded by 4 infrastructure anchors, set at the corners. The network deployment is similar to that presented on Figure 5.4, where 4 on-body nodes are placed on each body. All the on-body nodes are indexed from 1 to

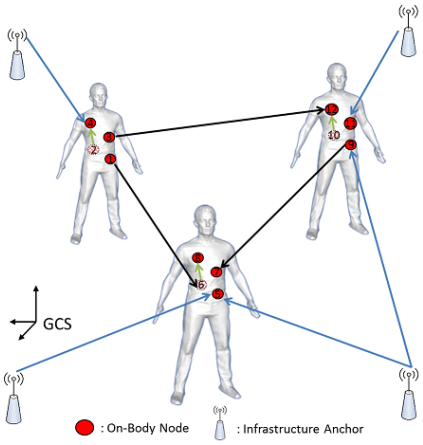

Figure 5.4: Typical WBAN deployment scenario for collective navigation (CGN) within a group of 3 equipped users.

12 (i.e. grouping the three sets of 4 on-body nodes).

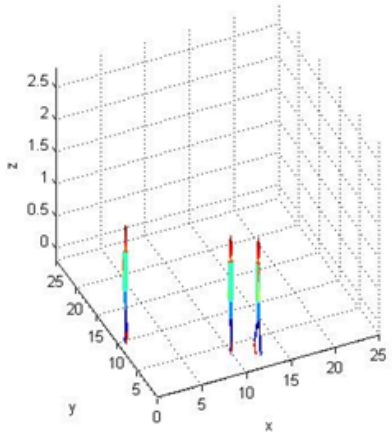

Figure 5.5: Mobility model, including a biomechanical representation based on piecewise cylinders and a macroscopic RGPM model, used for the generation of realistic distance measurements over body-to-body links in the collective navigation (CGN) scenario.

Still for simplicity, we assume hereafter that the distances over on-body links are a priori known and invariant over time, for instance by placing the on-body nodes at fixed and judicious locations (e.g. on the torso and the back).

5.4.2 Simulation Parameters

Radiolocation measurements can be delivered over off-body and body-to-body links, either through IR-UWB TOA or through N-B RSSI estimation. In case of IR-

UWB (e.g. according to the IEEE 802.15.4a standard), the conditional TOA-based ranging error model is assumed to be similar for both of off-body and inter-body links. The retained model is similar to that of equation (4.14), but noise parameters have been adjusted according to [8] and [108], as already reported in Table 4.2 for LSIMC simulations. Regarding N-B RSSI-based ranging (e.g. according to the IEEE 802.15.4a standard in the band centered around 2.4GHz), still inspired by the off-body and body-to-body channel models in [12] and [13], which have been specified in the ISM band (i.e. at 2.45 GHz) for WBAN planar monopole antennas, the used path loss model corresponds to equation (4.20), with the parameters already reported in Tables 3.3 and 3.5, with a conditional shadowing standard deviation of 2 dB. In both cases, NLOS conditions are assumed to be caused uniquely by body shadowing. Finally, similarly to LSIMC, single-link range measurements are derived from RSSI readings using the ML estimator proposed in [109], as shown in equation (4.21).

Concerning the localization algorithms and settings, each estimated body position is updated in average with a refreshment period of 30 ms. A first NLLS positioning algorithm is considered, whose settings are similar to that in Chapter 4 for LSIMC. An alternative EKF tracking algorithm is also considered, whose main formalism and principle are reminded in Appendix D. Accordingly, we consider a linear state-space mobility model, accounting for the evolution of the $6n$ dimensional state-space vector at time-stamp kT (or iteration k), $\mathbf{S}(k) = [X_1^T(k)\ V_1^T(k)\ X_2^T(k)\ V_2^T(k) \dots X_n^T(k)\ V_n^T(k)]$, which includes the three-dimensional positions and velocities of each blind node to be positioned, under the same notations as in Appendix D. Finally, we empirically and a priori determine the state-space noise covariance matrix $\mathbf{Q}$, relying on the variation of the true simulated on-body locations over a long period of time. In details, we apply the state-space equation onto these real positions, aggregate the noise residuals over each state component (i.e. computing $\mathbf{u}(k) = \mathbf{S}(k) - \mathbf{A}\mathbf{S}(k-1), \forall k$) over a long time period (still with the same time step of 30 ms) and finally compute the variance over each state component of $\mathbf{S}$, leading to the following numerical values:

$$\mathbf{Q} = \mathbf{I}_n \otimes \begin{pmatrix} 0.004 & 0 & 0 & 0 & 0 & 0 \\ 0 & 0.002 & 0 & 0 & 0 & 0 \\ 0 & 0 & 10^{-4} & 0 & 0 & 0 \\ 0 & 0 & 0 & 4.3 & 0 & 0 \\ 0 & 0 & 0 & 0 & 2.25 & 0 \\ 0 & 0 & 0 & 0 & 0 & 0.1253 \end{pmatrix} \tag{5.5}$$

5.4.3 Simulation Results

Based on the previous models and settings, simulations have been carried out to illustrate and compare the performances of both individual and collective navigation. Running 100 trials of the walk cycle with distinct independent realizations of the range measurement error processes, the empirical *Cumulative Density Function*

(CDF) of the RMSE of the estimated on-body nodes' centroid has been characterized (i.e. over all the trajectory trials and noise realizations).

First of all, addressing the individual navigation problem, we compare the localization performances of both NLLS and EKF algorithms, where the distance measurements over off-body links are based on TOA and/or RSSI estimation.
In particular, Figure 5.6 shows the nominal performance obtained with NLLS, where the TOA-based metrics clearly outperforms the RSSI-based metrics. Thus, the latter does not seem compliant with the requested level of precision, even if it may be useful as an indirect source of information (e.g. to solve ambiguities through hypothesis testing [110]).

Still based on the NLLS algorithm but uniquely with TOA-based range measurements over off-body links, Figure 5.7 illustrates the additional gains that could be achieved through distance reconstruction based on the shortest distance over neighborhood graph, as originally proposed for LSIMC to combat body shadowing obstructions. The median error decreases from $0.55\,m$ to $0.24\,m$ in this example, what looks definitely compliant with personal navigation needs.
On Figure 5.8, we show similar results with our additional proposal, which consists in estimating directly the body position, out of approximated distances between the external anchors and the centroid, relying on the prior knowledge of the on-body nodes' dispersion. Our proposal then leads to slightly better performances only, while reducing system complexity and energy consumption.

Figure 5.9 shows the results obtained with a classical EKF fed by TOA-based range measurements over off-body links. Rather surprisingly, the median error is still around $0.38\,m$, what is on the same order as that of the best NLLS embodiment. However, it is worth pointing out that the optimality of the EKF is under question here. In our case, the observation model indeed assumes systematically a zero-mean Gaussian noise process whereas actual range measurements are notoriously biased in NLOS conditions, as seen in Chapter 3. This suggests to modify the observation and/or even the state models in future works, accounting for the stochastic or semi-deterministic behaviour of such NLOS TOA biases (or even estimating them), following one of the approaches put forward in [111] or [112] for instance.

Collective navigation has been also investigated over several simulation scenarios. The first scenario is viewed as non-cooperative and proposed for benchmark purposes, where only the off-body measurements are integrated in the localization problem, so that each body position is computed independently of the others in the group. On the contrary, Scenario 2 considers a full cooperation scheme, where all the available kinds of links are involved (i.e. on-body, body-to-body and off-body links). Scenario 3 consists in using only the off-body and body-to-body links. Finally, Scenario 4 incorporates off-body and on-body links, so that each body position is also computed independently just like in the previous individual navigation case. This last scenario is proposed for benchmark purposes as well.
Based on the NLLS algorithm and on TOA-based range measurements, Figure 5.10 compares the empirical CDFs of the estimated centroids' RMSE (over the three

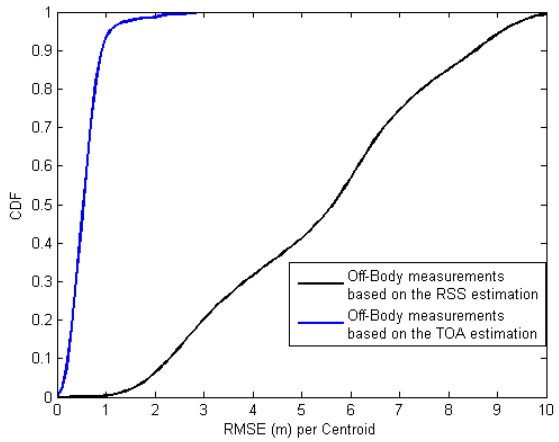

Figure 5.6: Empirical CDF of the RMSE of estimated on-body nodes' centroid for a single body, for a NLLS positioning algorithm fed by RSSI-based and TOA-based range measurements over off-body link.

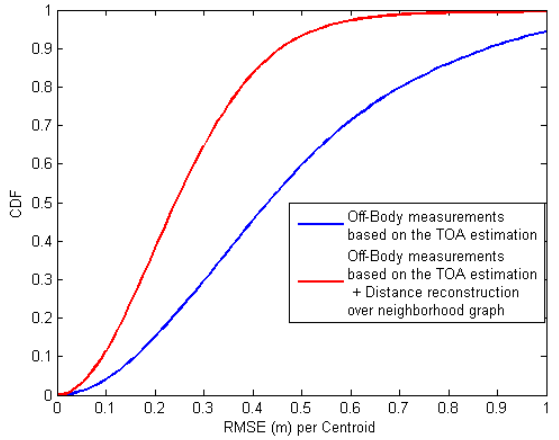

Figure 5.7: Empirical CDF of the RMSE of estimated on-body nodes' centroid for a single body, with and without distance reconstruction (i.e. using the shortest distance over neighborhood graph), for a NLLS positioning algorithm fed by TOA-based range measurements over off-body links.

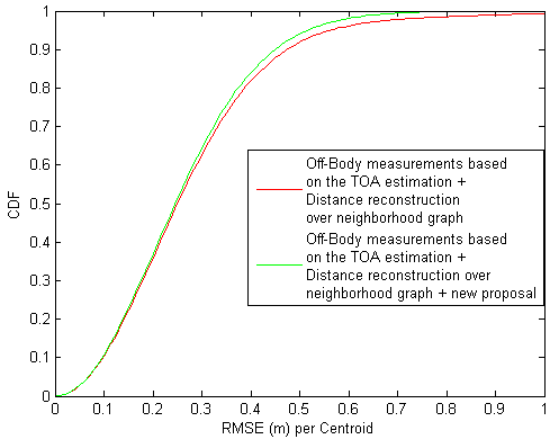

Figure 5.8: Empirical CDF of the RMSE of estimated on-body nodes' centroid for a single body, with distance reconstruction, for the classical cooperative scheme vs. the new proposal (i.e. with a priori known on-body dispersion), and a NLLS algorithm fed by TOA-based range measurements over off-body links.

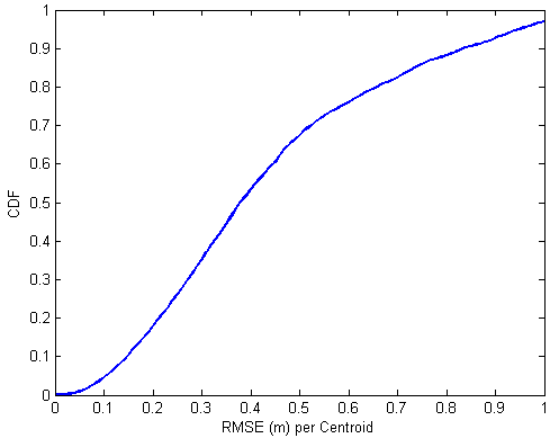

Figure 5.9: Empirical CDF of the RMSE of estimated on-body nodes' centroid for a single body and an EKF fed by TOA-based range measurements over off-body links.

users) in the different scenarios. First of all, and rather surprisingly, it appears that the non-cooperative scheme from Scenario 1 slightly outperforms the cooperative schemes from Scenarios 2, 3 and 4, when none of the proposed enhancements to combat body shadowing obstructions is implemented (but just the standard positioning algorithm). This phenomenon is most likely due to the strong error propagation (e.g. due to cumulative NLOS effects over off-body and body-to-body links) in all the network within cooperative schemes. Moreover, the number of off-body measurements available at each on-body node is systematically equal to 4, which is sufficient for estimating its $3D$ position in a non-cooperative scenario. Actually, in these simulations, we ensure full connectivity to the on-body nodes with respect to the infrastructure anchors (regardless of the NLOS conditions), while just applying more penalizing error models in case of body shadowing. In a realistic localization context however, as it will be seen in Chapter 6, some measurements may be missing due to frequent packet losses. Hence cooperative schemes shall help to compensate for such losses, contrarily to non-cooperative schemes, which may not be able to ensure the unicity of estimated on-body locations any more. Moreover, Figure 5.10 also shows that the improvements proposed to combat body shadowing, namely the distance reconstruction over neighborhood graph and the new navigation scheme assuming prior knowledge of on-body dispersion, could help to achieve rather significant gains, hence benefiting already from the cooperation potential.

Finally, on Figure 5.11, we show that the performance is significantly degraded

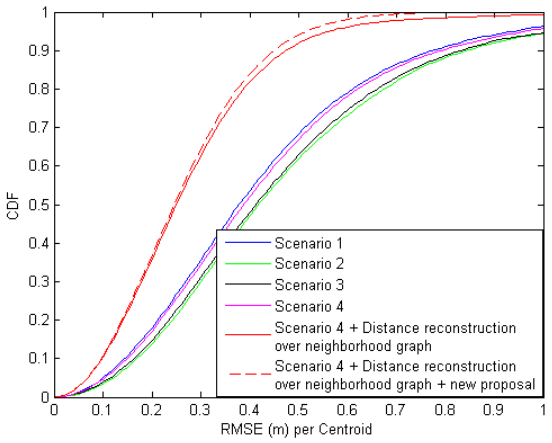

Figure 5.10: Empirical CDF of the RMSE of the RMSE of estimated on-body nodes' centroids in a group of 3 bodies, for different cooperation scenarios and a NLLS algorithm fed by TOA-based range measurements over off-body and body-to-body links.

in scenario 4, when assuming RSSI-based range measurements over off-body and body-to-body links at 2.4 GHz. Hence, those results confirm the same trends as before. The RSSI is not relevant for explicit ranging measurements in the context of

CGN applications either, but may be considered as an indirect source of information instead.

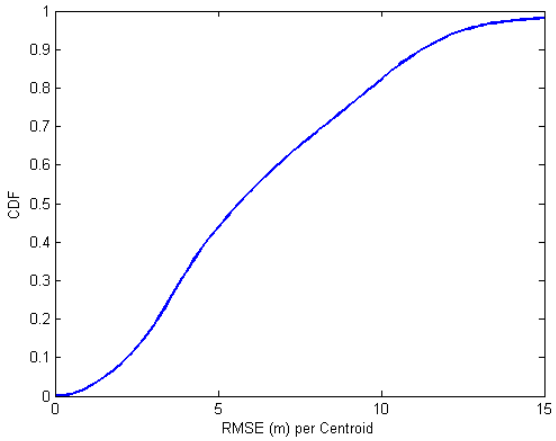

Figure 5.11: CDFs of the RMSE of the estimated centroid location of a group of 3 bodies. Localization is based on the NLLS algorithm and RSS-based range measurements over inter-body and off-body links.

5.5 Conclusion

In this chapter, we have addressed the problem of individual and collective navigation.

First of all, a cooperative NLLS algorithm has been adapted in the very context, by considering different radiolocation metrics over off-body and body-to-body links. Furthermore, we have proposed a new cooperation scheme for individual navigation, which consists in estimating directly the position of the on-body centroid, out of approximated distances with respect to the infrastructure anchors and based on the prior knowledge of on-body nodes' dispersion (under reasonable deployment constraints for the end user). This proposed scheme not only keeps on benefiting from the measurement diversity and redundancy authorized by cooperation and on-body deployment, but it also improves the average location accuracy by avoiding the error propagation due to strongly biased ranges and on-body nodes estimates. Furthermore, this proposal enables to estimate only one single position, thus reducing system complexity and energy consumption accordingly. Then this algorithm has been compared with a classical centralized EKF, showing that the latter may be optimized to account for biased observations due to NLOS body shadowing. Staying in the WBAN localization context, the next Chapter will account for experiments based on IR-UWB radio platforms to illustrate the practical limitations of the proposed MoCap solutions under realistic operating conditions.

Chapter 6

Experiments

Contents

6.1 Introduction

This Chapter accounts for real experiments based on integrated IR-UWB radio platforms. One goal is to test and partially validate some of the modeling and/or algorithmic proposals made in Chapters 3 and 4, respectively. Another objective is to illustrate the practical limitations of the latter developments under real operating conditions, in comparison with the initial target specifications claimed in Chapter 1.

First of all, various data sets of on-body and off-body range measurements have been collected for different body gestures and attitudes, so as to verify the modeling hypotheses put forward in Section 3.2 regarding conditional single-link errors based on IR-UWB TOA estimation. These experiments have been also used for preliminary calibration purposes (out of raw measurements, from a LS perspective). Hereafter, the so-called observed range measurements correspond to the calibrated measurements.

Secondly, IR-UWB devices have been deployed on a reference subject body, with infrastructure anchors placed in the surrounding indoor environment. In a first step, the intra-WBAN full mesh topology is exploited to collect only on-body range measurements (including real packet losses due to body shadowing) for relative MoCap in a body-strapped LCS, applying the CDWMDS algorithm described in Section 4.2. The second step consists in incorporating additional off-body links with respect to infrastructure anchors, in order to enable the absolute positioning

of on-body nodes in a GCS external to the body for LSIMC purposes. Hence, the 2-step localization approach described in Section 4.3 is considered. In both cases, the obtained experimental results are discussed and compared with simulation-based results from Sections 4.2.3 and 4.3.3. Unfortunately, due to time constraints, no group navigation scenarios could be tested experimentally by the time this thesis has been written.

The remaining part of this Chapter is organized as follows. Section 6.2 briefly describes the hardware equipment involved in our measurement campaign, including IR-UWB LDR platforms and a reference video acquisition system. In Section 6.3, we evaluate the real ranging errors observed over on-body and off-body links, in both LOS and NLOS conditions. Then Section 6.4 investigates relative and absolute individual MoCap applications, where the involved localization algorithms are fed with real range measurements. Finally, Section 6.5 draws a few conclusions and summarizes the main Chapter contributions.

6.2 Used Equipment and Experimental Settings

The used radio platform, which was developed at CEA-Leti, provides a representative example of integrated IR-UWB *Low Data Rate-Location and Tracking* (LDR-LT) device operating in the band [4.25, 4.75]GHz, with a complete protocol stack from the physical layer up to the localization application layer [113], [114]. Relying on internal 1 Gsps sampling and 1/1.5 bit quantization on the one hand, as well as on a *Differential Binary Phase Shift Keying* (DBPSK) modulation on the other hand, this platform enables data transmissions at the nominal rate of 350 kbps at up to 40 m in LOS, while performing peer-to-peer ranging through RT-TOF with clock drift compensation. Regarding unitary TOA estimates, the platform performs FAP detection. The index of the first sample exceeding the threshold is viewed as the TOA estimate in the local Rx observation window (i.e. direct detection is performed, but no cross-correlation with a template waveform adapted to the unitary expected pulse). Such detection is enabled within the fine time resolution of 1 ns, corresponding to the internal sampling capability (i.e. equivalently within the spatial resolution of 30 cm). The active power consumption, on the order of a few 10s of mW (typically, 10 mW in Tx and 30mW in Rx), is comparable with that of State-of-the-art technologies foreseen in the WBAN context, such as Bluetooth and ZigBee, but providing additional unprecedented ranging capabilities [108]. Figure 6.1 shows a picture of this platform in its plastic package.

Besides, fast measurement-oriented software, including simplified MAC and applications, have also been developed and ported for flexible demonstration purposes. In particular, the implemented MAC layer enables a beacon-enabled TDMA superframe structure, which appears adapted for small-size and coordinated mesh networks like in our WBAN context. Figure 6.2 shows the corresponding superframe structure [9], [115]. The *Beacon Period* (BP) is entirely specified by the coordinator, which handles resource allocation and scheduling for the entire network. A slotted

Aloha scheme is used in the *Contention Access Period* (CAP), in order to authorize a reduction of the energy consumption [9]. Furthermore, it was chosen to transmit data only during the *Contention Free Period* (CFP) using *Guaranteed Time Slots* (GTS) to prevent from collisions and improve the *Quality of Service* (QoS). Hence, in the nominal mode (i.e. in the absence of aggregation and broadcast), three adjacent GTS are reserved for each peer-to-peer range measurement between two distinct asyshronous devices, applying *3-Way* ranging transactions, as seen in Chapters 1 and 4. Unfortunately, the implemented MAC suffers from a few limitations in our specific WBAN localization context. One major problem concerns the refreshment rate that could be achievable for updating the nodes positions, which is strictly bounded by the superframe periodicity and by the number of available GTS per superframe. For practicability purposes in our study (but without loss of generality), the coordinator is external to the body and connected to a *Personal Computer* (PC) through a serial port for configuration and debug. Moreover, an additional USB link is used as a communication interface between this coordinator and the PC.

In our investigated scenarios, the TOA-based range measurements issued at IR-UWB platforms are compared with side reference measurements obtained with the optical Codamotion tracking system [10], which is able to provide very high localization accuracy (i.e. in the order of 0.05 mm). Considering the two levels of precisions, the Codamotion system will be used to determine the ranging errors. Hence, one optical marker was placed on each on-body device, in order to define its occupied position in real-time. Figure 6.3 shows the Codamotion tracking system in action, where the data files are fully traceable using legacy file formats such as ASCII text.

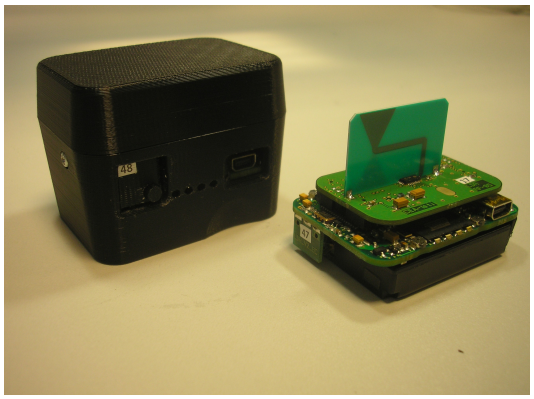

Figure 6.1: CEA-Leti's IR-UWB LDR-LT ranging-enabled platform (right) with its package (left).

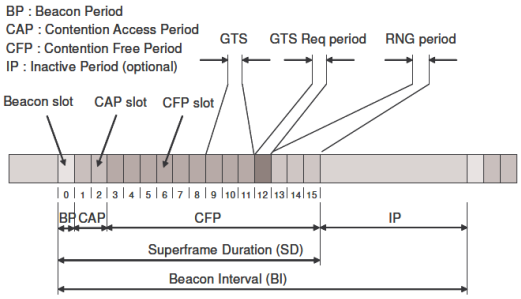

Figure 6.2: Implemented MAC superframe in the IR-UWB platform [9].

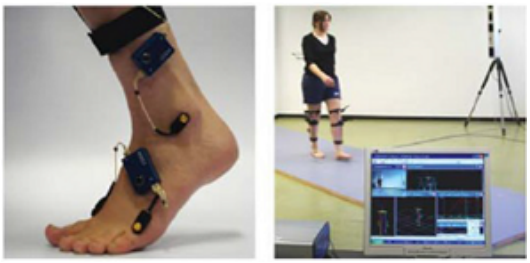

Figure 6.3: Codamotion tracking system, which considers on-body optical markers (left) and an external unit (CODA) equipped with 3 cameras [10].

6.3 Single-Link Ranging Experiments

In this section, we aim at empirically characterizing TOA-based ranging errors over IR-UWB on-body and off-body links, considering LOS and NLOS conditions in different body attitudes. Ranging accuracy will be assessed in terms of both the mean error and its standard deviation.

6.3.1 Ranging Over On-body Links

The first set of measurements is performed by placing two IR-UWB devices on the chest and the wrist of a static human body in LOS visibility of each other. Measurements have been collected during 20 sec by a time step of 1 sec. Figure 6.4 shows the implemented scenario, which is depicted in the following as Scenario 1. Figure 6.5 plots and compares the successive range measurements with respect to the real distance (delivered by the Codamotion) between the involved devices. The mean and standard deviation of ranging errors are respectively equal to 4.7 cm and 16 cm in this case.

Still considering the chest-wrist link, 3 other sets of measurements have been performed in the so-called Scenarios 2, 3 and 4. Figure 6.6 shows the corresponding body attitudes, which are defined by the wrist position. Figures 6.7, 6.8 and 6.9 compare the corresponding successive measurements and the real distances. Besides,

Figure 6.4: Experimental Scenario 1: On-body ranging over a static chest-wrist link in direct LOS visibility.

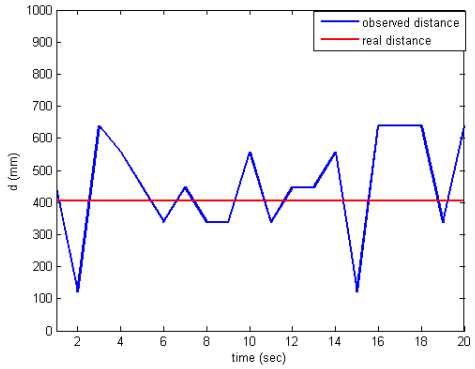

Figure 6.5: Comparison between measured and real distances over the static chest-wrist link in Scenario 1.

Table 6.1 summarizes the related ranging error parameters (i.e. mean and standard deviation) for each scenario. The obtained on-body ranging performances in LOS visibility are in compliance with the results presented in [108] for classical "body-free" LOS configurations at larger ranges in a typical indoor environment, showing that the standard deviation of ranging errors is below 30 cm. Moreover, the observed mean error is relatively small in comparison with the standard deviation and even with the true distance value. Thus, it could be neglected in first approximation over on-body links in direct LOS visibility. Those observations tend to confirm the zero-mean Gaussian hypothesis retained in Chapter 3 for IR-UWB TOA-based on-body measurements in LOS. However, the standard deviation observed with the real platforms is now larger than the values based on channel measurements (i.e. previously on the order of 10 cm in favorable SNR conditions) and hence, larger than the values assumed in the simulations of Chapter 4. This degraded accuracy is

Figure 6.6: Experimental Scenarios 2 (left), 3 (middle) and 4 (right): On-body ranging over the chest-wrist link in direct LOS visibity, for different body attitudes.

mostly due to the direct sample FAP detection scheme implemented in the real IR-UWB platforms, given the finest temporal granularity of 1 ns, whereas in Chapter 3, the performance was bounded by the signal bandwidth and resulting resolution capability (i.e. assuming an ideal and quasi-infinite temporal granularity at the receiver).

	STD (cm)	mean (cm)
Scenario 2	22	-4
Scenario 3	21	3
Scenario 4	24	5

Table 6.1: IR-UWB TOA-based ranging error parameters in Scenarios 2, 3 and 4.

The ranging error is now evaluated over static on-body links in systematic NLOS configurations. Two IR-UWB devices have been placed on the chest and the back of the subject body. Figure 6.10 shows the implemented scenario, depicted as Scenario 5 in the following. Similarly to the previous sets, the range measurements have been collected for 20 sec by a time step of 1 sec. Figure 6.11 plots and compares the observed range measurements with respect to the real distance between the involved devices. The mean and standard deviation of ranging errors are respectively equal to 5.68 m and 78 cm, which are likely redhibitory to the localization system. This phenomenon is due to a missed detection of the direct path, where TOA estimation adversely relies on a late secondary path, which may be reflected or diffracted by the surrounding materials (e.g. distant wall, distant metallic pieces of furniture), and hence, the length of the detected path is significantly biased from the direct one. One more complementary remark is that the devices' placements tend to limit also the sensitivity to close reflections (e.g. typically single-bound reflections on the ground) due to severe body obstructions also along the vertical dimension, which are most likely combined with penalizing relative antenna orientations. The propagation of radio waves diffracted around the body seems to be excluded as well in this case. The phenomenon is anyway all the more pessimistic in comparison with the results from Chapter 3 since no temporal restriction of the Rx observation window (i.e. in terms of excess delay) is applied in the IR-UWB platforms while estimating TOA (i.e. contrarily to the 5 ns window restriction assumed in Chapter 3, corresponding

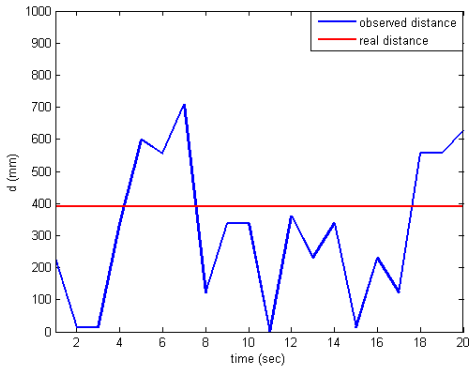

Figure 6.7: Comparison between measured and real distances over the chest-wrist link in Scenario 2.

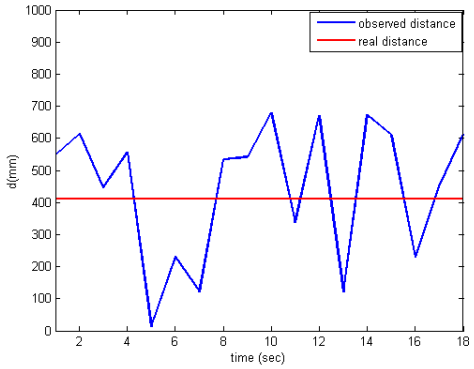

Figure 6.8: Comparison between measured and real distances over the chest-wrist link in Scenario 3.

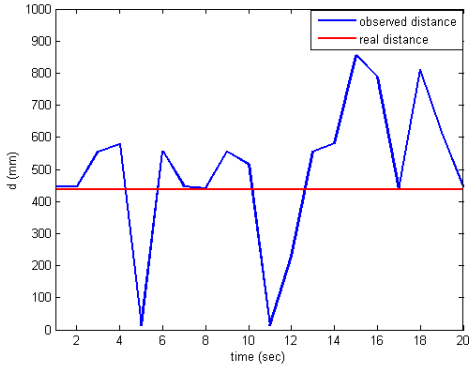

Figure 6.9: Comparison between measured and real distances over the chest-wrist link in Scenario 4.

to the confined WBAN spatial dimensions).

Figure 6.10: Experimental Scenario 5: On-body ranging over a static chest-back link, under systematic NLOS conditions.

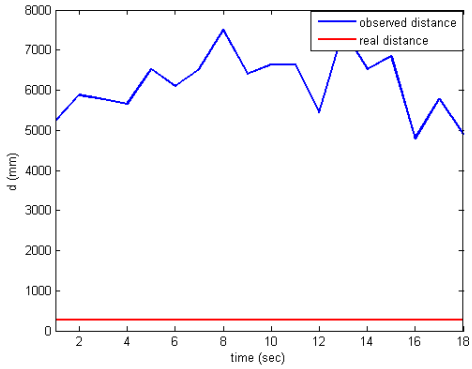

Figure 6.11: Comparison between measured and real distances over the chest-back link in Scenario 5.

Besides, another measurement set has been carried out according to Scenario 6. The chest-wrist link has been considered here, for being partially obstructed by human body shadowing (i.e. comprising also an unobstructed portion over-the-air), just like the link characterized in Chapter 3. Figure 6.12 shows the corresponding scenario, where the measurements have been collected similarly to the previous sets. Figure 6.13 plots and compares the observed range measurements with respect to the real distance separating the involved devices. The range measurement is again positively biased, with a mean error of 62 cm and a standard deviation of 25 cm. Like in Scenario 5, the positive bias is due to the detection of a late reflected path, but most likely resulting from a less distant interaction with the environment. This makes the use of partially obstructed links (like this chest-wrist link) much more

tractable for localization purposes. Moreover, the idea of positively biased range measurement over NLOS on-body links is compliant with the model that we have defined in Chapter 3, all except but the order of magnitude of this bias, which again depends on the kind of obstruction (i.e. full or partial) and Rx device capabilities (i.e. restriction of the Rx observation window, time granularity, antenna pattern and placement).

Figure 6.12: Experimental Scenario 6: On-body ranging over a static chest-wrist link, under systematic NLOS conditions.

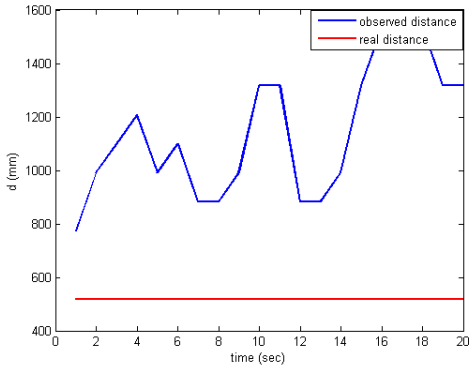

Figure 6.13: Comparison between measured and real distances over the chest-wrist link in Scenario 6.

6.3.2 Ranging Over Off-body Links

In order to evaluate the ranging errors over off-body links, we take benefit from Scenario 5, using the chest-placed device in direct LOS visibility with the coordinator, which is external to the body and located in the surrounding environment. On the other hand, the back-placed device is under systematic NLOS conditions from the same coordinator. Figure 6.14 plots and compares the measured distances

with respect to the real distance over the considered LOS off-body link (i.e. chest-coordinator). In this case, the mean ranging error is 5.6 cm and the standard deviation 17 cm. These results are compliant with the ranging error parameters observed over LOS on-body links. Figure 6.15 shows similar results over the considered NLOS off-body link, whose range measurements are again positively biased, with a mean error of 2.08 m and a standard deviation of 23 cm.

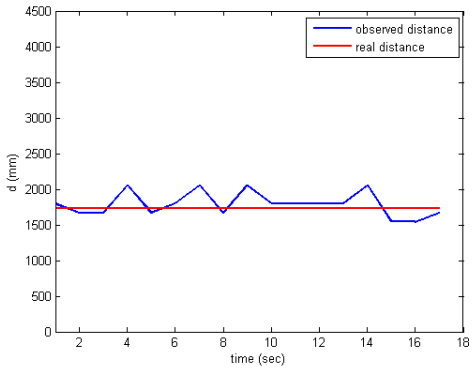

Figure 6.14: Comparison between measured and real distances over the chest-coordinator off-body link, under systematic LOS conditions.

6.4 Individual Motion Capture Experiments Based on Real Range Measurements

In this section, we account for other experiments addressing relative and absolute MoCap applications. For this sake, a full on-body mesh topology is considered, including 10 devices, as shown on Figure 6.16. Devices 1 to 4 are considered as on-body anchors, and the remaining devices as simple on-body nodes to be positioned. Table 6.2 summarizes the positions occupied by those devices, along with their status (i.e. simple mobile node or on-body anchor). Five additional infrastructure anchors are set at known positions in the indoor surrounding environment, which corresponds to a $4\,m \times 4\,m$ office room.

In our measurement setup, we had to face difficulties in synchronizing the Codamotion tracking system and the involved IR-UWB devices in case of dynamic scenarios. To overcome this problem, we defined 3 static body gestures corresponding to three key phases of the walk cycle. Range measurements have been collected in each gesture for 10 sec by a time-step of 1 sec. Figure 6.17 shows successive snapshots of the retained body gestures, based on a biomechanical model representation used in Chapter 4. The idea is to emulate mobility, assuming that a real body under moderate walk would switch between the last 3 gestures, taking approximately 1 sec between two adjacent gestures. Thus our localization problem could be considered as quasi-dynamic.

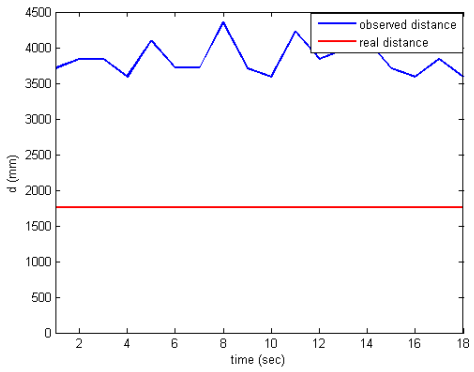

Figure 6.15: Comparison between measured and real distances over the back-coordinator off-body link, under systematic NLOS conditions.

Figure 6.16: On-body network deployment scenario for MoCap experiments.

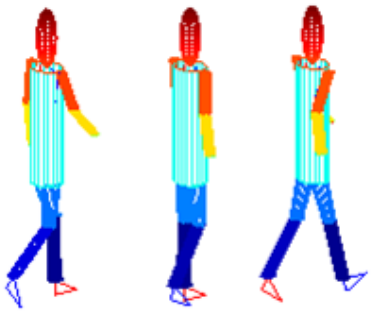

Figure 6.17: Retained body gestures for considering a quasi-dynamic localization problem.

In a first step, we consider relative positioning at the body scale (i.e. in a body-strapped LCS) based uniquely on on-body range measurements, thus applying the standard DWMDS and the new proposed CDWMDS algorithms described in Section

Device ID	On-body Position	Category
1	Chest	On-body anchor
2	Chest	On-body anchor
3	Left hip	On-body anchor
4	Back	On-body anchor
5	Right shoulder	On-body node
6	Right elbow	On-body node
7	Right wrist	On-body node
8	Left shoulder	On-body node
9	Left elbow	On-body node
10	Left wrist	On-body node

Table 6.2: IDs, positions and categories of the on-body devices used in MoCap experiments.

4.2. Figure 6.18 shows a comparison of the obtained localization RMSE per node (i.e. averaged over the three gestures). It can be noticed that the incorporation of fixed-length constraints globally improves the performance at all the peripheral mobile nodes, as expected. The average accuracy (i.e. over all the mobile nodes) is however degraded in comparison with the simulation results in Section 4.2.3, as a direct consequence of a higher standard deviation for single-link on-body range measurements (i.e. from 10 cm in simulations to 25 to 30 cm here), but in the same reasonable proportions. Given the ranging capabilities of the integrated IR-UWB devices used in our experiments, the achieved level of accuracy (e.g. with a minimum RMSE around 20 cm for the best on-body node) is thus questionable, especially when taking into account the MoCap specification of a few centimeters initially targeted in Chapter 1. Nevertheless, other applications necessitating relatively coarse levels of accuracy (e.g. gesture-based remote control or rough attitude detection) may still be covered.

The second step consists in incorporating off-body range measurements with respect to infrastructure anchors on top of on-body measurements, so as to enable the absolute positioning of on-body nodes in a GCS (e.g. associated with the room). Accordingly, we consider applying the 2-step localization approach described in Section 4.3, along with its distance approximation method based on graph neighborhood. Figure 6.19 shows the achieved localization performances, in terms of average RMSE per on-body device. Rather surprisingly, in this case, the results are no more in line but significantly degraded in comparison with the simulation-based previsions in Section 4.3.3. In particular, the application of the distance approximation method based on graph neighborhood seems no more beneficial. This may be due to the harmful conjunction of several factors, including the propagation of too strong on-body/off-body errors (hence, penalizing the transformation of the estimated coordinates from the LCS into the GCS), or even the reduced number of mobile on-body devices in comparison with the simulated scenarios, thus limiting the

benefits from full mesh cooperation... Again, these results do not seem sufficiently compliant with high precision MoCap requirements, but could be advantageously used for improved personal navigation though on-body diversity.

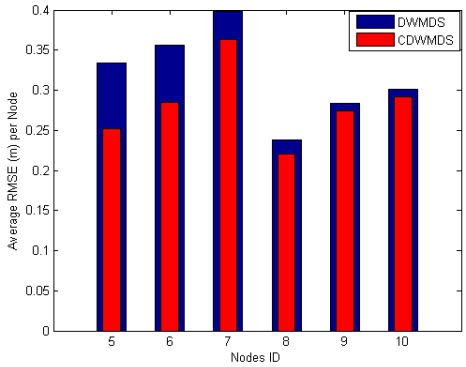

Figure 6.18: Relative localization average RMSE (m) per on-body node (ID), for DWMDS and CDWMDS localization algorithms.

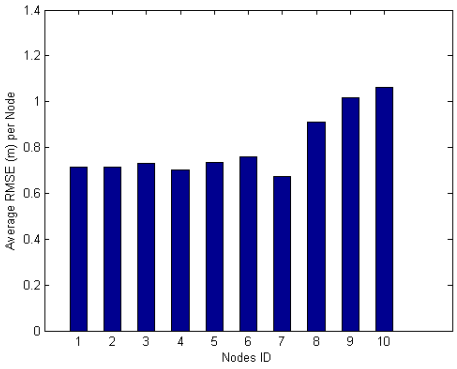

Figure 6.19: Absolute localization average RMSE (m) per on-body node (ID), based on the 2-step localization approach.

6.5 Conclusion

In this Chapter, we have described field experiments based on real IR-UWB platforms (and a reference video acquisition system) for on-body and off-body ranging error characterization, as well as for relative and absolute MoCap purposes.

Different sets of peer-to-peer measurements have been collected between IR-UWB devices, taking into account LOS and NLOS conditions over both on-body and off-body links. One first remark is that on-body and off-body ranging results

look consistent, especially in the NLOS configurations. Secondly, the observed results are at least partly compliant with the on-body models proposed in Chapter 3, where zero-mean random ranging errors have been assumed under LOS conditions, with an additive positive bias under NLOS conditions. However, experiments have revealed that the kind of on-body obstructions (i.e. full or partial) could lead to significantly different statistical bias behaviours (e.g. in terms of their maximum amplitude). In particular, it has been illustrated that the most severe chest-back measurements (not directly investigated in Chapter 3), under full and systematic NLOS conditions, could be biased by a few meters. This is most likely due to the systematic detection of distant multipath components in the TOA estimation process implemented at IR-UWB platforms, in conjunction with unfavorable antenna orientations and/or polarizations. It is worth reminding that these IR-UWB platforms have not been designed for WBAN localization (and definitely not for on-body localization), but for standard indoor localization at several tens of meters. Keeping the discussion at this single-link level, to combat NLOS biases, we suggest that the embedded TOA estimator could be judiciously adapted, without any serious hardware modification (e.g. by simply limiting the search window before the temporal synchronization point, taking into account the maximum measurable on-body distance, like in Chapter 3). Moreover, we also suggest that further studies are necessary regarding the antenna (i.e. jointly in terms of orientation, radiation diagram and/or polarization), so as to enable better sentivity to closer secondary multipath components (e.g. resulting from single-bounce reflections on the ground), or even, diffraction of the main direct path around the body.

In addition, we have addressed the relative and absolute on-body positioning problem, feeding the proposed localization algorithms with the range measurements issued at real IR-UWB platforms. The observed results show at least the robustness of the CDWMDS solution with respect to the standard DWMDS algorithm. Overall, the achieved levels of accuracy do not seem sufficiently compliant with the initial centimetric MoCap requirements. However, considering the relative localization results obtained at the body scale, some applications necessitating a relatively coarse precision (e.g. gesture-based remote control or rough attitude detection) may be covered, without necessitating any additional sensor or technology, but just relying one the current on-body IR-UWB devices, as they stand now. One step ahead, the absolute localization results could be advantageously used for improved personal navigation (at least) through on-body nodes diversity, so as to reinforce the estimated absolute macroscopic position of the user (e.g. "averaging" over on-body nodes to get a centroid).

Finally, reconciling single-link and positioning concerns, it is also worth mentioning that more recent generations of integrated IR-UWB solutions could theoretically provide centimetric ranging precision [116], [117]. The final on-body localization accuracy being somehow proportional to the latter ranging performance, as revealed herein by a quick comparison between simulation results and experiments, one could extrapolate that much higher precision, compatible with MoCap applications, could be available based on stand-alone IR-UWB systems in a reasonably short future.

Chapter 7

Conclusions and Perspectives

Contents

7.1 Conclusions

In this PhD dissertation, we have addressed the cooperative localization problem in WBAN. Various research topics and domains have thus been explored, related to physical modeling, algorithmic developments, as well as to medium access mechanisms or networking. The main personal contributions issued in the frame of these PhD investigations can be summarized as follows:

- Modeling: A dynamic on-body model has been proposed for IR-UWB TOA-based ranging in two key frequency bands and for two representative links. The drawn model, which relies on UWB channel measurements, takes into account dynamic channel obstruction configurations (i.e. LOS/NLOS) and SNR variations under body mobility. Then the related model parameters have been studied as a function of a controlled SNR within synthetic received multipath signals. On this occasion, false and missed detection phenomena have been illustrated under low SNR and NLOS conditions, as well as asymptotically ideal detection behaviour under more favourable SNR and LOS conditions. The performances of first peak and strongest peak detection schemes have also been compared. We have shown that the ranging error distribution could be fairly well modeled as a centered Gaussian distribution in LOS conditions in case of systematic strongest path detection, and as a weighted mixture between uniform and Gaussian distributions in the case of first path detection. In NLOS conditions, ranging errors are also shown to follow a weighted mixture between uniform and Gaussian distributions in case of strongest path detection.
  Secondly, representative lower bounds have been derived for the standard deviation of N-B RSSI-based and IR-UWB TOA-based range measurements over off-body and body-to-body links. One first conclusion, as expected, is that RSSI readings in NLOS conditions due to body shadowing are hardly

exploitable for ranging purposes on both kinds of links, whereas LOS conditions may provide more acceptable ranging performance, but most likely at short ranges (typically below 20 m). One second remark is that off-body and body-to-body links exhibit approximately the same behaviours in terms of ranging error statistics, in first approximation.

- Design of localization algorithms:
  - Relative on-body positioning for MoCap: A decentralized and cooperative DWMDS algorithm, which can asynchronously estimate unknown on-body nodes locations, has been adapted. In particular, we have introduced fixed-length geometric constraints (possibly self-learnt) that correspond to time-invariant Euclidean inter-node distances under body mobility. This initial CDWMDS has been enhanced through scheduling and censoring mechanisms to mitigate error propagation due to the location-dependent disparities observed among on-body nodes (e.g. in terms of connectivity, GDOP and accelerations). It has been also shown that forcing the symmetry of pair-wise measurements could help to mitigate measurement outliers and packet losses. Moreover, CDWMDS has been proved to outperform a classical MDS algorithm in terms of localization accuracy for various single-link PER values and ranging standard deviations even under realistic MAC superframe, hence illustrating rather fine robustness against latency effects.
  - Absolute on-body positioning for MoCap: Two approaches have been presented to estimate the absolute locations of on-body nodes in a global coordinates system, considering different radiolocation metrics over off-body links with respect to infrastructure anchors. One 2-step solution relies on the preliminary relative localization of on-body nodes at the body scale, before applying further transformations based on the absolute localization of on-body anchors. At first sight, body shadowing seems very challenging, not to say redhibitory, to achieve levels of precision compatible with high-precision MoCap needs. However we have proposed another algorithm that estimates the shortest path between on-body and infrastructure anchors over neighborhood graph to compensate for possible radio obstructions and penalizing measurement errors. Thanks to the latter improvement, approximately the same levels of precision as that obtained for relative on-body localization could be achieved over simulated large-scale trajectories.
  - Absolute body centroid positioning for individual and collective navigation: A cooperative NLLS algorithm has been adapted and compared with a classical tracking EKF, while considering different radiolocation metrics over off-body and body-to-body links. Furthermore, we have proposed a new cooperation scheme for individual navigation, which consists in estimating directly the position of the on-body centroid, out

of approximated distances with respect to the infrastructure anchors. The latter are based on the prior knowledge of on-body nodes' dispersion (under reasonable deployment constraints for the end user). This scheme not only keeps on benefiting from the measurement diversity and redundancy authorized by cooperation and on-body deployment, but it also improves the average localization accuracy by mitigating error propagation. Finally, only one single position needs to be computed, thus reducing system complexity and energy consumption accordingly.

- Experiments: Field experiments, based on real IR-UWB platforms (and a reference video acquisition system) have been described. These measurements aim at both single-link ranging error characterization and relative/absolute MoCap evaluation. Due to time constraints, no collective navigation could be tested however.
  On-body and off-body ranging results look consistent, especially in NLOS configurations. The observed results are also partly compliant with the originally proposed on-body models, assuming zero-mean random ranging errors under LOS conditions and additive positive bias under NLOS conditions. However, these experiments have also revealed that on-body obstructions could lead to significantly different bias behaviours, depending whether the obstruction is full or partial (e.g. chest-back range measurements could be biased by a few meters). Possible reasons have been pointed out, such as the detection of late multipath components in the used IR-UWB platforms, which have been designed for standard indoor localization at several tens of meters (but not for WBAN applications), or even unfavorable antenna orientations and polarizations, which favor neither diffracted path around the body, nor early/close secondary paths (e.g. single-bounce reflections on the ground).
  Additional experimental scenarios have been considered for relative and absolute on-body positioning, feeding the proposed localization algorithms with on-body (and off-body) range measurements from the real IR-UWB platforms. Significant performance improvements have been noted when applying fixed-length constraints, even if the achieved accuracy cannot be really compliant with MoCap requirements at first sight. Nevertheless, relying uniquely on the current on-body IR-UWB devices (i.e. even if not optimized in the very context), gesture-based remote control or rough attitude detection could be already covered on the one hand. The absolute localization results could be also advantageously used for improved individual or collective navigation, relying on on-body diversity (not shown herein).

Overall, one can conclude that the cooperative localization problem in WBAN, as initially stated in Chapter 1 for stand-alone and opportunistic MoCap and navigation applications, has been only partly solved out here (especially regarding high precision MoCap) and numerous points still remain open. On the one hand, practical experiments and empirical channel-based observations tend to suggest that a few working hypotheses have been underestimated at the beginning of our PhD

investigations, as well as in our simulations (e.g. body shadowing effects on both ranging errors and packet losses). On the other hand, we believe that the current state-of-the-art radio capabilities are not yet arrived at their full potential in terms of single-link precision. Finally, some of our initial proposals detailed above (e.g. body-constrained decentralized localization, use of on-body diversity...), though non-definitive, may deserve complementary future research efforts, as seen in the next subsection.

7.2 Perspectives

After recalling the main PhD contributions and their limitations, we draw hereafter some related perspectives and possible axes of research for future works:

- Consider coupling the CDWMDS localization algorithm with tracking/smoothing algorithms, better initialization policy and/or a soft weighting of the available single-link measurements in the optimized cost function (e.g. depending on the link quality, the channel obstruction status or the empirically observed "instantaneous" PER).

- Enable more efficient links selection and parsimonious/timely cooperation over on-body, body-to-body and off-body links (i.e. relying uniquely on the most relevant and necessary links), hence improving robustness, while reducing over-the-air traffic and latency.

- Design ranging-enabled IR-UWB receivers and impulse detection algorithms, which could be more suitable into the WBAN localization context. For instance, so as to combat NLOS biases over on-body links due to body shadowing within the current IR-UWB devices (e.g. those used in our experiments), the embedded TOA estimation procedure could be adapted without changing the hardware capabilities, by simply limiting the search window (e.g. taking into account the maximum measurable on-body distance). Regarding the antenna, optimizations are also expected (i.e. jointly in terms of mastered orientation, radiation diagram and/or polarization), to enable better sensibility to early/close secondary multipath components, or even, a diffraction of the direct path around the body. Finally, more recent generations of integrated low-power IR-UWB solutions, which already claim centimetric levels of ranging precisions, should be considered in the WBAN context to scalably achieve localization performances compatible with MoCap applications in a reasonably short future.

- Perform hybrid data fusion to combine IR-UWB radiolocation metrics with other modalities, such as inertial measurements issued at embedded IMU (e.g. delivering at least accurate information about the body-limbs orientation). Such multimodal solutions are likely to offer the highest and most promising potential in terms of precision, but additional research efforts must be made

in terms of algorithmic design and implementation, so as to limit computational complexity and power consumption, while coping with sychronization constraints between the two sub-systems.

- Mitigate the effects of latency introduced by communication protocols on localization performance, and thus, emphasizing the needs for cross-layer design approaches ("by nature").

- Develop more adapted evaluation tools, through semi-deterministic radio modeling under complex human mobility, for realistic performance assessment and benefit from the latest advances in the field of WBAN radio propagation prediction (e.g. diffraction theory applied to dielectric cylinders, deterministic ray-tracing...) to elaborate even more robust ranging/localization algorithms.

Appendix A

Cramer-Rao Lower Bound for the TOA Estimation of UWB Signals

A.1 System Structure

The Cramer-Rao Lower Bound (CRLB) of the TOA estimator, based on the IR-UWB signals is derived here.

Let $p(t)$ be the transmitted UWB signal. Hence, in a pure AWGN channel $n(t)$, the received signal $r(t)$ is

$$r(t) = p(t-\tau) + n(t) \tag{A.1}$$

where every sample of n(t) is Gaussian distributed with zero mean and variance σ_0^2, and τ is the time delay to be estimated.

In a multipath channel, the received signal is given by:

$$r(t) = \sum_{j=1}^{L_p} \alpha_j p(t-\tau_j) + n(t) = h(t) \otimes p(t) + n(t) \tag{A.2}$$

where $h(t) = \sum_{j=1}^{L_p} \alpha_j \delta(t-\tau_j)$ is the multipath CIR, $\delta(.)$ is the Dirac delta function, L_p is the number of multipath components, α_j and τ_j are respectively the amplitude and delay of the j-th multipath component.

For the AWGN model in A.1, the received signal can be represented as a vector of K samples as follows:

$$\mathbf{r} = \mathbf{p} + \mathbf{n} \tag{A.3}$$

where $\mathbf{r} = [r_1, r_2, ..., r_K]$, $\mathbf{p} = [p_1, p_2, ..., p_K]$ and $\mathbf{n} = [n_1, n_2, ..., n_K]$.

Suppose an unbiased estimator of τ, then the estimation error variance is lower bounded by the CRLB, and thus, $E_{\mathbf{r}}|(\hat{\tau}-\tau)^2| \geq CRLB(\tau)$, where

$$CRLB(\tau) = (E_{\mathbf{r}|\tau}[-\frac{d^2}{d\tau^2} ln(p(\mathbf{r}|\tau))])^{-1} \tag{A.4}$$

in A.4, $p(\mathbf{r}|\tau)$ is the conditional pdf.

Since the additional noise $n(t)$ is white and zero mean, $p(\mathbf{r}|\tau)$ can be expressed as

$$p(\mathbf{r}|\tau) = \prod_{k=1}^{K} \frac{1}{\sqrt{2\pi}\sigma_0} exp(-\frac{1}{2\sigma_0^2}(r_k - p_k)^2) = (\frac{1}{\sqrt{2\pi}\sigma_0})^K exp(-\frac{1}{2\sigma_0^2}\sum_{k=1}^{K}(r_k - p_k)^2) \tag{A.5}$$

A continuous-time equivalent of $p(\mathbf{r}|\tau)$ can be developed [118], [119], and the log-likelihood function $L(\mathbf{r},\tau)$ can be represented as follows

$$L(\mathbf{r},\tau) = \frac{1}{2\sigma_0^2}(2\int_{T_0} r(t)p(t-\tau)dt - \int_{T_0} p^2(t-\tau)dt) \tag{A.6}$$

A.2 CRLB For Single Pulse Systems in AWGN

In this case, the CRLB can be derived from A.6 or directly from [120] as the following form

$$CRLB(\tau) = \frac{\sigma_0^2}{\int_{T_0} \dot{p}^2(t-\tau)dt} \tag{A.7}$$

where $\dot{p}(t-\tau)$ denotes one partial differentiation with respect to τ. Hence, this equation conducts to the same form of equation 1.2.

A.3 CRLB For UWB Signal in Multpath Channel

In this section, we focus on multipath channels and derive the CRLBs using joint detection for multiple multipath parameters $\boldsymbol{\alpha} = [\alpha_1, ..., \alpha_j, ..., \alpha_{L_p}]$ and $\boldsymbol{\tau} = [\tau_1, ..., \tau_j, ..., \tau_{L_p}]$, which are treated as unknown but deterministic.

Start with A.2, the log-likelihood function in A.6 can be rewritten as $L(\mathbf{r},\tau,\boldsymbol{\alpha})$ as

$$L(\mathbf{r},\tau,\boldsymbol{\alpha}) = \frac{1}{\sigma_0^2}\int_{T_0} r(t)\sum_j \alpha_j p(t-\tau_j)dt - \frac{1}{2\sigma_0^2}(\int_{T_0}[\sum_j \alpha_j p(t-\tau_j)]^2 dt \tag{A.8}$$

Lower bounds on the variances of estimates for the components of α_j and τ_j are given in terms of the diagonal elements of the inverse of the Fisher information matrix $\mathbf{J^{-1}}$. After some manipulations, the Fisher information matrix $\mathbf{J}$ can be given as:

$$\mathbf{J} = \begin{pmatrix} \mathbf{J}_{\tau\tau} & \mathbf{J}_{\tau\alpha} \\ \mathbf{J}_{\alpha\tau} & \mathbf{J}_{\alpha\alpha} \end{pmatrix} \tag{A.9}$$

where $\mathbf{J}_{\tau\tau}$, $\mathbf{J}_{\tau\alpha}$, $\mathbf{J}_{\alpha\tau}$ and $\mathbf{J}_{\alpha\alpha}$ are all $L_p \times L_p$ matrices, as well as the $[j,m]^{th}$ element is given by

$$J_{\tau\tau}[j,m] = \frac{1}{\sigma_0^2}\int_{T_0} \alpha_j\alpha_m\dot{p}(t-\tau_j)\dot{p}(t-\tau_m)dt \tag{A.10}$$

$$J_{\alpha\alpha}[j,m] = \frac{1}{\sigma_0^2}\int_{T_0} p(t-\tau_j)p(t-\tau_m)dt \tag{A.11}$$

$$J_{\tau\alpha}[j,m] = J_{\alpha\tau}[j,m] = -\frac{1}{\sigma_0^2}\int_{T_0} \alpha_j\dot{p}(t-\tau_j)p(t-\tau_m)dt \tag{A.12}$$

Appendix B

Adaptive Self-Learning and Detection of On-Body Fixed-Length Links

On-body links can be classified into two categories. The first one corresponds to the mobile links with variable lengths, which are characterized by a distance that varies over time under body mobility. The second category concerns the fixed-length links, where the distance is considered as time-invariant under body mobility. Hence, we formulate the classification/identification issue into a decision problem. For a given pair of nodes, the first hypothesis H_0 corresponds to the fixed-length link, whereas hypothesis H_1 corresponds to a variable mobile-length link under mobility.

$$\begin{aligned} H_0 &: \text{ Fixed-length link} \\ H_1 &: \text{ Mobile-length link} \end{aligned} \tag{B.1}$$

For the considered on-body link between two devices, $\widetilde{d} = [\widetilde{d}(1), \widetilde{d}(2), ..., \widetilde{d}(N)]$ denotes the vector, which contains N consecutive distance measurements, for instance based on IR-UWB TOA or N-B RSSI estimation. Hereafter, a simple new method is proposed for the detection of the fixed-length links.

The detector is depicted as a variance-based detector. We assume that the observed distance at time-stamp k can be represented by the following equation:

$$\widetilde{d}(k) = d(k) + n(k) \tag{B.2}$$

where, $d(k)$ denotes the true distance at time k and $n(k)$ is a random variable, which represents the ranging error process. For simplicity, we assume that ranging errors are i.i.d. variables that follow a centered Gaussian distribution, with a variance σ^2. We define two unbiased estimators. The first one corresponds to the mean of the observed distance measurements, denoted by $\bar{d}$ and represented by equation B.3. The second one consists in estimating the variance of the observed distance vector, where the estimated variance $\hat{var}(\widetilde{d})$ is given by equation B.4 [121]. This empirical variance estimator is unbiased and thus, it can be written as a sum of the statistical variance of the range measurements $\widetilde{d}$ seen as r.v., and an additive random variable e resulting from the estimation process, which is zero-mean with the variance of $(var(\widetilde{d})\sqrt{\frac{2}{N-1}})^2$, according to equation B.5.

$$\bar{d} \triangleq \frac{1}{N}\sum_{i=1}^{N}\widetilde{d}(i) \tag{B.3}$$

$$\hat{\sigma}^2 \triangleq \frac{1}{N-1}\sum_{i=1}^{N}(\widetilde{d}(i)-\bar{d})^2 \tag{B.4}$$

$$\hat{var}(\widetilde{d}) = var(\widetilde{d}) + e \tag{B.5}$$

Under H_0, for the fixed-length links, $\hat{var}(\widetilde{d})$ is close to σ^2 for a sufficiently large N, whereas it becomes significantly larger than σ^2 under mobility. We defined the missed detection probability P_M, which represents the probability to detect a fixed-length link as variable-length one, as follows:

$$P_M = P(Decision = H_1|H_0) = \int_{threshold}^{+\infty} p(e|H_0)de \tag{B.6}$$

where $p(e|H_0)$ denotes the pdf of the variable e, when a fixed-length link is involved. Once P_M is specified a priori, the detection threshold value can be easily calculated, and thus, a new form of the variance-based detector can be represented in equation B.7

$$\begin{aligned} &\text{Decision} = H_0 \quad if\ (\hat{var}(\widetilde{d}) - \sigma^2) \leq \text{threshold} \\ &\text{Decision} = H_1 \quad if\ (\hat{var}(\widetilde{d}) - \sigma^2) \geq \text{threshold} \end{aligned} \tag{B.7}$$

Appendix C

Cramer-Rao Lower Bound for Relative On-Body Nodes Positioning

As described in Chapter 2, the CRLB defines the lower bound on the variance of any unbiased estimator. In this context, the present section derives the CRLB of any unbiased estimator for the relative on-body nodes positions, under ranging error based on the TOA estimation that is considered as centered Gaussian variable with a variance $\sigma^2(t)$.

As for MoCap, which is investigated by estimating the 3D positions of the on-body nodes, and thus, we are seeking for the CRLB, which characterizes the 3D positions estimators, relying on [122].

As seen previously, a WBAN is first characterized by n on-body mobile nodes and m anchors, with respective positions $X_i(t) = (x_i(t), y_i(t), z_i(t))_{i=1}^{m+n}$ forming the overall network-level vector of positions $X(t) = [X_1(t), ..., X_m(t), ..., X_{m+n}(t)]$ at time t. Hence, the Fisher information matrix (FIM) can be derived as follows:

$$F(t) = \begin{pmatrix} F_{xx}(t) & F_{xy}(t) & F_{xz}(t) \\ F_{xy}^T(t) & F_{yy}(t) & F_{yz}(t) \\ F_{xz}^T(t) & F_{yz}^T(t) & F_{zz}(t) \end{pmatrix} \tag{C.1}$$

where:

$$[F_{xx}(t)]_{k,l} = \begin{cases} \frac{1}{\sigma^2(t)} \sum_{i \in H(k)} \frac{(x_k(t)-x_i(t))^2}{||X_k(t)-X_i(t)||^2}, & k = l \\ \frac{-1}{\sigma^2(t)} I_{H(k)}(l) \frac{(x_k(t)-x_l(t))^2}{||X_k(t)-X_i(t))||^2}, & k \neq l \end{cases} \tag{C.2}$$

$$[F_{yy}(t)]_{k,l} = \begin{cases} \frac{1}{\sigma^2(t)} \sum_{i \in H(k)} \frac{(y_k(t)-y_i(t))^2}{||X_k(t)-X_i(t)||^2}, & k = l \\ \frac{-1}{\sigma^2(t)} I_{H(k)}(l) \frac{(y_k(t)-y_l(t))^2}{||X_k(t)-X_i(t))||^2}, & k \neq l \end{cases} \tag{C.3}$$

$$[F_{zz}(t)]_{k,l} = \begin{cases} \frac{1}{\sigma^2(t)} \sum_{i \in H(k)} \frac{(z_k(t)-z_i(t))^2}{||X_k(t)-X_i(t)||^2}, & k = l \\ \frac{-1}{\sigma^2(t)} I_{H(k)}(l) \frac{(z_k(t)-z_l(t))^2}{||X_k(t)-X_i(t))||^2}, & k \neq l \end{cases} \tag{C.4}$$

$$[F_{xy}(t)]_{k,l} = \begin{cases} \frac{1}{\sigma^2(t)} \sum_{i \in H(k)} \frac{(x_k(t)-x_i(t))(y_k(t)-y_i(t))}{||X_k(t)-X_i(t)||^2}, & k = l \\ \frac{-1}{\sigma^2(t)} I_{H(k)}(l) \frac{(x_k(t)-x_l(t))(y_k(t)-y_l(t))}{||X_k(t)-X_i(t)||^2}, & k \neq l \end{cases} \tag{C.5}$$

$$[F_{xz}(t)]_{k,l} = \begin{cases} \frac{1}{\sigma^2(t)} \sum_{i \in H(k)} \frac{(x_k(t)-x_i(t))(z_k(t)-z_i(t))}{||X_k(t)-X_i(t)||^2}, & k = l \\ \frac{-1}{\sigma^2(t)} I_{H(k)}(l) \frac{(x_k(t)-x_l(t))(z_k(t)-z_l(t))}{||X_k(t)-X_i(t)||^2}, & k \neq l \end{cases} \tag{C.6}$$

$$[F_{yz}(t)]_{k,l} = \begin{cases} \frac{1}{\sigma^2(t)} \sum_{i \in H(k)} \frac{(y_k(t)-y_i(t))(z_k(t)-z_i(t))}{||X_k(t)-X_i(t)||^2}, & k = l \\ \frac{-1}{\sigma^2(t)} I_{H(k)}(l) \frac{(yk(t)-y_l(t))(z_k(t)-z_l(t))}{||X_k(t)-X_i(t)||^2}, & k \neq l \end{cases} \quad \text{(C.7)}$$

Herein, $F_{xx}(t)$, $F_{yy}(t)$, $F_{zz}(t)$, $F_{xy}(t)$, $F_{xz}(t)$ and $F_{yz}(t)$ are submatrices, each of $n \times n$ elements. T denotes the matrix transpose operator. $H(k) = j \in [1 : n+m]$ that makes pair-wise observations with node k. $I_{H(k)}(l)$ is equal to 1 if $l \in H(k)$ or 0 otherwise. $d_{ij}(t) = ||X_i(t) - X_j(t)||^{1/2}$ denotes the Euclidean distance between devices i and j.

Let $\hat{X}_i(t) = (\hat{x}_i(t), \hat{y}_i(t), \hat{z}_i(t))$ be an unbiased estimators of $X_i(t)$. Thus, the trace of the covariance matrix (i.e. $F(t)^{-1}$) of the ith location estimates satisfies:

$$\begin{aligned} CRLB_i(t) &= cov(\hat{x}_i(t)) + cov(\hat{y}_i(t)) + cov(\hat{z}_i(t)) \\ &\geq [F(t)^{-1}]_{i,i} + [F(t)^{-1}]_{i+n,i+n} + [F(t)^{-1}]_{i+2n,i+2n} \end{aligned} \quad \text{(C.8)}$$

Appendix D

Reminder of the Extended Kalman Filter Formulation

The KF represents a special case of the Bayesian filter, requiring a linear state-space equation and a linear observation model, in addition to zero-mean Gaussian noise process. Furthermore, the KF conducts to an optimum tracking solution if the criteria on linearity and Gaussianity are fulfilled. However, if the observation is based on the direct range measurements, which are highly non linear with respect to the occupied positions, then, the linear KF could be not reasonable to solve the tracking problem.

As an alternative solution to such non-linearity issues, the EKF solution [76], [77] considers the following state-space and observation models:

$$\begin{aligned} \mathbf{S}(k) &= \mathbf{A}\mathbf{S}(k-1) + \mathbf{u}(k) \\ \widetilde{\mathbf{d}}(k) &= h(\mathbf{S}(k)) + \mathbf{n}(k) \end{aligned} \tag{D.1}$$

where $\mathbf{S}(k) = [X_1^T(k)\ V_1^T(k)\ X_2^T(k)\ V_2^T(k) \dots X_n^T(k)\ V_n^T(k)]$ denotes the $6\,n$ dimensional state-space vector at time-stamp kT or iteration k, including the three-dimensional positions and velocities of each blind node, which must be positioned. The vector $\widetilde{\mathbf{d}}(k) = [\{\{\widetilde{d}_{ij}(k)\}_{j=n+1:n+m}\}_{i=1:n}\ \{\{\widetilde{d}_{ij}(k)\}_{j=1:n}\}_{i=1:n}\}]$ denotes the vector of available range measurements of nodes, either with respect to other nodes or infrastructure anchors. The state transition matrix $\mathbf{A}$ is given by:

$$\mathbf{A} = \mathbf{I_n} \otimes \left(\mathbf{I_6} + \left(\begin{pmatrix} 0 & 1 \\ 0 & 0 \end{pmatrix} \otimes \begin{pmatrix} T & 0 & 0 \\ 0 & T & 0 \\ 0 & 0 & T \end{pmatrix} \right) \right) \tag{D.2}$$

where $\mathbf{I_l}$ denotes the $l-$ dimensional identity matrix and $\otimes$ is the Kronecker product. Hence, $\mathbf{A}$ is based on a priori information bridging the occupied positions at two consecutive time stamps: kT and $(k+1)T$. In this approach, we assume that each node moves independently of each other. $\mathbf{u}(k)$ is the state-space noise vector, with covariance matrix $\mathbf{Q}$, and $\mathbf{n}(k)$ is the observation noise vector with covariance matrix $\mathbf{\Sigma}(k)$. The noise covariance matrix can vary dynamically over time as a function of the number of available range measurements. Finally, $h(.)$ denotes the non-linear relation between the observed measurements and the state vector.
The implementation of the EKF starts with the initialization phase. Afterward,

the occupied positions are iteratively estimated, based on the state-space and the observation according to the following phases:

Prediction Phase: This phase consists in predicting the occupied position at time-stamp kT, as a function of the estimated position $\hat{\mathbf{S}}(k-1|k-1)$ at the previous time-stamp $(k-1)T$, then, the predicted position is given as follows:

$$\hat{\mathbf{S}}(k|k-1) = \mathbf{A}\hat{\mathbf{S}}(k-1|k-1) \tag{D.3}$$

where, $(k|k-1)$ means that the estimate at time-stamp kT is based on the knowledge of the measurements and the history up to time-stamp $(k-1)T$. After that prediction, the corresponding MMSE matrix is expressed as:

$$\mathbf{M}(k|k-1) = \mathbf{A}\mathbf{M}(k-1|k-1)\mathbf{A}^T + \mathbf{Q} \tag{D.4}$$

Correction Phase: This phase consists in correcting the error committed during the prediction, based on the observed measurements at time-stamp kT. Hence, the Kalman gain matrix includes a weighting between the predicted estimates and the current measurements, and is given as:

$$\mathbf{K}(k) = \mathbf{M}(k|k-1)\mathbf{H}^T(k)(\mathbf{\Sigma}(k) + \mathbf{H}(k)\mathbf{M}(k|k-1)\mathbf{H}^T(k))^{-1} \tag{D.5}$$

In the classical equations (e.g. in the case of KF), the matrix $\mathbf{H}(k)$ includes a linear relation between the state and the measurements. Since for positioning applications, we usually have a non-linear dependency, thus the observation equation is linearized around the predicted state-space vector as follows:

$$h(\mathbf{S}(k)) \approx h(\hat{\mathbf{S}}(k|k-1)) + \mathbf{H}(k)(\mathbf{S}(k) - \hat{\mathbf{S}}(k|k-1)) \tag{D.6}$$

where the Jacobian observation matrix is:

$$\mathbf{H}(k) = \frac{\partial h(\mathbf{S}(k))}{\partial \mathbf{S}(k)} \mid_{\mathbf{S}(k)=\hat{\mathbf{S}}(k|k-1)} \tag{D.7}$$

Hence, it includes the derivations of the observation equation with respect to the variables of the state-space vector. Finally, the correction step combines the predicted estimates with the current measurements weighted with the Kalman gain matrix. Thus, the final estimate of the state-space vector is given as follows:

$$\hat{\mathbf{S}}(k|k) = \hat{\mathbf{S}}(k|k-1) + \mathbf{K}(k)(\widetilde{\mathbf{d}}(k) - h(\hat{\mathbf{S}}(k|k-1))) \tag{D.8}$$

The corresponding MMSE matrix is obtained as:

$$\mathbf{M}(k|k) = (\mathbf{I}_{6n} - \mathbf{K}(k)\mathbf{H}(k))\mathbf{M}(k|k-1) \tag{D.9}$$

Bibliography

[1] M. Hanson, H. Powell, A. Barth, K. Ringgenberg, B. Calhoun, J. Aylor, and J. Lach. Body area sensor networks: Challenges and opportunities. *Computer*, 42(1):58–65, 2009. (Cited on pages xi and 2.)

[2] H. Shaban. *A novel highly accurate wireless wearable human locomotion tracking and gait analysis system via UWB radios.* PhD thesis, Virginia Polytechnic Institute and State University, 2010. (Cited on pages xi, 7, 27, 39 and 41.)

[3] S. Gezici, Zhi Tian, G.B. Giannakis, Hisashi Kobayashi, A.F. Molisch, H.V. Poor, and Z. Sahinoglu. Localization via ultra-wideband radios: a look at positioning aspects for future sensor networks. *Signal Processing Magazine, IEEE*, 22(4):70–84, 2005. (Cited on pages xi, 10 and 11.)

[4] K. Kyung-Sup, S. Ullah, and N. Ullah. An overview of ieee 802.15.6 standard. In *Applied Sciences in Biomedical and Communication Technologies (ISABEL), 2010 3rd International Symposium on*, pages 1–6, 2010. (Cited on pages xi, 1, 22, 23 and 86.)

[5] A. Fort, C. Desset, J. Ryckaert, P. De Doncker, L. Van Biesen, and P. Wambacq. Characterization of the ultra wideband body area propagation channel. In *Ultra-Wideband, 2005. ICU 2005. 2005 IEEE International Conference on*, pages 6–pp, 2005. (Cited on pages xi, 25 and 26.)

[6] R. D'Errico and L. Ouvry. Time-variant ban channel characterization. In *Personal, Indoor and Mobile Radio Communications, 2009 IEEE 20th International Symposium on*, pages 3000–3004, 2009. (Cited on pages xii, 26, 40, 42, 45, 53 and 55.)

[7] P. Pasquero and R. D'Errico. Joint delay and angle-of-arrival characterization and modelling of uwb off-body channels. *To be submitted on Antenna and Propagation, IEEE Transactions.* (Cited on pages xiii, 62 and 64.)

[8] E. Ben Hamida, M. Maman, B. Denis, and L. Ouvry. Localization performance in wireless body sensor networks with beacon enabled mac and space-time dependent channel model. In *Personal, Indoor and Mobile Radio Communications Workshops (PIMRC Workshops), 2010 IEEE 21st International Symposium on*, pages 128–133, 2010. (Cited on pages xiii, xvii, 27, 28, 37, 39, 70, 77, 78, 92 and 104.)

[9] I. Bucaille, A. Tonnerre, L. Ouvry, and B. Denis. Mac layer design for uwb ldr systems: Pulsers proposal. In *Positioning, Navigation and Communication, 2007. WPNC'07. 4th Workshop on*, pages 277–283, 2007. (Cited on pages xv, 112, 113 and 114.)

[10] http://www.codamotion.com. (Cited on pages xv, 6, 113 and 114.)

[11] http://www.ieee8012.org/15/pub/TG6.html. (Cited on pages xvii, 1, 11, 22, 24, 80 and 91.)

[12] R. Rosini and R. D'Errico. Off-body channel modelling at 2.45 ghz for two different antennas. In *Antennas and Propagation (EUCAP), 2012 6th European Conference on*, pages 3378–3382, 2012. (Cited on pages xvii, 26, 56, 57, 92 and 104.)

[13] R. Rosini, R. d'Errico, and Verdone R. Body-to-body communications: a measurement-based channel model at 2.45 ghz. In *Personal Indoor and Mobile Radio Communications (PIMRC 2012)*, pages 1763–1768, 2012. (Cited on pages xvii, 25, 26, 59 and 104.)

[14] S. Ullah, H. Higgins, B. Braem, B. Latre, C. Blondia, I. Moerman, S. Saleem, Z. Rahman, and K. Kwak. A comprehensive survey of wireless body area networks. *Journal of Medical Systems*, 36(3):1065–1094, 2012. (Cited on page 1.)

[15] Y. Hovakeemian, K. Naik, and A. Nayak. A survey on dependability in body area networks. In *Medical Information Communication Technology (ISMICT), 2011 5th International Symposium on*, pages 10–14, 2011. (Cited on page 1.)

[16] http://www.ee.qub.ac.uk/wireless/interactive.html. (Cited on page 2.)

[17] T.B. Moeslund, A. Hilton, and V. Krager. A survey of advances in vision-based human motion capture and analysis. *Computer Vision and Image Understanding Special Issue on Modeling People - Visionbased understanding of a persons shape, appearance, movement and behaviour*, 104(2-3):90–126, 2006. (Cited on page 6.)

[18] A. Leardini, L. Chiari, A. Cappozzo, and U. DellaCroce. Human movement analysis using stereophotogrammetry part 2: instrumental errors. *Gait and Posture*, 21(2):197–211, 2005. (Cited on page 6.)

[19] T. Sakaguchi, T. Kanamori, H. Katayose, K. Sato, and S. Inokuchi. Human motion capture by integrating gyroscopes and accelerometers. In *Proceedings IEEE/SICE/RSJ MFI96*, pages 470–475, 1996. (Cited on page 6.)

[20] A. Andreadis, A. Hemery, A. Antonakakis, G. Gourdoglou, P. Mauridis, D. Christopoulos, and J. Karigiannis. Real-time motion capture technology on a live theatrical performance with computer generated scenery. In *Informatics (PCI), 2010 14th Panhellenic Conference on*, pages 148–152, 2010. (Cited on page 6.)

[21] S. Aloui, C. Villien, and S. Lesecq. A framework for motion capture system design using cramer-rao lower bound. In *Communications, Computers and*

Signal Processing (PacRim), 2011 IEEE Pacific Rim Conference on, pages 79–84, 2011. (Cited on page 6.)

[22] E. Foxlin. Pedestrian tracking with shoe-mounted inertial sensors. *Computer Graphics and Applications, IEEE*, 25(6):38–46, 2005. (Cited on page 6.)

[23] Chin-Woo Tan and Sungsu Park. Design of accelerometer-based inertial navigation systems. *Instrumentation and Measurement, IEEE Transactions on*, 54(6):2520–2530, 2005. (Cited on page 6.)

[24] Lei Fang, P.J. Antsaklis, L.A. Montestruque, M.B. McMickell, M. Lemmon, Yashan Sun, Hui Fang, I. Koutroulis, M. Haenggi, Min Xie, and Xiaojuan Xie. Design of a wireless assisted pedestrian dead reckoning system - the navmote experience. *Instrumentation and Measurement, IEEE Transactions on*, 54(6):2342–2358, 2005. (Cited on page 6.)

[25] J.F. OBrien, R.E. Bodenheimer, G.J. Brostow, and J.K. Hodgins. Automatic joint parameter estimation from magnetic motion capture data. *Georgia Institute of Technology*, 1999. (Cited on page 7.)

[26] F.H. Raab, E.B. Blood, T.O. Steiner, and H.R. Jones. Magnetic position and orientation tracking system. *Aerospace and Electronic Systems, IEEE Transactions on*, AES-5(2):197–211, 1979. (Cited on page 7.)

[27] Z. Knoll, R. Kiss, and L. Kocsis. Joint kinematics next term and spatial temporal parameters of gait measured by an ultrasound-based system. *Gait and Posture*, 7(26):197–211, 2004. (Cited on pages 7 and 8.)

[28] T. Sato, S. Nakamura, K. Terabayashi, M. Sugimoto, and H. Hashizume. Design and implementation of a robust and real-time ultrasonic motion-capture system. In *Indoor Positioning and Indoor Navigation (IPIN), 2011 International Conference on*, pages 1–6, 2011. (Cited on page 8.)

[29] Rim. Bahroun. Localisation de personnes à l'intérieur des batiments par ondes sismiques. PhD Thesis (in French), Polytechnique de Grenoble, december 2013. (Cited on page 8.)

[30] D. Vlasic, R. Adelsberger, G. Vannucci, J. Barnwell, M. Gross, W. Matusik, and J. Popović. Practical motion capture in everyday surroundings. *ACM Transactions on Graphics (TOG)*, 26(3):35, 2007. (Cited on page 8.)

[31] Y. Gu, A. Lo, and I. Niemegeers. A survey of indoor positioning systems for wireless personal networks. *IEEE Communications Survey & Tutorals*, 11(1):13–32, 2009. (Cited on page 8.)

[32] M. Maman, B. Denis, M. Pezzin, B. Piaget, and L. Ouvry. Synergetic mac and higher layers functionalities for uwb ldr-lt wireless networks. In *Ultra-Wideband, 2008. ICUWB 2008. IEEE International Conference on*, pages 101–104, 2008. (Cited on pages 9, 77 and 78.)

[33] B. Denis. Exploitation des capacités de radiolocalisation des transmissions ultra-large bande dans les réseaux sans-fil. PhD Thesis (in French), Institut National des Sciences Appliquées de Rennes, D05-18, 2005. (Cited on page 10.)

[34] Z. Sahinoglu, S. Gezici, and I. Guvenc. Ultra-wideband positioning systems: Theoretical limits, ranging algorithms, and protocols. Cambridge University Press Cambridge, U.K., 2008. (Cited on pages 10, 47 and 71.)

[35] T. Rappaport. Wireless communications : Principles and practice. Upper Saddle River, NJ, USA : Prentice Hall PTR, 2001. (Cited on page 11.)

[36] D. Neirynck, K. Philips, H. De Groot, and J. Espina. Practical comparison of ranging in ieee 802.15.4 and ieee 802.15.4a medical body sensor networks. In *BodyNets'10*, pages 16–22, 2010. (Cited on pages 12 and 35.)

[37] D. Hol, F. Dijkstra, H. Luinge, and T. Schon. Tightly coupled uwb/imu pose estimation. In *Ultra-Wideband, 2009. ICUWB 2009. IEEE International Conference on*, pages 688–692, 2009. (Cited on page 12.)

[38] D. Jourdan, Jr. Deyst, J.J., M.Z. Win, and N. Roy. Monte carlo localization in dense multipath environments using uwb ranging. In *Ultra-Wideband, 2005. ICU 2005. 2005 IEEE International Conference on*, pages 314–319, 2005. (Cited on page 12.)

[39] J. Youssef, B. Denis, C. Godin, and S. Lesecq. Pedestrian tracking solution combining an impulse radio handset transmitter with an ankle-mounted inertial measurement unit. *International Journal of Navigation and Observation*, 2012. (Cited on page 12.)

[40] Sylvain Pittet, Valerie Renaudin, Bertrand Merminod, and Michel Kasser. Uwb and mems based indoor navigation. *The Journal of Navigation*, 61(3):369–384, 2008. (Cited on page 12.)

[41] V. Renaudin, B. Merminod, and M. Kasser. Optimal data fusion for pedestrian navigation based on uwb and mems. In *Position, Location and Navigation Symposium, 2008 IEEE/ION*, pages 341–349, 2008. (Cited on page 12.)

[42] F. Evennou and F. Marx. Advanced integration of wifi and inertial navigation systems for indoor mobile positioning. *Eurasip Journal on Applied Signal Processing*, 2006:164–164, 2006. (Cited on page 12.)

[43] H. Wymeersch, J. Lien, and M.Z. Win. Cooperative localization in wireless networks. *Proceedings of the IEEE*, 97(2):427–450, 2009. (Cited on pages 13 and 35.)

[44] J. Hamie, B. Denis, R. D'Errico, and C. Richard. Empirical modeling of intra-ban ranging errors based on ir-uwb toa estimation. In *Proceedings of the 7th International Conference on Body Area Networks*, BodyNets'12, pages 139–144, 2012. (Cited on pages 18, 40, 65, 71 and 80.)

[45] J. Hamie, B. Denis, R. D'Errico, and C. Richard. On-body toa-based ranging error model for motion capture applications within wearable uwb networks. *to appear in Journal on Mobile Networks and Applications*, 2013. (Cited on pages 18, 40, 65 and 80.)

[46] J. Hamie, B. Denis, and C. Richard. Constrained decentralized algorithm for the relative localization of wearable wireless sensor nodes. In *Sensors, 2012 IEEE*, pages 1–4, 2012. (Cited on pages 18, 75 and 95.)

[47] J. Hamie, B. Denis, and C. Richard. Nodes updates censoring and scheduling in constrained decentralized positioning for large-scale motion capture based on wireless body area networks. In *Proceedings of the 7th International Conference on Body Area Networks*, BodyNets'12, pages 100–105, 2012. (Cited on pages 18 and 95.)

[48] J. Hamie, B. Denis, and C. Richard. Decentralized positioning algorithm for relative nodes localization in wireless body area networks. *to appear in Journal on Mobile Networks and Applications*, 2013. (Cited on pages 18 and 95.)

[49] J. Hamie, B. Denis, and C. Richard. Joint motion capture and navigation in heterogeneous body area networks with distance estimation over neighborhood graph. In *Positioning Navigation and Communication (WPNC), 2013 10th Workshop on*, pages 1–6, 2013. (Cited on pages 18 and 95.)

[50] S. Ullah, M. Mohaisen, and M. Alnuem. A review of ieee 802.15.6 mac, phy, and security specifications. *International Journal of Distributed Sensor Networks*, 2013, 2013. (Cited on page 22.)

[51] J. Zhang, D.B. Smith, L.W. Hanlen, D. Minutti, D. Rodda, , and B. Gilbert. Stability of narrowband dynamic body area channel. *Antennas and Wireless Propagation Letters, IEEE*, 8:53–56, 2009. (Cited on page 23.)

[52] K. Takizawa H. Sawada N. Katayama K.Y Yazdandoost T. Kobayashi H.B. Li T. Aoyagi, J.I. Takada and R. Kohno. Channel models for wearable and implantable wbans-nict. Technical report, IEEE 802.15-08-0416-04-0006, IEEE 802.15 Task Group 6 Document, November 2010. (Cited on pages 23 and 24.)

[53] G. Dolmans, , and A. Fort. Channel models wban-holst centre/imec-nl. Technical report, IEEE 802.15-08-0418-01-0006, IEEE 802.15 Task Group 6 Document, July 2008. (Cited on page 24.)

[54] D. Smith A. Zhang D. Lewis D. Rodda D. Miniutti, L. Hanlen and B. Gilbert. Narrowband on body to off body channel characterization for ban. Technical report, IEEE 802.15-08-0559-00-0006, IEEE 802.15 Task Group 6 Document, August 2008. (Cited on page 25.)

[55] J. Takada K.Y. Yazdandoost H. Sawada, T. Aoyagi and R. Kohno. Channel model between body surface and wireless access point for uwb band. Technical

report, IEEE 802.15-08-0576-00-0006, IEEE 802.15 Task Group 6 Document, August 2008. (Cited on page 25.)

[56] S.L. Cotton and W.G. Scanlon. Channel characterization for single-and multiple-antenna wearable systems used for indoor body-to-body communications. *Antennas and Wireless Propagation, IEEE Transaction on*, 57(4):980–990, 2008. (Cited on page 25.)

[57] G. Koutitas. Multiple human effects in body area networks. *IEEE Antennas and Wireless Propagation Letters, IEEE*, 9:938–941, 2010. (Cited on page 25.)

[58] Y. Wang, I. Bonev, J. Nielsen, I. Kovacs, and G.F. Pedersen. Characterisation of the indoor multiantenna body-to-body radio channel. *Antennas and Propagation, IEEE Transactions on*, 57(4):972–979, 2009. (Cited on page 25.)

[59] Ieee std 802.15.4-2006, part 15.4: Wireless medium access control (mac) and physical layer (phy) specifications for low-rate wireless personal area networks (lr-wpans), september 2006. (Cited on page 25.)

[60] Ieee 802.15.4a channel model- final report (p802.15-04-0662-04-004a-channel-model-final-report-r1), october 2005. (Cited on pages 25 and 63.)

[61] M. Mhedhbi, M. Laaraiedh, and B. Uguen. Constrained lmds technique for human motion and gesture estimation. In *Positioning Navigation and Communication (WPNC), 2012 9th Workshop on*, pages 89–93, 2012. (Cited on pages 27, 28, 70, 73 and 80.)

[62] Z. Mekonnen, E. Slottke, H. Luecken, C. Steiner, and A. Wittneben. Constrained maximum likelihood positioning for uwb based human motion tracking. In *Indoor Positioning and Indoor Navigation (IPIN), 2010 International Conference on*, pages 1–10, 2010. (Cited on pages 27, 28, 31, 36 and 39.)

[63] H. Ren and L. Meng, M.and Xu. Indoor patient position estimation using particle filtering and wireless body area networks. In *Engineering in Medicine and Biology Society, 2007. EMBS 2007. 29th Annual International Conference of the IEEE*, pages 2277–2280, 2007. (Cited on pages 27, 28, 33 and 36.)

[64] W. Cully, S. Cotton, W. Scanlon, and J. McQuiston. Body shadowing mitigation using differentiated los/nlos channel models for rssi-based monte carlo personnel localization. In *Wireless Communications and Networking Conference (WCNC), 2012 IEEE*, pages 694–698, 2012. (Cited on page 28.)

[65] A. Costa, N. Patwari, and O. Hero. Distributed weighted-multidimensional scaling for node localization in sensor networks. *ACM Trans. Sen. Netw.*, 2(1):39–64, 2006. (Cited on pages 29, 30, 70, 74 and 80.)

[66] P. Biswas, T. Lian, T. Wang, and Y. Ye. Semidefinite programming based algorithms for sensor network localization. *ACM Trans. Sen. Netw.*, 2(2):188–220, 2006. (Cited on page 29.)

[67] AA. Cox, T.and Cox. *Multidimensional scaling*, volume 88. CRC Press, 2001. (Cited on pages 30, 72 and 73.)

[68] B. Denis, Liyun He, and L. Ouvry. A flexible distributed maximum log-likelihood scheme for uwb indoor positioning. In *Positioning, Navigation and Communication, 2007. WPNC'07. 4th Workshop on*, pages 77–86, 2007. (Cited on page 30.)

[69] B. Denis and N. Daniele. Nlos ranging error mitigation in a distributed positioning algorithm for indoor uwb ad-hoc networks. In *Wireless Ad-Hoc Networks, 2004 International Workshop on*, pages 356–360, 2004. (Cited on page 30.)

[70] G. Destino, D. Macagnano, G. Abreu, B. Denis, and L. Ouvry. Localization and tracking for ldr-uwb systems. In *Mobile and Wireless Communications Summit, 2007. 16th IST*, pages 1–5. IEEE, 2007. (Cited on page 30.)

[71] SM Kay. Fundamentals of statistical signal processing, volume i: Estimation theory. 1993. (Cited on pages 31 and 32.)

[72] A. Doucet, S. Godsill, and C. Andrieu. *On sequential simulation-based methods for Bayesian filtering*. Department of Engineering, University of Cambridge UK, 1998. (Cited on page 33.)

[73] F. Gustafsson, F. Gunnarsson, N. Bergman, U. Forssell, J. Jansson, R. Karlsson, and P. Nordlund. Particle filters for positioning, navigation, and tracking. *Signal Processing, IEEE Transactions on*, 50(2):425–437, 2002. (Cited on page 33.)

[74] F. Evennou, F. Marx, and E. Novakov. Map-aided indoor mobile positioning system using particle filter. In *Wireless Communications and Networking Conference, 2005 IEEE*, pages 2490–2494, 2005. (Cited on page 33.)

[75] K. Yu and E. Dutkiewicz. Improved kalman filtering algorithms for mobile tracking in nlos scenarios. In *Wireless Communications and networking Conference (WCNC), 2012 IEEE*, pages 2390–2394, 2012. (Cited on page 33.)

[76] X. Yun and E. Bachmann. Design, implementation, and experimental results of a quaternion-based kalman filter for human body motion tracking. *Robotics, IEEE Transaction on*, 22(6):1216–1277, 2006. (Cited on pages 33 and 137.)

[77] T. Perala and R. Piché. Robust extended kalman filtering in hybrid positioning applications. In *Positioning, Navigation and Communication, 2007. WPNC'07. 4th Workshop on*, pages 55–63, 2007. (Cited on pages 33 and 137.)

[78] J.S. Yedidia, W.T. Freeman, and Y. Weiss. Understanding belief propagation and its generalizations. *Exploring artificial intelligence in the new millennium, ACM*, 97(2):239–269, 2003. (Cited on page 34.)

[79] A.T. Ihler, J.W. Fisher, R.L. Moses, and A.S. Willsky. Nonparametric belief propagation for self-localization of sensor networks. *Selected Areas in Communications, IEEE Journal on*, 23(4):809–819, 2005. (Cited on page 34.)

[80] V. Savic, H. Wymeersch, F. Penna, and S. Zazo. Optimized edge appearance probability for cooperative localization based on tree-reweighted nonparametric belief propagation. In *Acoustics, Speech and Signal Processing (ICASSP), 2011 IEEE International Conference on*, pages 3028–3031, 2011. (Cited on page 34.)

[81] H. Noureddine. *Signal Processing Techniques for Wireless Cooperative Localization and Tracking*. PhD thesis, Telecom Bretagne, 2012. (Cited on page 34.)

[82] H. Noureddine, N. Gresset, D. Castelain, and R. Pyndiah. A new variant of nonparametric belief propagation for self-localization. In *Telecommunications (ICT), 2010 IEEE 17th International Conference on*, pages 822–827, 2010. (Cited on page 34.)

[83] U. Ferner, H. Wymeersch, and M.Z. Win. Cooperative anchor-less localization for large dynamic networks. In *Ultra-Wideband, 2008. ICUWB 2008. IEEE International Conference on*, pages 181–185, 2008. (Cited on page 35.)

[84] C. Pedersen, T. Pedersen, and B.H. Fleury. A variational message passing algorithm for sensor self-localization in wireless networks. In *Information Theory Proceedings (ISIT), 2011 IEEE International Symposium on*, pages 2158–2162, 2011. (Cited on page 35.)

[85] M. Di Renzo, R. Buehrer, and J. Torres. Pulse shape distortion and ranging accuracy in uwb-based body area networks for full-body motion capture and gait analysis. In *Global Telecommunications Conference, 2007. GLOBECOM'07. IEEE*, pages 3775–3780, 2007. (Cited on pages 35 and 45.)

[86] A.A. Goulianos and S. Stavrou. Uwb path arrival times in body area networks. *Antennas and Wireless Propagation Letters, IEEE*, 6:223–226, 2007. (Cited on page 35.)

[87] C.P. Figueiredo, N.S. Dias, and P.M. Mendes. 3d localization for biomedical wireless sensor networks using a microantenna. In *Wireless Technology, 2008. EuWiT 2008. European Conference on*, pages 45–48, 2008. (Cited on page 35.)

[88] Cheng Guo, Jing Wang, R.V. Prasad, and M. Jacobsson. Improving the accuracy of person localization with body area sensor networks: An experimental study. In *Consumer Communications and Networking Conference, 2009. CCNC 2009. 6th IEEE*, pages 1–5, 2009. (Cited on page 36.)

[89] L. Cheolhyo, L. Hyung-Soo, and K. Jae-Young. Performance of a one-way ranging method for wban healthcare services. In *Communications and Information Technology, 2009. ISCIT 2009. 9th International Symposium on*, pages 1460–1463, 2009. (Cited on page 36.)

[90] F. Chiti, R. Fantacci, F. Archetti, E. Messina, and D. Toscani. An integrated communications framework for context aware continuous monitoring with body sensor networks. *Selected Areas in Communications, IEEE Journal on*, 27(4):379–386, 2009. (Cited on page 36.)

[91] H. Shaban, M. El-Nasr, and R. Buehrer. Toward a highly accurate ambulatory system for clinical gait analysis via uwb radios. *Information Technology in Biomedicine, IEEE Transactions on*, 14(2):284–291, 2010. (Cited on pages 39 and 45.)

[92] S. Gezici, M. Chiang, H. Poor, and H. Kobayashi. A genetic algorithm based finger selection scheme for uwb mmse rake receivers. In *Ultra-Wideband, 2005. ICU 2005. 2005 International conference on*, pages 164–169, 2005. (Cited on page 42.)

[93] B. Denis and J. Keignart. Post-processing framework for enhanced uwb channel modeling from band-limited measurements. In *Ultra Wideband Systems and Technologies, 2003 IEEE Conference on*, pages 260–264, 2003. (Cited on pages 42 and 63.)

[94] L. Yang. *The Applicability of the Tap-Delay Line Channel Model to Ultra Wideband*. PhD thesis, Virginia Polytechnic Institute and State University, 2004. (Cited on page 45.)

[95] J. Zhang, R. Kennedy, and T. Abhayapala. Cramer-rao lower bounds for the time delay estimation of uwb signals. In *Communications, 2004 IEEE International Conference on*, volume 6, pages 3424–3428, 2004. (Cited on pages 62 and 63.)

[96] L. De Nardis and M. Di Benedetto. Overview of the ieee 802.15. 4/4a standards for low data rate wireless personal data networks. In *Positioning, Navigation and Communication, 2007. WPNC'07. 4th Workshop on*, pages 285–289, 2007. (Cited on page 63.)

[97] F. Doremani, H. Javadi, and A. Farahi. A new distributed weighted multidimensional scaling algorithm for localization in wireless sensor networks. *International journal of Computer Science and Engineering Survey*, 20(1), 2011. (Cited on page 70.)

[98] Z. Chen, H. Wei, Q. Wan, S. Ye, and W. Yang. A supplement to multidimensional scaling framework for mobile location: A unified view. *signal Processing, IEEE Transaction on*, 57(5):2030–2034, 2009. (Cited on page 72.)

[99] A. Costa, N. Patwari, and O. Hero. Achieving high-accuracy distributed localization in sensor networks. In *Acoustics, Speech, and Signal Processing, 2005. Proceedings. (ICASSP'05). IEEE Conference on*, pages iii–641, 2005. (Cited on page 74.)

[100] P. Groenen. *The Majorization Approach to Multidimensional Scaling: some problems and extensions*. DSWO Press, Leiden University Leiden, 1993. (Cited on page 74.)

[101] M. Maman, F. Dehmas, R. D'Errico, and L. Ouvry. Evaluating a tdma mac for body area networks using a space-time dependant channel model. In *Personal, Indoor and Mobile Radio Communications, 2009 IEEE 20th International Symposium on*, pages 2101–2105, 2009. (Cited on pages 77, 78 and 91.)

[102] D. Macagnano, G. Destino, F. Esposito, and G. Abreu. Mac performances for localization and tracking in wireless sensor networks. In *Positioning, Navigation and Communication, 2007. WPNC'07. 4th Workshop on*, pages 297–302, 2007. (Cited on page 78.)

[103] T. Camp, J. Boleng, and V Davies. A survey of mobility models for ad hoc network research. *Wireless Communications and Mobile Computing*, 2(5):483–502, 2002. (Cited on page 78.)

[104] I. Pantazis. Tracking human walking using marg sensors. Technical report, DTIC Document, 2005. (Cited on page 78.)

[105] C. Wang, J. Chen, Y. Sun, and X. Shen. Wireless sensor networks localization with isomap. In *Communications, 2009. ICC'09. IEEE International Conference on*, pages 1–5, 2009. (Cited on pages 88 and 90.)

[106] Béla Bollobás. *Extremal Graph Theory*. DoverPublications. com, 1978. (Cited on page 90.)

[107] D. Goldenberg, A. Krishnamurthy, W. Maness, Y. Yang, R. Young, A. Young, A. Morse, and A. Savvid. Network localization in partially localizable networks. In *INFOCOM 2005. 24th Annual Joint Conference of the IEEE Computer and Communication Societies. Proceedings IEEE*, volume 1, pages 313–326, 2005. (Cited on page 90.)

[108] M. Pezzin, I. Bucaille, T. Schulze, A. Pato, and L. DeCelis. An open ir-uwb platform for ldr-lt applications prototyping. In *Positioning, Navigation and Communication, 2009. WPNC 2009. 6th Workshop on*, pages 285–293, 2009. (Cited on pages 92, 104, 112 and 115.)

[109] M. Laaraiedh, S. Avrillon, and B. Uguen. Enhancing positioning accuracy through direct position estimators based on hybrid rss data fusion. In *Vehicular Technology Conference, 2009. VTC Spring 2009. IEEE 69th*, pages 1–5, 2009. (Cited on pages 92 and 104.)

[110] N. Amiot, T. Pedersen, M. Laaraiedh, and B. Uguen. A hybrid positioning method based on hypothesis testing. *Wireless Communications Letters, IEEE*, 1(4):348–351, 2012. (Cited on page 105.)

[111] J. Youssef, B. Denis, C. Godin, and S. Lesecq. Enhanced uwb indoor tracking through nlos toa biases estimation. In *Global Telecommunications Conference, 2008. IEEE GLOBECOM 2008. IEEE*, pages 1–5, 2008. (Cited on page 105.)

[112] B. Denis, L. Ouvry, B. Uguen, and F. Tchoffo-Talom. Advanced bayesian filtering techniques for uwb tracking systems in indoor environments. In *Ultra-Wideband, 2005. ICU 2005. 2005 IEEE International Conference on*, pages 6–pp, 2005. (Cited on page 105.)

[113] D. Lachartre, B. Denis, D. Morche, L. Ouvry, M. Pezzin, B. Piaget, J. Prouvee, and P Vicent. A 1.1nj/b 802.15.4a-compliant fully integrated uwb transceiver in 0.13 micrometer cmos. In *Solid-State Circuits Conference - Digest of Technical Papers, 2009. ISSCS 2009. IEEE International*, pages 312–313,313a, 2009. (Cited on page 112.)

[114] M. Pezzin and D. Lachartre. A low power, low data rate impulse radio ultra wide band transceivers. In *Future Network and Mobile Summit, 2010*, pages 1–10, 2010. (Cited on page 112.)

[115] B. Denis, M. Maman, and L. Ouvry. On the scheduling of ranging and distributed positioning upadtes in cooperatives ir-uwb networks. In *Ultra-Wideband, 2009. ICUWB 2009; IEEE International Conference on*, pages 370–375, 2009. (Cited on page 112.)

[116] G. Masson, D. Morche, H. Jacquinot, P. Vincent, F. Dehmas, S. Paquelet, A. Bisiaux, O. Fourquin, J. Gaubert, and S. Bourdel. A 1 nj/b 3.2-to-4.7 ghz uwb 50 mpulses/s double quadrature receiver for communication and localization. In *ESSCIRC, 2010 Proceedings of the*, pages 502–505, 2010. (Cited on page 124.)

[117] `http://bespoon.com/`. (Cited on page 124.)

[118] L. Harry and V. Trees. Detection, estimation, and modulation theory, part i. *Massachussets institute of technology, Jhon Wiley and Sons*, 1968. (Cited on page 132.)

[119] J. Proakis. *Intersymbol Interference in Digital Communication Systems*. 1995. (Cited on page 132.)

[120] A. D'Andrea, U. Mengali, and R. Reggianini. The modified cramer-rao bound and its applications to synchronization problems. *Communications, IEEE Transaction on*, 42(234):1391–1399, 1994. (Cited on page 132.)

[121] E. Lehman and G. Casella. *Theory of point estimation*, volume 31. springer, 1998. (Cited on page 133.)

[122] N. Patwari, A. Hero, M. Perkins, N. Correal, and R. O'dea. Relative location estimation in wirelsess sensor networks. *Signal Processing, IEEE Transaction on*, 51(8):2137–2148, 2003. (Cited on page 135.)